



# **Design and Analysis of SRAMs for Energy Harvesting Systems**

By

**Abdullah Baz**

School of Electrical, Electronic and Computer Engineering  
Newcastle University

A thesis submitted in fulfilment of the requirements for the  
degree of Doctor of Philosophy

April 2014

## Abstract

At present, the battery is employed as a power source for wide varieties of microelectronic systems ranging from biomedical implants and sensor networks to portable devices. However, the battery has several limitations and incurs many challenges for the majority of these systems. For instance, the design considerations of implantable devices concern about the battery from two aspects, the toxic materials it contains and its lifetime since replacing the battery means a surgical operation. Another challenge appears in wireless sensor networks, where hundreds or thousands of nodes are scattered around the monitored environment and the battery of each node should be maintained and replaced regularly, nonetheless, the batteries in these nodes do not all run out at the same time.

Since the introduction of portable systems, the area of low power designs has witnessed extensive research, driven by the industrial needs, towards the aim of extending the lives of batteries. Coincidentally, the continuing innovations in the field of micro-generators made their outputs in the same range of several portable applications. This overlap creates a clear opportunity to develop new generations of electronic systems that can be powered, or at least augmented, by energy harvesters. Such self-powered systems benefit applications where maintaining and replacing batteries are impossible, inconvenient, costly, or hazardous, in addition to decreasing the adverse effects the battery has on the environment.

The main goal of this research study is to investigate energy harvesting aware design techniques for computational logic in order to enable the capa-

bility of working under non-deterministic energy sources. As a case study, the research concentrates on a vital part of all computational loads, SRAM, which occupies more than 90% of the chip area according to the ITRS reports.

Essentially, this research conducted experiments to find out the design metric of an SRAM that is the most vulnerable to unpredictable energy sources, which has been confirmed to be the timing. Accordingly, the study proposed a truly self-timed SRAM that is realized based on complete handshaking protocols in the 6T bit-cell regulated by a fully Speed Independent (SI) timing circuitry. The study proved the functionality of the proposed design in real silicon. Finally, the project enhanced other performance metrics of the self-timed SRAM concentrating on the bit-line length and the minimum operational voltage by employing several additional design techniques.

## Preface

The results in this PhD thesis are realized within the framework of the project “Next Generation Energy harvesting Electronics: A Holistic Approach”, which is a £1.6M project funded by EPSRC. The project involves four universities, namely, the University of Southampton, Newcastle University, Imperial College, and the University of Bristol. All academic institutions are undertaking the three-year collaborative research project in partnership with four industrial companies: Dialog Semiconductor, Diodes Incorporated, ARM, and Mentor Graphics.

More information can be found in the project website:

<http://www.holistic.ecs.soton.ac.uk/index.php>

## Acknowledgments

Since November 2009, I have been a research student with the Holistic project and currently, I am approaching the end of my third PhD year. During this time, I have fabricated three chips, published four papers in international conferences, an invited journal paper, and several more are being prepared for submission. The results obtained throughout the study period were realized by developing several program codes, mastering different EDA/CAD tools, and testing numerous hardware components, equipment, and boards in the laboratory. Certainly, carrying out all this work alone is difficult if not impossible. Accordingly, it is the aim of this text to acknowledge those key people, without their invaluable help, the mentioned achievements would not be possible.

First of all, I wish to express my extreme gratitude to my research supervisor Professor Alex Yakovlev for his incredibly wise guidance and motivations during my research. I appreciate his support for attending all training courses, meetings, and conferences I have requested throughout my study. I owe him special thanks for sponsoring me to fabricate three chips while very few supervisors around the world do that.

Next, my sincere thanks go to Dr. Delong Shang, my colleague and mentor, for his help throughout this research. He always had the time to propose new ideas to me and discuss my results.

In addition, I acknowledge the efforts that my colleague, Mr. Reza Ramezani, has made to complete part of the digital part of my first SRAM chip. Fol-

lowing my first chip, I helped him in designing the full-custom and analogue part of his sensor chip. I really enjoyed that collaborative work.

The same thanks go to my friend, Mr. Xuefu Zhang, who has successfully designed and fabricated his novel power delivery method, coined Capacitor Bank Block (CBB). His portable demonstration box was controlled by mine to prove the functionality of the SRAM in several venues including PATMOS 2012 in Newcastle, the final advisory board meeting of holistic project in the University of Southampton, the final project showcase held in Imperial College, the 3<sup>rd</sup> annual Energy harvesting conference in London, and the Async 2013 conference in Santa Monica.

Most importantly, Umm Al-Qura University, the Ministry of Higher Education in the Kingdom of Saudi Arabia, and the Saudi Cultural Bureau in London have financially supported my study as well as my living expenses in the UK. Definitely, without their support the aforementioned achievements would not have been possible, my sincere thanks go to them.

Above and beyond all else, my parents, my first teachers in this life, have been continuously supporting and encouraging me throughout my study as well as my life. Without their incredibly wise guidance, such a level would never be reached and such a work would never be achieved. Despite that I lost my father in the second year of my PhD, he still inspires me to reach ever further.

Next in importance, I express my special and sincere thanks and extreme gratitude to my wife, son, and daughter for their love, support, and patience throughout my study. I really appreciate the time they sacrificed to allow me progress more.

Finally, I apologize in advance, to those I might have forgotten to mention.

# Contents

Abstract.....	I
Preface .....	III
Acknowledgments.....	IV
Contents.....	VI
List of Tables .....	IX
List of Figures .....	X
Chapter 1. Introduction .....	1
1.1 Introduction .....	1
1.2 Motivation.....	3
1.3 Research Originality and Contributions .....	5
1.4 Research Management and Involved Risks .....	7
1.5 Thesis Outline and Achievements.....	7
1.6 Publications.....	8
1.7 References .....	9
Chapter 2. Background .....	11
2.1 Introduction .....	11
2.2 Energy Harvesting Systems: Next Generation of Microelectronics .....	11
2.2.1 Micro Generators.....	12
2.2.2 Energy Harvesting Electronics.....	17
2.3 SRAM.....	18
2.3.1 SRAM Structure and Operational States.....	18
2.3.1.1 Holding State.....	19
2.3.1.2 Reading State .....	21
2.3.1.3 Writing State .....	24
2.3.2 SRAM Design Challenges.....	25
2.3.3 SRAM Design Approaches .....	29

2.3.3.1 Bit-Cell Based Techniques .....	30
2.3.3.2 Voltage Level Based Techniques .....	34
2.3.3.3 Timing Circuit Based Techniques .....	38
2.3.3.4 Peripheral Circuit Based Techniques .....	40
2.4 Summary .....	40
2.5 References .....	41
Chapter 3. Truly Self-Timed SRAM.....	46
3.1 Introduction .....	46
3.2 Problem Statement: Timing Variations in Non-Deterministic Environments.....	46
3.2.1 SRAM Latency under Different VDDs.....	47
3.3 Methodology and Design Strategy: Power Adaptive Computing .....	49
3.3.1 Self-Timed SRAM.....	50
3.4 Investigations on the Proposed SI SRAM .....	55
3.4.1 Behaviour of SI SRAM under Variable VDD.....	56
3.4.2 Timing and Energy Computations.....	57
3.4.3 Energy Overhead.....	59
3.5 More Efficient Design Technique: Smart Latency Bundled Self-Timed SRAM.....	60
3.5.1 Bundling Techniques in Self-Timed SRAM .....	61
3.5.2 Timing and Energy Comparisons.....	66
3.6 Conclusion .....	69
3.7 References .....	71
Chapter 4. Design, Fabrication and Testing of HoliSRAM.....	73
4.1 Introduction .....	73
4.2 Chip Architecture .....	73
4.2.1 Dual Power Domain Design Phase .....	78
4.2.2 Dual Cell Design Phase .....	80
4.3 Chip Design Flow .....	81
4.3.1 Results of Chip Simulation .....	81
4.4 Chip Testing.....	85
4.4.1 Stream II Demonstration: a Portable HoliSRAM Box .....	85
4.4.2 Interactive Interface for Interactive Demonstration .....	90
4.4.3 Measurements and Testing Results .....	91
4.5 Conclusions .....	96
4.6 References .....	97
Chapter 5. Improving the Robustness of Self-Timed SRAM .....	98



5.1 Introduction .....	98
5.2 Preliminary Analysis .....	98
5.3 New Robust Self-Timed SRAM: a Bit-Cell Based Technique .....	101
5.3.1 Investigations on the Proposed Bit-Cell Based Technique .....	104
5.4 Bit-line Keeper: a Peripheral Circuit Based Technique .....	106
5.4.1 Investigations on the Proposed Peripheral Circuit Based Technique .....	107
5.5 Virtual Ground: a Voltage Level Based Technique.....	110
5.5.1 Investigations on the Proposed Voltage Level Based Technique .....	113
5.6 Conclusions .....	114
5.7 References .....	116
Chapter 6. Conclusions and Future Work.....	117
6.1 Introduction .....	117
6.2 View and Review .....	117
6.3 Prospective Future Research .....	121
6.4 References .....	123
Appendix A. Hardware Supplements .....	124
A.1 Tool Path .....	124
A.2 Introduction .....	127
A.3 Chip Gallery .....	127
A.4 Demonstration PCB .....	128
A.5 PIC32 Interface Code .....	134

## List of Tables

Table 2.1 Amount of power that can be harvested from different ambient energy sources. ....	12
Table 2.2 Comparisons between transduction mechanisms of vibration energy harvesters ....	14
Table 2.3 Scaling parameters. ....	25
Table 4.1 Functional yield of the SI SRAM. ....	84
Table 4.2 Components list of the portable demonstration box. ....	89
Table 4.3 $\mu$ C ports employed during the demonstration. ....	90
Table 6.1 Comparison between the designs proposed in the thesis.....	120
Table A.1 Chip Gallery.....	128

## List of Figures

Figure 2.1 Electromagnetic transduction technique. ....	13
Figure 2.2 Piezoelectric transduction technique. ....	13
Figure 2.3 Two different configurations for electrostatic transduction technique. ....	14
Figure 2.4 Schematic of thermocouple and of a thermopile. ....	15
Figure 2.5 Cross coupled inverters with two voltage sources to model static noise. ....	19
Figure 2.6 Basic SRAM system block diagram. ....	20
Figure 2.7 Butterfly curves of the 6T cell during holding state. ....	21
Figure 2.8 Butterfly curves of the 6T cell during reading. ....	22
Figure 2.9 The schematic used to extract the N-curve and the resulted N-curve. ....	23
Figure 2.10 The schematic used to extract the WSNM together with the extracted curves. ....	25
Figure 2.11 Leakage currents in the 6T cell. ....	27
Figure 2.12 Worst case data scenario for bit-line leakage. ....	28
Figure 2.13 Published SRAM bit-cells. ....	31
Figure 3.1 A method to investigate timing discrepancy between SRAM and inverter chain. ....	48
Figure 3.2 Timing mismatch between SRAM and its bundling delay element. ....	48
Figure 3.3 Block diagram of the proposed self-timed memory system. ....	52
Figure 3.4 STG specifications of the reading and writing operations in the 6T cell. ....	53
Figure 3.5 Possible implementation of the STG's in Figure 3.4. ....	54
Figure 3.6 Critical waveforms of self-timed SRAM under variable VDD. ....	56
Figure 3.7 Operation delay of the proposed self-timed SRAM. ....	58
Figure 3.8 Energy consumptions of the proposed self-timed SRAM. ....	58
Figure 3.9 Energy overhead of the proposed timing controller during writing. ....	59
Figure 3.10 Energy overhead of the proposed timing controller during reading. ....	60
Figure 3.11 Bundling scheme in self-timed SRAM. ....	61
Figure 3.12 Modified writing STG for latency bundled SRAM. ....	64
Figure 3.13 Modified timing circuit based on the modified STG. ....	66
Figure 3.14 Writing latency comparison between fully SI and smartly bundled SRAM. ....	68
Figure 3.15 Reading latency comparison between fully SI and smartly bundled SRAM. ....	68
Figure 3.16 Writing energy comparison between fully SI and smartly bundled SRAM. ....	69
Figure 3.17 Reading energy comparison between fully SI and smartly bundled SRAM. ....	69
Figure 4.1 Main part of the HoliSRAM chip. ....	74
Figure 4.2 STG specification of the SRAM demonstration chip. ....	76
Figure 4.3 Power domain view of the HoliSRAM chip. ....	78
Figure 4.4 A method to investigate suitable way of signal communications. ....	79

Figure 4.5 Waveforms of the signal communication experiment. ....	80
Figure 4.6 Timing waveforms of the closed loop self-timed SRAM. ....	82
Figure 4.7 Corner analysis of the HoliSRAM core. ....	83
Figure 4.8 Stream II demonstration system diagram. ....	86
Figure 4.9 Block diagram of the SRAM demonstration box. ....	88
Figure 4.10 Portable demonstration box pictured from all sides. ....	91
Figure 4.11 Oscilloscope screenshot for the HoliSRAM critical signals during reading. ....	92
Figure 4.12 Oscilloscope screenshot for the HoliSRAM critical signals during writing. ....	92
Figure 4.13 Oscilloscope screenshot of the HoliSRAM chip under a sawtooth voltage. ....	94
Figure 4.14 Oscilloscope screenshot of the HoliSRAM under a sinusoidal voltage. ....	94
Figure 4.15 Waveforms of the circuits causing the mismatch. ....	96
Figure 5.1 Timing waveforms of a typical failure case in self-timed SRAM. ....	99
Figure 5.2 Bit-line voltage after successful writing for different bit-line sizes. ....	101
Figure 5.3 Proposed 10T SRAM cell. ....	102
Figure 5.4 STG specifications for writing and reading in self-timed 10T SRAM. ....	103
Figure 5.5 Proposed SI controller for the self-timed 10T SRAM. ....	104
Figure 5.6 Waveforms of the proposed self-timed SRAM for (a) reading and (b) writing. ....	104
Figure 5.7 Waveforms of a timing failure case in the 10T self-timed SRAM. ....	106
Figure 5.8 The circuit diagram of the bit-line keeper. ....	107
Figure 5.9 Waveforms of the 10T self-timed SRAM with no timing failure. ....	107
Figure 5.10 Writing time for 256x128 SRAM bank at 0.3V. ....	108
Figure 5.11 Timing diagram of writing operation that shows the data in the bundling and bundled columns. ....	110
Figure 5.12 10T SRAM cell with the virtual ground terminal. ....	112
Figure 5.13 STGs specifications for writing and reading of the 10T SRAM with VGND. ....	112
Figure 5.14 Possible realization of the timing circuit for the 10T SRAM with VGND. ....	113
Figure 5.15 Energy saving during writing and reading in the 10T SRAM with VGND. ....	114
Figure A.1 The final view of the SRAM chip after P&R. ....	125
Figure A.2 SRAM chip after replacing abstract views with corresponding real layouts. ....	126
Figure A.3 HoliSRAM chip completely designed and packaged in PGA84. ....	127
Figure A.4 Schematic of the demonstration PCB page 1/3. ....	129
Figure A.5 Schematic of the demonstration PCB page 2/3. ....	130
Figure A.6 Schematic of the demonstration PCB page 3/3. ....	131
Figure A.7 Layer-1 of the demonstration PCB. ....	132
Figure A.8 Layer-2 of the demonstration PCB. ....	132
Figure A.9 Layer-3 of the demonstration PCB. ....	133
Figure A.10 Layer-4 of the demonstration PCB. ....	133
Figure A.11 Components name in the demonstration PCB. ....	134

# Chapter 1. Introduction

## 1.1 Introduction

The story, of the technology, began in late 1950s after two important inventions. The first was the ability to build an electronic circuit in which all of the components, both active and passive, were fabricated in a single piece of semiconductor. This idea was successfully implemented for the first time by Jack Kilby in the summer of 1958 [1] and was coined Integrated Circuit (IC) thereafter. The second was the introduction of the silicon Metal Oxide Semiconductor Field Effect Transistor (MOSFET), which was patented by M. M. Atalla and Dawon Kahng at Bell Labs in 1959 [2]. These two inventions allow the engineers to design high density ICs that have higher performance and noise immunity and lower power consumption than all other technologies, which is the primary reason that 99% of ICs production today uses MOS transistors [3].

Since this achievement, the technology has been driven by industrial needs to increase the performance, functionality, and density of ICs while decreasing the manufacturing cost, which has been accomplished via shrinking device feature size. The shrinking process was clearly understood and described by the co-founder of Intel, Gordon Moore, in 1965 following his observation of the scaling process since 1959 [4]. Moore found that, for each technology node, there is a certain number of components per IC which yields the minimum manufacturing cost of the device. As the technology scales down, this minimal cost point significantly increases the number of devices per die, roughly it doubles every two years.

The scaling process has not only improved the performance and functionality, moreover, it rendered a wide variety of new applications (e.g. high performance processors, portable systems, and ultra-low voltage devices). These proposed applications were enabled by the new features of the introduced technology node, since each node has its own properties in terms of operational voltage, switching speed, input capacitance, etc. Both the application requirements and the characteristics of the technology persuade designers to propose new design strategies to overcome the involved challenges. Usually, the design technique entails trading off some of the performance metrics of the whole system at the expense of others. For instance, in unrestricted power applications, performance and functionality are improved at the cost of more energy. In contrast, the design techniques of battery powered devices focus on minimizing the power consumption for specific performance constraints, where the performance is defined by the specifications of the applications. As a final example, high speed portable systems consider improving the performance of computation for a predefined amount of power in which the total energy is determined by the battery capacity and its lifetime [5]. The reader can refer to [6-9] for some examples of the previously introduced design techniques.

Recently and after conducting intensive research in both the area of micro-generators in order to improve their output and size, and the field of low power design techniques, a clear opportunity was made to develop a new generation of microelectronic systems that can be self-powered via energy harvesters [10]. Yet, the design strategies for this new generation are not crystal-clear and several attempts have been made towards shaping this generation. Nevertheless, the contributions proposed in this thesis can be considered as one of these attempts.

The remainder of this introductory chapter is organized into five sections, the next section introduces the concepts that motivated this work, and the third section summarizes the research originality and contributions. The fourth section discusses the expected risks and management plans, the fifth

section sketches out the outline of the whole text, and the last section lists all the publications resulting from this study.

## **1.2 Motivation**

At present, a battery is used as an energy source for several types of electronic systems ranging from biomedical devices and sensor networks to mobile phones and handheld computers. The only benefit that batteries grant to these computing systems is portability and the cost is several difficulties and limitations. Some of these difficulties affect some types of systems while others affect them all.

First, the electrical characteristics of the employed battery strongly affect the design of the power management and power minimization or optimization circuitry of the electronic systems. For instance, most portable electronic devices requires DC/DC converters, the design of which requires considering the voltage, and the minimum, maximum, and average discharge current of the battery [11]. This implies that changing the properties of the battery demands reviewing the design of these circuits.

Nickel Cadmium (NiCd) is a type of battery that has some advantages like long life and economical price, which made biomedical equipment one of its main applications, however, NiCd contains toxic substances and moreover it is environmentally unfriendly [12].

In the case of wireless sensor networks, hundreds to thousands of nodes are scattered around the monitored environment and the battery of each node should be maintained and replaced regularly, nevertheless, the batteries in these nodes do not all run out at the same time. In such a case, maintaining the batteries is costly and inconvenient [13, 14].

Some popular batteries like Lithium Ion (Li-ion), which is popularly used in cellular phones and notebook computers, require protection circuitry for safety purposes. However, the protection circuit itself limits the charging and discharging peak voltage and/or current of the battery and consumes an amount of the stored energy [12].

Some other limitations of batteries are self discharging, oxidation, performance degradation, high maintenance, and chemical breakdown [12].

Moreover, the dimension, weight, and cost of the electronic device are constrained by the corresponding properties of the battery, which strongly depend upon its energy density and cost [12].

Discussing the cost of the energy stored in batteries makes the problem even worse. It was reported in [12] that only during the year 2000, 2500MW was consumed by the batteries of cellular phones and mobile computers. In actual fact, batteries should not be blamed for this huge amount of power, however, they should be blamed for the cost they incur to store such an amount of energy. Financially, the total cost of acquiring a kWh of energy from a rechargeable battery is more than seven times the cost to supply the same to domestic customers. In the case of primary battery, the cost of a kWh is 3000 times more expensive than the cost of similar amount from the electric grid [12].

Finally, according to [15-17] the power consumption of ICs roughly doubles every two years while the power density of batteries doubles only every ten years. This difference creates a considerable gap between the power required by System on Chips (SoCs) and the maximum power deliverable by batteries. Unfortunately, this gap has been accumulating for a while and it is anticipated that in the near future the battery will not be a suitable source for many portable systems since its capacities will lag substantially behinds the needs of those systems [17].

All these challenges implied in the battery encourage some researchers to enhance its parameters while others decided to switch to different ways of supplying power to portable electronic devices. According to the literature and due to the advancement in the field of micro-generators and low power electronics, powering computing systems from energy scavengers is a promising area of research, based on that, it is better known as next generation of electronic systems [10].



Nevertheless, enabling energy harvesting systems do not aim to replace batteries in all portable systems, but rather to benefit those systems where maintaining and replacing batteries are impossible, inconvenient, costly, and/or hazardous. The benefit here means that the electronics are powered, or at least augmented, by the harvester. At the same time, it is anticipated that batteries will still serve power to several applications whenever it outperforms its alternatives. Yet, the battery is a vital component used nowadays and a portable power source for large numbers of applications and since it has been introduced, it controls the enabling and advancement of numerous technologies [12].

### **1.3 Research Originality and Contributions**

As discussed above, each generation of microelectronics has its own theme of design techniques, which are shaped by the requirements of the application together with the restrictions imposed by the surrounding environment and the employed technology node. Exploring the literature, during different eras of technology, concludes that design strategies involve trading off one or more performance metrics of the design at the expense of others. Frequently, there is a fundamental trade-off between power and performance, when there is no concern about the former, the latter is considerably improved while it was sacrificed when the former was scarce. Moreover, other design parameters are traded-off as well. For instance, many power minimization techniques like power gating, body-bias and multi-threshold voltage devices incur design overheads in terms of speed, area, and yield of the whole system [6-9, 18].

At present, it is the energy harvesting era, which requires researchers and designers to explore the challenges existing in the environment and the employed technologies in order to determine the theme of this generation in terms of design strategies [18].

The main objectives of this contribution are to investigate the existing design techniques used to employ energy scavenger as a power source for microelectronic systems. Upon the investigation, this study aims to introduce novel design techniques in order to enhance the state of the art of this gen-

eration. Comparing the existing techniques with the proposed ones would produce valuable results and that should be included in the thesis as well. While the mentioned aims cover a massive area of research, the main goal is kept reasonable within the available timescale and resources by concentrating on the most important part of the computational load.

Generally, the work is divided into several stages, which starts by selecting one of the fundamental and most vital parts of the computation logic as a case study for the whole research, then exploring the challenges involved in powering such a component, together with the whole system, from an energy scavenger. Following this stage, it is intended to examine the existing design techniques of the chosen case study, and propose novel design strategies based upon the researcher's understanding to the whole framework and his vision. Next stage consists of testing and verifying the functionality of the proposed design method via the most accurate resources available. Finally, the research plans to compare between the relevant design strategies in terms of the performance metrics of the chosen case study.

It is the fact that examining any, simple or complex, computational logic results in finding a memory component somewhere in the system. This element is vital for all computation processes in order to store instructions, operands, and results. Static Random Access Memory (SRAM) is an important type of memory typically used in an L1 and L2 on-chip cache as well as a wide range of SoCs [19]. International Technology Roadmap for Semiconductors (ITRS) reported that SRAM occupies more than 90% of the chip area and predicted that by 2018 the density of SRAM transistors will be six times more than the density of logic in the SoC [20]. Accordingly, the main SRAM performance metrics like throughput, energy, and area dominate those of the whole chip. Moreover, the challenges involved in designing and optimizing the SRAM are beyond those involved in any other electronic circuits [21]. All these facts allowed SRAM to gain special attention from designers and researchers, the feature that makes it the best case study for this research.

## **1.4 Research Management and Involved Risks**

This research will include analysis and designs of electronic circuits, which must be conducted via the available Electronic Design Automation (EDA) and Computer Aided Design (CAD) tools. Once the tools confirm the claimed contributions, the relevant circuitry might be fabricated and tested. Accordingly, the success of this research relies upon the researcher's skill in mastering the available tools and his ability to mimic the real environment by the tools. Therefore, it is anticipated that the main researcher requires some advance training courses. Importantly, fabrication and testing of hardware might involve manufacturing defeats, which needs to be spotted and corrected if possible. The excellent track record the supervisory team has in this field will support this research and hence regular meetings with them are compulsory.

## **1.5 Thesis Outline and Achievements**

This section describes the main work conducted during this research and that contains design techniques and data analysis for SRAM's in the context of energy harvesting systems. The body of the thesis is organized into six chapters along with an appendix outlined as follows:

Chapter 2: As a preliminary discussion, this chapter covers the important background of the main two areas of this research, energy scavenging, and SRAM. Firstly, the chapter presents the contributing factors in enabling the energy harvesting electronics as a promising field of research along with the challenges involved. After that, the most important aspects of the SRAM literature are covered.

Chapter 3: This chapter describes several experiments conducted to examine the current design techniques for SRAM in the context of energy harvesting systems. According to obtained results, which confirm the lack of adaptability of these techniques, the text proposes a truly self-timed SRAM to address this issue. Then, the chapter ends up with some analysis and computations.

Chapter 4: The aim of this chapter is to prove the functionality of the proposed design techniques in real hardware. Towards that aim, the chapter takes the reader through the stages the researcher has followed in order to design and test the fully self-timed SRAM chip. Importantly, the obtained measurements confirm the expectations and raise proposals for future research.

Chapter 5: In order to complete the whole framework of this study, this chapter provides several design strategies to improve the design metrics of self-timed SRAM via increasing its area density and extending its operational range. The proposed design techniques cover different levels of abstraction including circuit and transistor level.

Chapter 6: This chapter concludes the whole project and outlines some promising proposals for future studies.

Appendix A: This appendix is entitled hardware supplements and it contains some materials that the reader might be eager to read about the fabrication and testing works involved in this study.

## **1.6 Publications**

The work conducted throughout this project resulted in several contributions, some are already published, and others are in preparation. The following list includes all published ones.

1. A. Baz, D. Shang, F. Xia, and A. Yakovlev, "Self-Timed SRAM for Energy Harvesting Systems," in Integrated Circuit and System Design. Power and Timing Modeling, Optimization, and Simulation. vol. 6448, R. Leuken and G. Sicard, Eds., ed: Springer Berlin Heidelberg, 2011, pp. 105-115.
2. A. Baz, D. Shang, F. Xia, and A. Yakovlev, "Self-Timed SRAM for Energy Harvesting Systems," Journal of Low Power Electronics, vol. 7, pp. 274-284, 2011.

3. A. Baz, D. Shang, F. Xia, A. Yakovlev, and A. Bystrov, "Improving the Robustness of Self-timed SRAM to Variable Vdds," in *Integrated Circuit and System Design. Power and Timing Modeling, Optimization, and Simulation*. vol. 6951, J. Ayala, B. García-Cámara, M. Prieto, M. Ruggiero, and G. Sicard, Eds., ed: Springer Berlin Heidelberg, 2011, pp. 32-42.
4. F. Burns, A. Baz, D. Shang, and A. Yakovlev, "Variability Analysis of Self-Timed SRAM Robustness," in press.
5. A. Baz, D. Shang, F. Xia, R. Ramezani, R. Emery, and A. Yakovlev, "Self-Timed SRAM with Smart Latency Bundling," Technical Report, NCL-EECE-MSD-TR-2010-161, published by <http://async.org.uk>, available: <http://async.org.uk/tech-reports/NCL-EECE-MSD-TR-2010-161.pdf>.

## 1.7 References

1. Texas Instruments, *An Interview with Jack Kilby* [online]. Available: [www.ti.com/corp/docs/kilbyctr/interview.shtml](http://www.ti.com/corp/docs/kilbyctr/interview.shtml)
2. D. Kahng, "A Historical Perspective on the Development of MOS Transistors and Related Devices," *Electron Devices, IEEE Transactions on*, vol. 23, no. 7, pp. 655-657, 1976.
3. J. N. Helbert, *Handbook of VLSI Microlithography, 2nd Edition*: Elsevier Science, 2001.
4. G. E. Moore, "Cramming More Components onto Integrated Circuits," *Electronics*, vol. 38, no. 8, pp. 114-117, 1965.
5. C. Piguet, "History of Low-Power Electronics," in *Low-Power Electronics Design*, Switzerland: CRC Press, 2004.
6. C. Dong-Young and L. Seung-Hoon, "Design Techniques for a Low-Power Low-Cost CMOS A/D Converter," *Solid-State Circuits, IEEE Journal of*, vol. 33, pp. 1244-1248, 1998.
7. K. Uming, T. Balsara, and L. Wai, "Low-Power Design Techniques for High-Performance CMOS Adders," *Very Large Scale Integration (VLSI) Systems, IEEE Transactions on*, vol. 3, pp. 327-333, 1995.
8. W. Jinn-Shyan et al., "Design Techniques for Single-Low-V<sub>DD</sub> CMOS systems," *Solid-State Circuits, IEEE Journal of*, vol. 40, pp. 1157-1165, 2005.
9. L. Sigal et al., "Circuit Design Techniques for the High-Performance CMOS IBM S/390 Parallel Enterprise Server G4 Microprocessor," *IBM Journal of Research and Development*, vol. 41, pp. 489-503, 1997.
10. University of Southampton, *Next Generation Energy-Harvesting Electronics: A Holistic Approach* [online]. Available: <http://www.holistic.ecs.soton.ac.uk/>
11. M. Pedram and W. Qing, "Design Considerations for Battery-Powered Electronics," in *Design Automation Conference, 1999. Proceedings. 36th*, 1999, pp. 861-866.
12. I. Buchmann, *Batteries in a Portable World: A Handbook on Rechargeable Batteries for Non-Engineers*, 2nd ed.: Cadex Electronics, 2001.
13. R. Vijay et al., "Design Considerations for Solar Energy Harvesting Wireless Embedded Systems," in *Information Processing in Sensor Networks, 2005. IPSN 2005. Fourth International Symposium on*, 2005, pp. 457-462.
14. J. A. Paradiso and T. Starner, "Energy Scavenging for Mobile and Wireless Electronics," *Pervasive Computing, IEEE*, vol. 4, pp. 18-27, 2005.
15. J. Donovan, *Portable Electronics: World Class Designs: World Class Designs*: Elsevier Science, 2009.
16. H. Iwai, "CMOS Technology-Year 2010 and Beyond," *Solid-State Circuits, IEEE Journal of*, vol. 34, pp. 357-366, 1999.

17. J. M. Rabaey, *Low Power Design Essentials*: Springer London, Limited, 2009.
18. B. M. Al-Hashimi, *System-on-Chip: Next Generation Electronics*: The Institution of Engineering and Technology, 2006.
19. A. Pavlov, and M. Sachdev, *CMOS SRAM Circuit Design and Parametric Test in Nano-scaled Technologies: Process-Aware SRAM Design and Test*: Springer London, Limited, 2008.
20. The International Technology Roadmap for Semiconductors, *ITRS Home* [online]. Available: <http://www.itrs.net/>
21. M. Qazi, M. E. Sinangil, and A. P. Chandrakasan, "Challenges and Directions for Low-Voltage SRAM," *Design & Test of Computers, IEEE*, vol. 28, pp. 32-43, 2011.

## **Chapter 2. Background**

### **2.1 Introduction**

This chapter covers the background and literature of this research topic. Fundamentally, there are two main subjects behind this research, energy harvesting electronics and SRAM, accordingly, this chapter contains two main sections for each subject. Most of the materials in the following chapters depend upon the information provided here.

### **2.2 Energy Harvesting Systems: Next Generation of Microelectronics**

Energy harvesting is the process by which energy existing in the environment is converted into electrical energy via an equipment called energy harvester or scavenger, where the generated power is typically in the scale of  $\mu$  to m-Watts [1]. Energy harvesting systems are those electronic systems powered by energy harvesters only or harvesters augmented with batteries [1].

It is worth highlighting that the idea of powering portable electronic equipment from the surrounding energy has been around before the MOSFET transistor itself. For instance, Zenith Space Command TV and the first Citizen thermoelectric watch are two industrial examples from the literature showing that the battery-free electronic device is not a new research topic. The former is a battery-less remote control for the TV while the latter is a wristwatch employing a thermoelectric generator, they were developed in 1956 and 1975 respectively [2].

Based on the mentioned definitions, this section contains two subsections to cover the background of the harvester and its load respectively.

### 2.2.1 Micro Generators

According to the literature, powering microelectronics systems from the environment can employ three main types of ambient energy: kinetic, thermal and radiant. Kinetic energy exists in various forms like vibrations, motions, rotations, etc. Thermal energy mainly appears as a temperature gradient between different materials. Radiant energy includes light or solar energy and electromagnetic radiation or Radio Frequency (RF) signals [3, 4]. Table 2.1 shows the amount of power that can be harvested from different ambient energy sources. According to the table below, energy harvesters can provide power in the 0.1uW to 10mW range, which is typical for wireless sensor network [3].

**Table 2.1 Amount of power that can be harvested from different ambient energy sources.**

Source	Harvested Power
Ambient light-Indoor	10uW/cm <sup>2</sup>
Ambient light-Outdoor	10mW/cm <sup>2</sup>
Vibration-Human	4uW/cm <sup>2</sup>
Vibration-Industrial	100uW/cm <sup>2</sup>
Thermal-Human	30uW/cm <sup>2</sup>
Thermal-Industrial	10mW/cm <sup>2</sup>
RF-Cell phone	0.1uW/cm <sup>2</sup>

Each kind of energy requires a specific generator (e.g. vibration based power generator, thermoelectric generator and photovoltaic energy harvester are used to harvest kinetic, thermal and solar energy respectively) in order to extract the electric power from the ambient energy where the extraction process is done via what is called a transduction mechanism. Transduction mechanism can be defined as the circuit technique employed inside the harvester to convert the ambient energy to useful electric power. For vibration based harvesters, there are three main types of transduction techniques, namely, electromagnetic, electrostatic, and piezoelectric.

Electromagnetic transduction mechanism is based on the law of electromagnetic induction, which states that an electrical current will be induced in any closed circuit when the magnetic flux through a surface bounded by



the conductor changes [1]. For instance, if an inductor coil is attached to any vibration source and permanent magnets are used to produce magnetic field through the coil (as shown in the figure below [1]). Then the relative displacement caused by the vibrations will change the magnetic flux through the coil and hence generate electric current inside it.

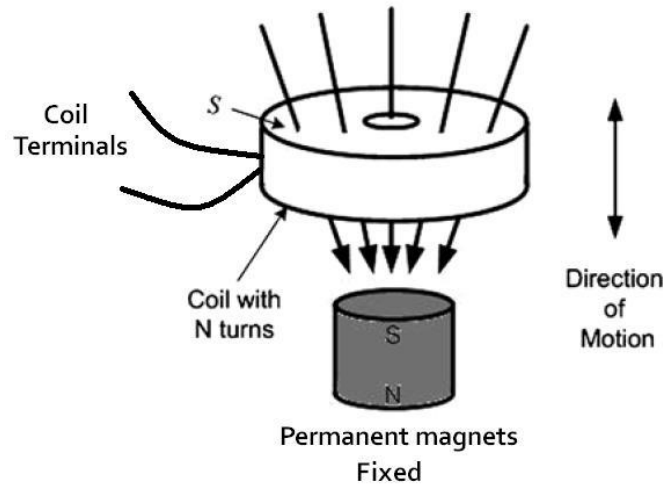


**Figure 2.1 Electromagnetic transduction technique.**

In this transduction mechanism, the voltage across the coil is proportional to the strength of the magnetic field, the velocity of vibration, and the number of turns of the coil [1, 3-5]. Piezoelectric harvesters employ the piezoelectric effect that exists in some materials like crystals and certain ceramics. Piezoelectric effect is the ability of generating an electrical potential in response to applied mechanical stress [3-5] as shown in the figure below [1].

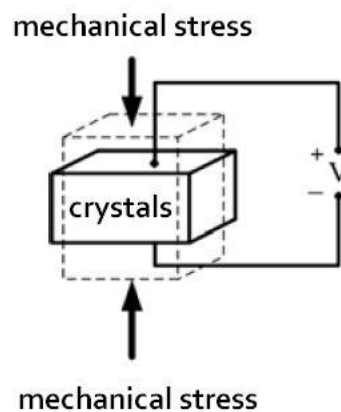


**Figure 2.2 Piezoelectric transduction technique.**

Electrostatic generators employ the vibration to relatively move one of the electrodes of a polarized capacitor with respect to the other as shown in the figure below. This motion develops potential difference across the capacitor, which causes electric current to flow in an external circuit [3].

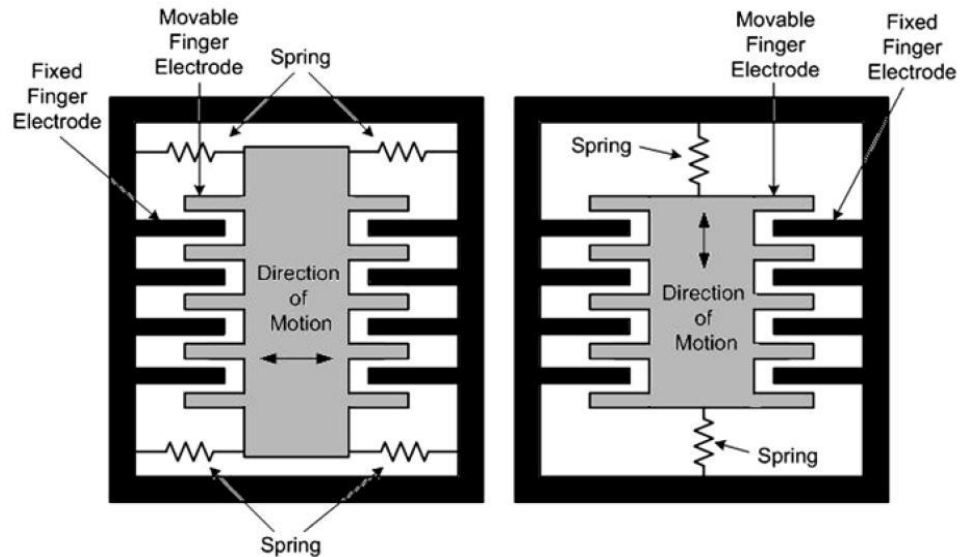


**Figure 2.3 Two different configurations for electrostatic transduction technique.**

**Table 2.2 Comparisons between transduction mechanisms of vibration energy harvesters**

Transduction technique	Advantages	Disadvantages
Piezoelectric	<ul style="list-style-type: none"> <li>-Simple structure</li> <li>-No external voltage source</li> <li>-Compatible with MEMS</li> <li>-High output voltage</li> <li>-No mechanical constraints needed</li> </ul>	<ul style="list-style-type: none"> <li>-Thin films have poor coupling</li> <li>-Poor mechanical properties</li> <li>-High output impedance</li> <li>-Charge leakage</li> <li>-Low output current</li> </ul>
Electromagnetic	<ul style="list-style-type: none"> <li>-No external voltage source</li> <li>-No mechanical constraints needed</li> <li>-High output current</li> </ul>	<ul style="list-style-type: none"> <li>-Difficult to integrate with MEMS fabrication process</li> <li>-Poor performance in micro-scale</li> <li>-Low output voltage</li> </ul>
Electrostatic	<ul style="list-style-type: none"> <li>-Easy to integrate with MEMS fabrication process</li> <li>-High output voltage</li> </ul>	<ul style="list-style-type: none"> <li>-Mechanical constraints needed</li> <li>-External voltage source or precharged electret needed</li> <li>-High output impedance</li> <li>-Low output current</li> </ul>

Thermal energy harvester are based on what is called Seebeck effect, which states that when a temperature difference is established between different conductors of special semiconductor materials, potential voltage develops between them and that causes electric current to flow in an external circuit [3]. The mentioned semiconductor materials are called thermocouples, which can be connected together in a large number to form the core element of the thermal energy harvester (thermopile) [5].

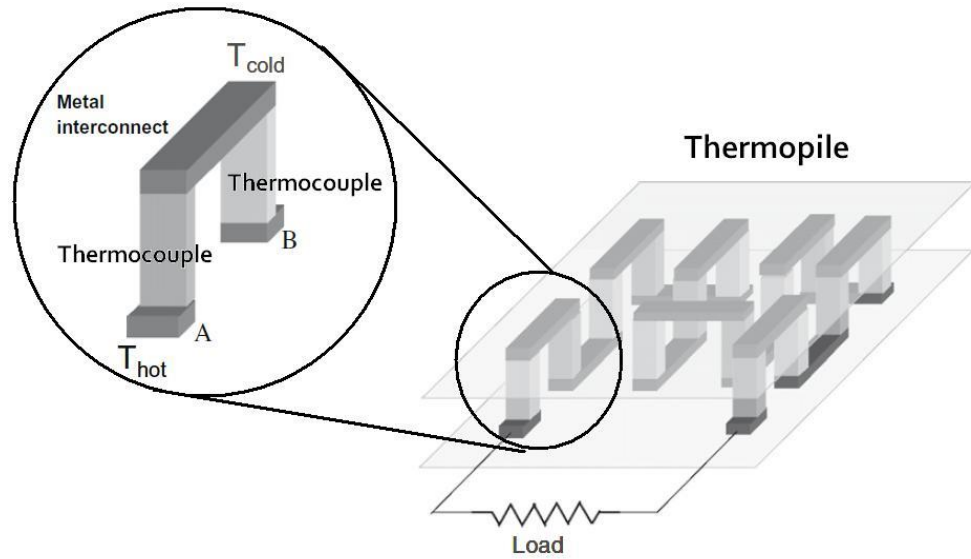


Figure 2.4 Schematic of thermocouple and of a thermopile.

Photovoltaic harvesters employ the photovoltaic effect that exists in some material and it allow these materials to develop potential voltage upon exposure to light by converting the energy in the received photons to an electric energy. According to the previous table, the power density of the outdoor photovoltaic cell reach up to  $10\text{mW}/\text{cm}^2$ , which is enough to power some applications include wireless sensor node.

A scavenger has the option to employ one or more transduction mechanisms according to its requirements. For instance, a vibration based harvester can employ any or all of piezoelectric, electromagnetic, and electrostatic transduction techniques [1, 3-5]. Table 2.2 compares between the main advantages and disadvantages of these transduction techniques [1].

It was proven analytically and experimentally that for each kind of harvester the generated power reaches its maximum at some operational conditions

and it drops otherwise [3]. Vibration based power generator is a resonant system, therefore, it produces maximum power when its resonant frequency matches the kinetic vibration frequency [3]. In the case of harvesting energy from temperature difference, the maximum power is generated when the thermal resistance of the thermocouples equates to that of the air gap [3, 6]. Photovoltaic maximum power depends upon light intensity and temperature [7]. Accordingly, adaptive techniques are required, in the micro-generator, in order to boost its efficiency and decrease the loss resulting from environmental and operational conditions [1, 3].

Extracting maximum power from a scavenger, that can be delivered to the load is another issue called Maximum Power Point Tracking (MPPT). This design technique requires considering the internal impedance of the harvester, which significantly varies based upon the type of the harvester, ranging from a few ohms for the thermal harvester to tens of kilohms for vibration ones [4].

In the case that two or more sources of energy are available in the environment surrounding the electronic system, a technique called Multi-Modal energy harvesting can be employed to improve the amount of supplied energy. A prototype is reported in [8] that combines electromagnetic and piezoelectric energy harvesters, where the power generated from the fabricated device was found to be 0.25W and 0.25mW using the electromagnetic and piezoelectric mechanism respectively.

The most important performance metrics of the harvester that the application needs to consider are the range of output voltages and power density, which is the amount of generated power per unit volume. These two properties are significantly dominated by the material used to implement the device, the transduction scheme, the type of the ambient energy, and the source of it (e.g. human or industrial [5]). Output voltage ranges from hundreds mV, in the case of photovoltaic cells, to a few volts, in the case of vibration harvester [4]. Power density is in the range of a few to a few hundreds of  $\mu\text{W}/\text{cm}^3$  and might reach up to tens of  $\text{mW}/\text{cm}^3$  in the case of outdoor solar harvesters.

### 2.2.2 Energy Harvesting Electronics

The portable electronics era put hard pressure on several performance metrics of the electronic systems, power consumption is at the top of them. Consequently, several energy and power minimization techniques were introduced to the area, which resulted in operating fully functional SoC with very low energy consumption. Examples include an 8-bit sub-threshold processor that is fully functional from as low as 200mV and consumes 3.5pJ/instruction at 350mV [9], and a 16-bit microcontroller that consumes 27.2pJ/cycle at its minimum energy voltage [10]. In the case of power restricted applications, the processor can adaptively operate down to 160mV and draws 11nW at 710Hz [9] while the microcontroller consumes around 12 $\mu$ W [10].

Comparing the range of power consumption of those carefully designed microelectronic systems with the range of power generated from optimized harvesters, as mentioned earlier, results in the fact that both are in the same order of magnitude. This has created a clear opportunity to develop a new generation of microelectronics systems that can be self-powered. Towards this goal, many projects were funded and hundreds of research papers were published around the world [11, 12]. All these studies were conducted because numerous challenges in this era have not yet been addressed.

For instance, energy harvesting systems rely upon random amounts of energy and nondeterministic voltage levels, which can be interrupted at any time. Therefore, they require new design strategies that are more adaptive, clever, and energy-aware. Such a design technique might provide the system with the highest performance whenever energy is available and at the same time provide a fallback strategy when the available energy drops to a certain level. This strategy must have the highest priority of saving the important data as well as completing the requested tasks within the supplied amount of energy even if the performance is sacrificed. This design technique should be energy aware in the sense that all the time it does not spend more than the harvested amount of energy. Moreover, the overall cir-

cuitry has to consider other challenges involved in the technology node such as high off-currents and process variations if exist.

Starting from this vision, the researcher begins his study towards proposing new design techniques for these systems powered by harvesters in order to enable the era of self-powered electronics.

## **2.3 SRAM**

Static Random Access Memory (SRAM) is a fundamental and vital subsystem for all computational systems. This type of memory is volatile as it does lose its contents when the power supply is lost and it is called static because the stored data do not require refreshing as in the case of DRAM. The term random access means that any memory word can be accessed arbitrary and not necessarily sequentially. SRAM is a subsystem because it is employed as a crucial part of computational systems to store instructions, operands, and results. In personal computers, SRAM is used as on-chip Level 1 (L1) and Level 2 (L2) caches to exchange data between main memory and CPU registers [13].

### **2.3.1 SRAM Structure and Operational States**

Figure 2.6 shows the block diagram of a basic SRAM system, its workhorse is the bit-cell, which is a component able to store only one bit of data, either 0 or 1. This cell is repeated tens of thousands of times and organized in rows and columns to form a sub array. Each bank is surrounded by several auxiliary circuits, which include decoder, prechargers, write drivers, read buffers, column multiplexers, and sense amplifiers, to complete the functionality of the memory. All cells in the same column share a common connection from sides called a pair of bit-lines and all cells in the same row share a common link called a word-line. A pair of bit-lines is used by the write drivers to write the data into the cells during writing operation as well as is used by the read buffers to read the data from the cells during reading process. Word-line is activated by the decoder to allow the bit-lines accessing the cross coupled inverters via the access transistors. Several bit-lines might share the same auxiliary circuits using a column multiplexer so as to im-

prove the area density of the SRAM. The size of the SRAM can be increased by including many banks in the same SRAM system.

All signals in the SRAM system are monitored and controlled by a vital component called timing control block, which synchronizes all signals in the memory in order to guarantee safe and successful operation during each operational state of the memory as will be described in the following.

### 2.3.1.1 Holding State

Ideal SRAM has to have the capability of holding its content under all operational conditions of the application, a property known as stability. The cell preserves its content, into the cross coupled inverters, so long as one of the inverters continuously outputs logic one voltage level that is above the trip point of the other inverter and that inverter continuously outputs logic zero voltage level that is below the trip point of the opposite inverter. Unfortunately, noise and Single Event Upset (SEU) can decrease/increase the voltage level of one of the inverters or increase/decrease the trip point of the opposite one to cause holding failure. Static Noise Margin (SNM) is an important metric used to measure how much the cell is immune to noise and it models all noises imposed on the cell by a pair of DC voltage sources as shown in Figure 2.5 [14].

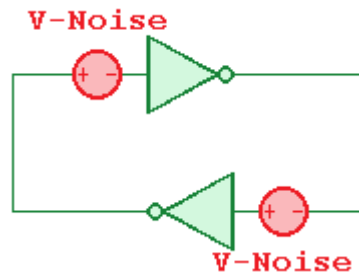


**Figure 2.5 Cross coupled inverters with two voltage sources to model static noise.**

If this circuit is simulated for different VDDs, the butterfly curve shown in Figure 2.7 is produced. SNM is defined as the side length of the largest square that can be embedded inside the smallest lobes of the butterfly curve [14]. Importantly, if the SNM is less than the thermal voltage, the thermal noise can flip the cell content and the cell is assumed unstable [15].

# SRAM Bit Cell

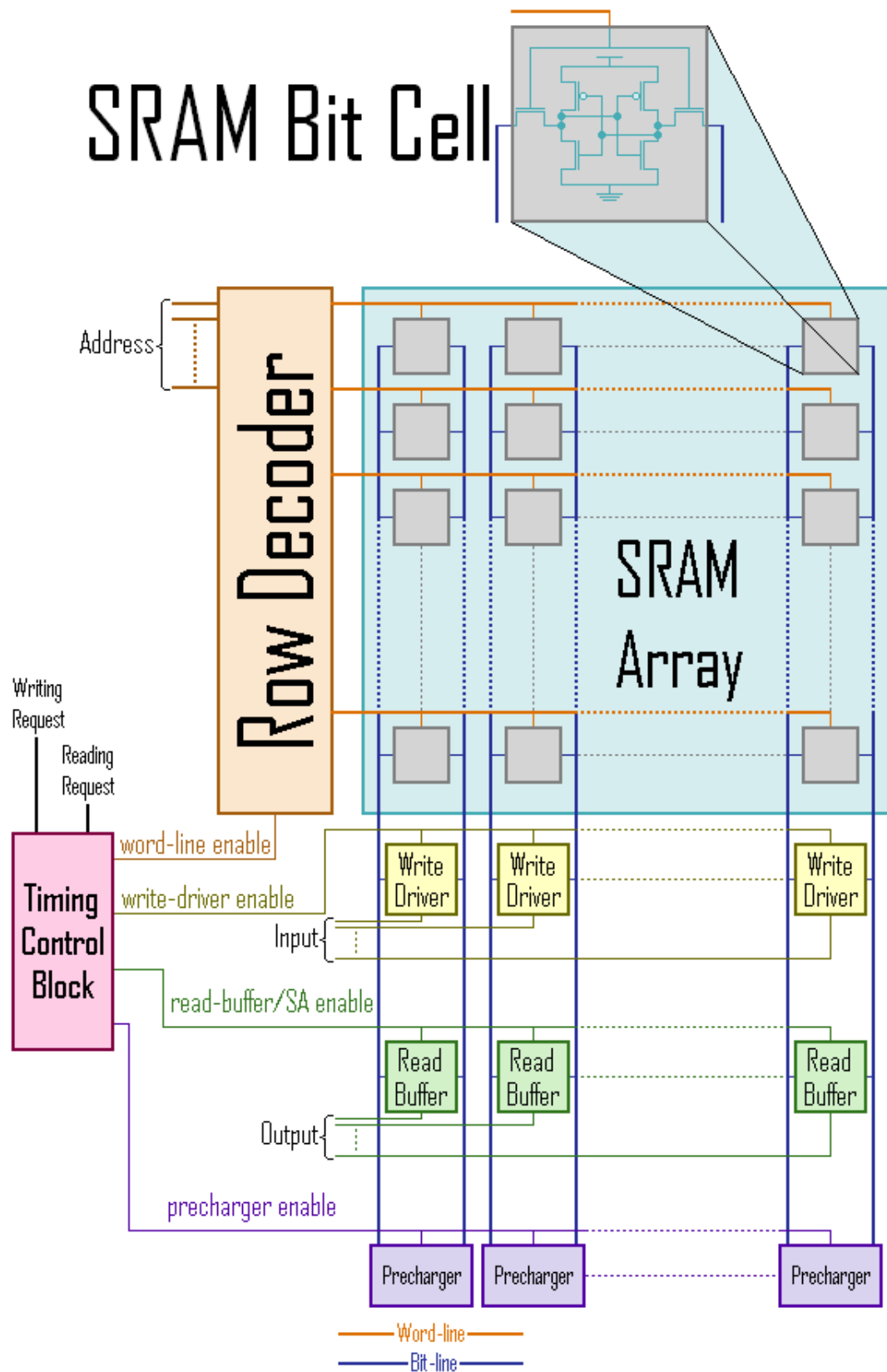


**Figure 2.6 Basic SRAM system block diagram.**

Supply voltage scaling significantly degrades the stability of the cell because it decreases the output high voltage level of one of the inverters, if this level becomes below the trip point of the other one the bit-cell loses its content.



Local process variations dramatically exacerbate this situation by decreasing the ON voltage level of the first inverter or increasing the trip point of the opposite one further [16-18]. Increasing the temperature weakens the pMOS device with respect to nMOS, which slightly declines the SNM in the super-threshold region while it almost has no effect in the sub-threshold regime [16].

### 2.3.1.2 Reading State

The second operational state of the SRAM is the reading, during which the word-line is driven high to connect the bit-lines to the cross coupled inverters. Since the bit-cell is quite small, with respect to the large bit-lines capacitance, and very weak to charge the whole bit-lines, the reading is achieved by precharging the bit-lines to high voltage prior to opening the access transistors, which results in discharging one of them, according to the stored data, after enabling the access transistors. Reading buffers/sense amplifiers are connected to the other end of the bit-lines and they are enabled at the right time to catch and hold the data.

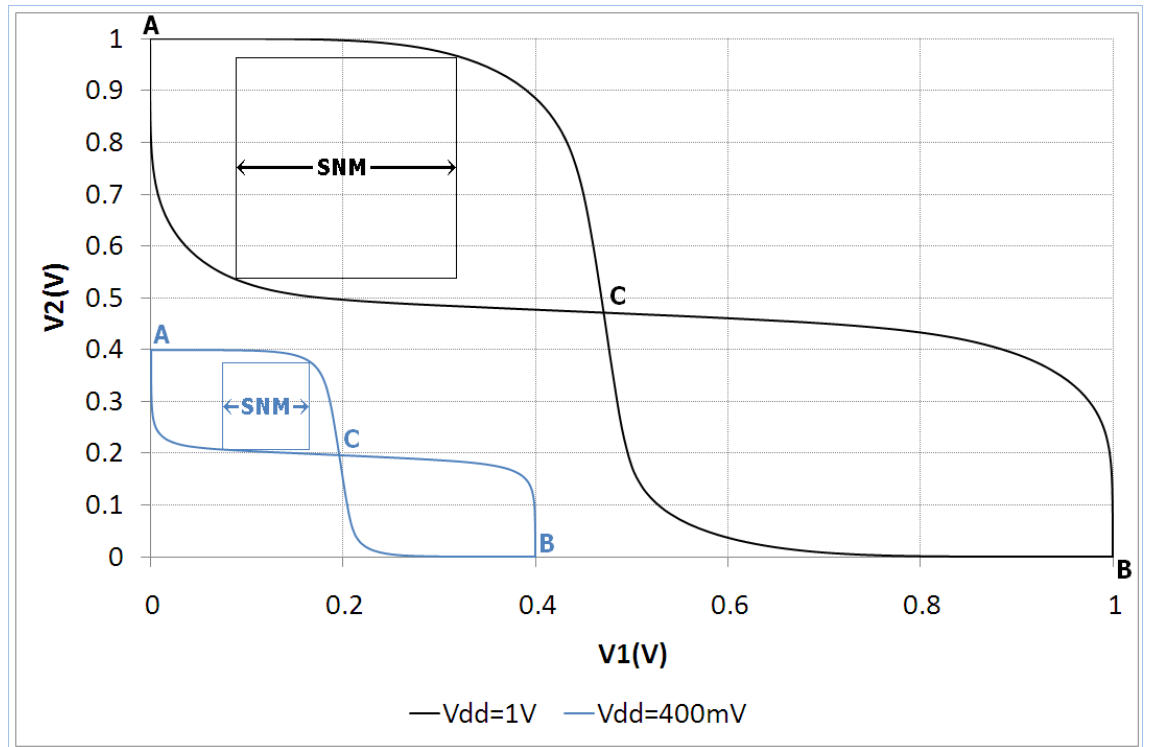


Figure 2.7 Butterfly curves of the 6T cell during holding state.

Reading process has to end up safely and correctly, a primary concern for current and future technologies. Correct reading implies that the data stored in the cells, being read, are mapped onto output latches while safe reading means that the operation does not corrupt any stored cells.

Safe reading is called reading stability and can be measured using reading SNM in the same way as holding SNM is measured but with clamping the word-line to the supply voltage. Comparing Figure 2.7 and Figure 2.8 shows that for the same level of VDD, reading SNM is worse than holding SNM and that because opening the access transistors shifts the VTC curve of each inverter by the amount of voltage drop across the corresponding access transistor. This property makes reading SNM more attractive by designers as it represents the worst case SNM.

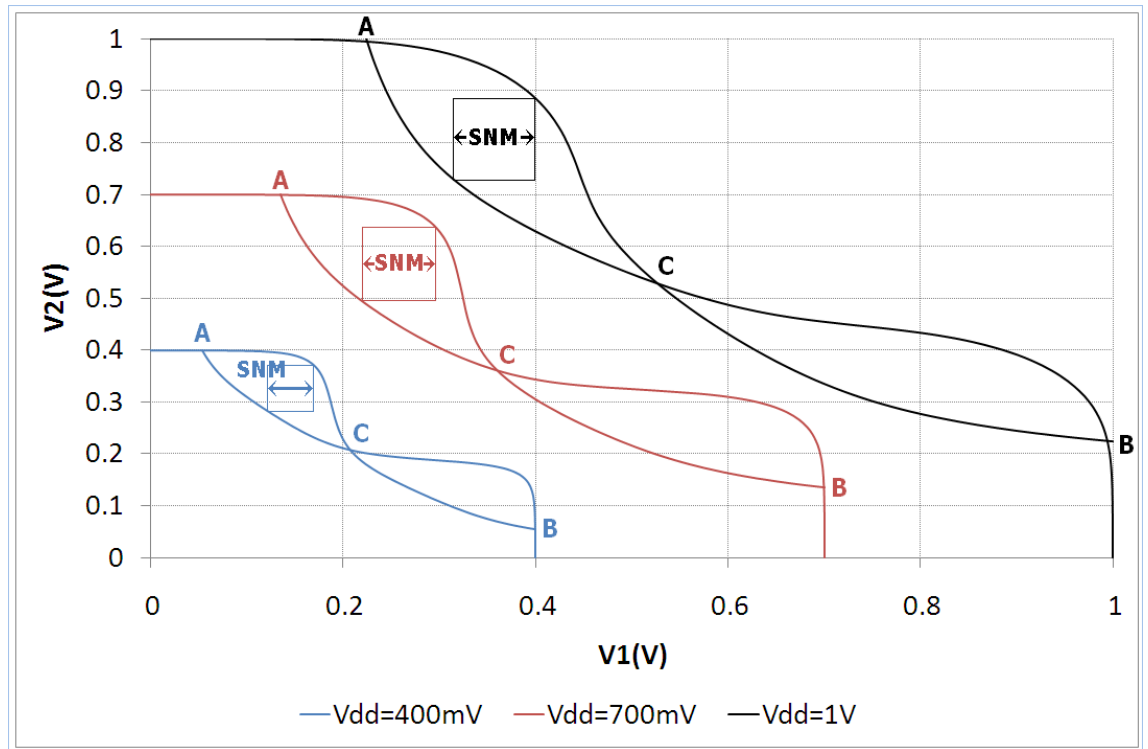


Figure 2.8 Butterfly curves of the 6T cell during reading.

The inability of the SNM to be measured with automatic inline testers was the motivation behind introducing the N-curve [18]. Figure 2.9 shows in the left the circuit setup usually employed to extract the N-curve along with the extracted N-curve in the right. The setup involves clamping both the bit-lines and word-line to the supply voltage, then, a voltage source  $V_1$  is ap-

plied to the node storing zero and swept from 0V to VDDV. Meanwhile the corresponding current I1 is measured and plotted versus the voltage V1. The figure shows that the current injected in the bit-cell node is zero at three values of voltages A, B and C which correspond to the three points in the butterfly curve shown above where A and B are the two stable points and C is the meta-stable point. Maximum DC noise, which can be applied at the cell before disturbing it, is the voltage difference between A and B.

In the same way as holding failure, reading failure happens if the voltage level of output low of one inverter is above the trip point of the opposite inverter. This situation is exacerbated by precharging the bit-lines and opening the access transistors and the problem is significantly affected by scaling the supply voltage owing to decreasing the trip point of opposite inverter [16, 17]. Local process variations play with the threshold voltage of each device individually and that results in changing the strength of each transistor with respect to others. Changing the transistor's relative strength affects the trip point of the inverter as well as its output voltage level, which considerably increases the probability of reading failure [15, 16, 20].

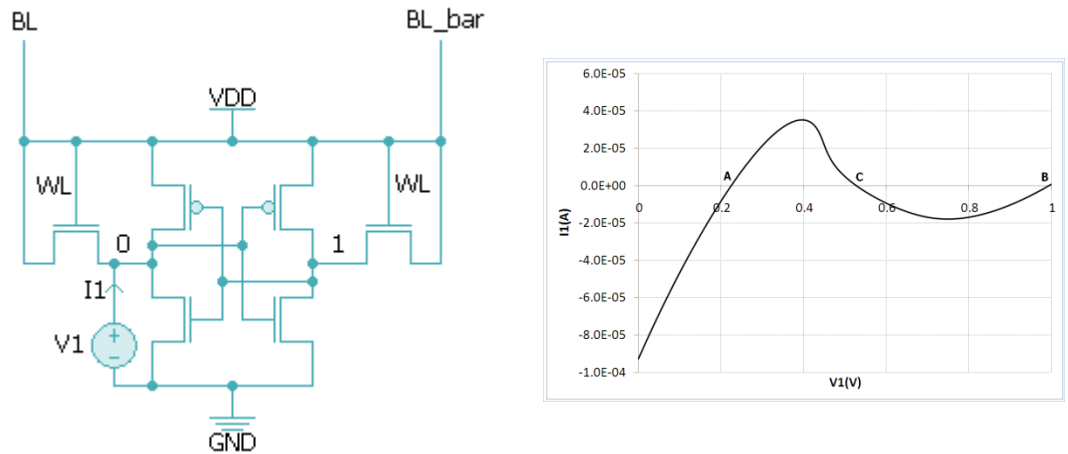


Figure 2.9 The schematic used to extract the N-curve and the resulted N-curve.

The other compulsory condition of the reading operation is the correct reading. According to the described mechanism of reading operation, wrong data is read if the output buffers/sense amplifiers were enabled before the bit-lines reflect the stored data and/or the access transistors enabling time is not enough for the bit-lines to convey the data. Based on that, this type of

failure manifests itself as a timing issue, hence, it is also known as access time failure [15, 17].

Again, supply voltage scaling and local process variations change the characteristic of individual device differently and that results in considerable variations in reading timing, which was calibrated during the design time, to end up with access time failure in the real silicon.

### **2.3.1.3 Writing State**

The last operational state of the SRAM is the writing operation, during which the system has to have the ability to successfully write new data to the bit-cells. The new data might be the same as or opposite of the stored ones, nevertheless, opposite data is always assumed as it involves more actions (e.g. flipping the cells) and hence it represents the worst case writing.

Based on that successful writing involves discharging the node holding high voltage, through its corresponding bit-line, below the opposite inverter trip point within the time when access transistors are enabled. Write driver is the component in charge of driving the bit-line to discharge that node, where the final voltage of the high voltage node is determined by the voltage divider between the corresponding pull-up transistor and access transistor. Moreover, since the access transistors are enabled for a limited time only, the final voltage is also affected by the discharging current, that is the difference in ON current between the pull-up and access transistor [17].

Successful writing as described above is a feature called write-ability, which can be measured by the writing SNM as shown in the right of Figure 2.10, where the circuit setup appears in the left. If the side of the largest square that can be embedded between the two curves is larger than zero, the cell is then writeable. Similar to the case of reading, the same N-curve can be used to measure the write-ability, which equals to the voltage difference between point C and B in Figure 2.9.

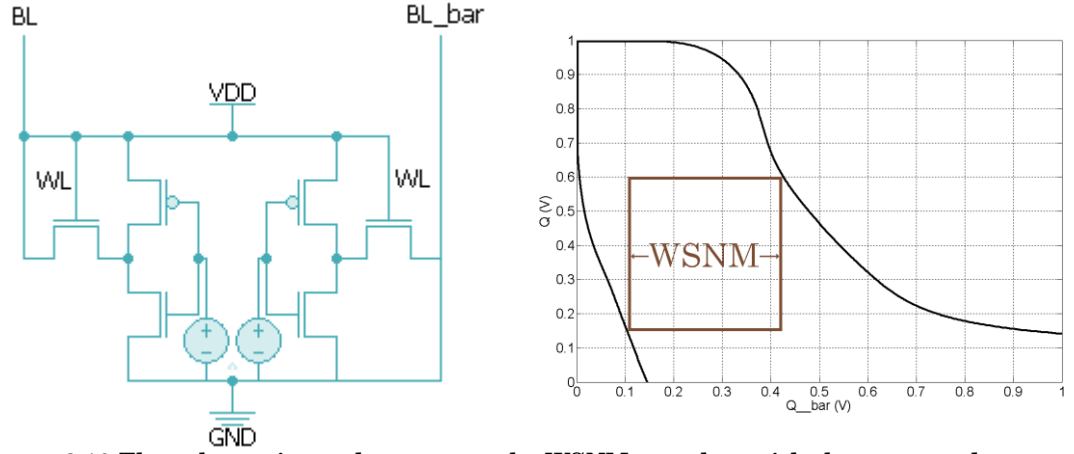


**Figure 2.10** The schematic used to extract the WSNM together with the extracted curves.

Increasing the temperature and/or decreasing the VDD decrease the ON-current of the transistors [21] and that significantly degrades the write-ability of the bit-cell [17, 18]. Local process variations have severe negative effects on write-ability owing to its ability to change the strength and ON current of each transistor in the cell individually [17, 18].

### 2.3.2 SRAM Design Challenges

SRAM design margin shrinks as the technology scales down and that increases the challenges associated with it, especially for current and future processes. Table 2.3 shows how the scaling of transistor size affects various parameters of the device [19].

**Table 2.3** Scaling parameters.

Parameter	Scaling factor
Gate length	1/s
Oxide thickness	1/s
Junction depth	1/s
Drain voltage	1/s
Drain current	1/s
Threshold voltage	1/s
Gate area	1/s <sup>2</sup>
Supply voltage	1/s
Number of transistors	s <sup>2</sup>

The elusive aim of all memory designers is to propose a single design that is optimized in terms of performance, density, power dissipation/energy consumptions, robustness, manufacturing yield, testability, scalability, and modularity. Unfortunately, such an SRAM has not yet been developed nor expected to appear in the future [22]. Accordingly, this section is dedicated to discuss the most common challenges in SRAM design, which are listed in

the following paragraphs followed by a section containing possible solutions if any exists.

The first challenge results from the fundamental conflict in the design requirements of the 6T bit-cell. According to the aforementioned discussion, write-ability requires decreasing the relative strength of the pull-up transistors to access transistors (pull-up ratio) and increasing the relative strength of the pull-up transistors to pull-down transistors. For the same cell, read-stability requires increasing the relative strength of the pull-down transistors to access transistors (cell ratio) [17, 18].

High density SoCs require a bit-cell designed upon minimum or near minimal feature size devices [23-25]. Nevertheless, the standard deviation of the device threshold voltage variations is inversely proportional to the square root of the effective device area (Pelgrom's law) [26, 27]. Accordingly, the smaller the cell area is the higher variations it experiences and the less robustness it has [24].

With more than 90% of the chip area occupied by the memory [28] and as much as 40% of the total power in 90nm generation wasted in leakage [29, 30], leakage power became one of the crucial SRAM design challenges in submicron process technologies, especially during the standby mode. Figure 2.11 depicts the current leakage from the 6T bit-cell, during holding state. Moreover, systematic and/or random parameter variations, especially those affecting threshold voltage, considerably play with the leakage energy from two aspects. On the one hand, as the variations decrease the threshold voltage of the device, it leaks more current. On the other hand, as the threshold voltage decreases, the device becomes faster and its operation time decreases which reflected back upon its energy.

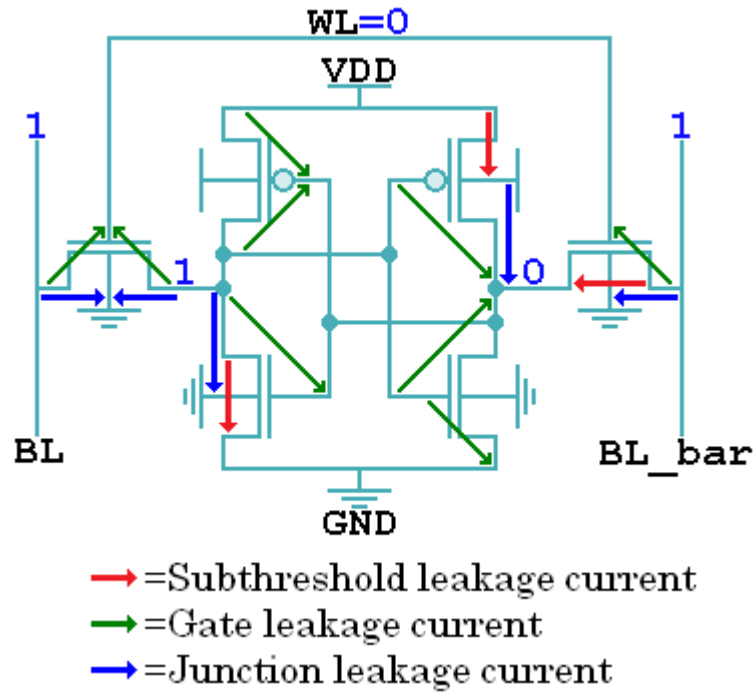


Figure 2.11 Leakage currents in the 6T cell.

In addition to wasting energy, leakage can corrupt data during SRAM operations. This occurs because bit-lines are the only way the peripheral circuits communicate with bit-cells, however, while the signals carried by the bit-lines have to be controlled by the accessed cells only, the leakage current from un-accessed cells strongly affect them. One of the scenarios representing this issue might be a pair of bit-lines, one of them is correctly pulled-down by the stored data of the accessed cell while the other one is erroneously pulled-down by the leakage from un-accessed cells. The problem deteriorates as the number of cells per bit-lines increases [31], temperature increases and/or process variations decrease the threshold voltage of the devices [32]. The worst case data scenario is shown in Figure 2.12 and it occurs when accessing one of the bit-cells that stores data complement to the data stored in all other cells in the same pair of bit-lines. This case involves fighting between the accessed cell and all un-accessed cells, while the former tries to keep the charge in the bit-lines the latter discharges it.

The performance of a SoC is dominated by that of its corresponding memory, as the latter is involved in all stages of computations. Accordingly, it is the aim of the designers to cut down the operation time, especially the reading operation as it consists of discharging the large capacitance of one of the bit-

lines. For this reason, it is common to attach a sense amplifier to each pair of bit-lines in order to divide the reading task between the bit-cell and the amplifier as follows. The bit-cell discharges a marginal amount of the bit-line voltage and the sense amplifier carries on the rest by detecting that and amplifying it to the full voltage swing. Nonetheless, it is worth highlighting that the sense amplifier is not an essential component for SRAM as the case of DRAM, since the former is capable of driving one of the bit-lines all the way down to the ground, while the latter cannot. However, sense amplifier is a troublesome component, especially in the context of SRAM, because of several reasons. Importantly, the sense amplifier is an analogue power hungry circuit that operates correctly only when it is enabled at the right time, which is set during design time. This time has to be large enough to accommodate all reliability concerns and small enough not to waste system performance. In addition, the energy consumed during the amplification must be considered [33].

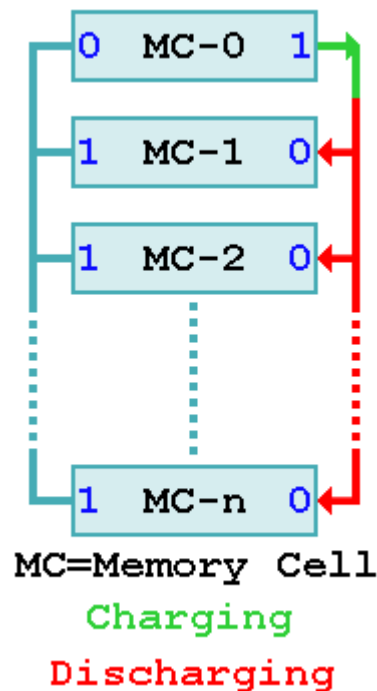


Figure 2.12 Worst case data scenario for bit-line leakage.

As stated earlier, process variations increase with the scaling process, hence, one of the designer's essential goals is exploring the effects of process variations upon the behaviour of the design before fabrication. Most EDA tools employ corner analysis and/or Monte-Carlo simulation for this pur-



pose. Corner analysis assumes the same worst (Slow), typical (Typical) and/or best (Fast) case timing scenario for all devices of the same type (nMOS or pMOS) in the same die, which allows measuring the boundary of some SRAM performance metrics (e.g. leakage current, speed of operations) but not all of them. For instance, as described earlier, writing failure happens if the node storing zero was not discharged below the trip point of the opposite inverter within the time when word-line is enabled. Based on that, the probability of writing failure increases if the threshold voltage of the: 1) pull-up transistor reduces, 2) access transistor increases, 3) pull-up transistor of the opposite inverter rises and/or 4) pull-down transistor of the opposite inverter declines [17]. Such a scenario cannot be caught by corner analysis, in addition to that, corner analysis cannot predict the failure probability of the die. On the other hand, Monte-Carlo allows the user to vary device parameters of each transistor in the design independently and it is the most accurate available method for computing the design yield [26]. However, the accuracy of Monte-Carlo estimation strongly depends on the number of simulations, which exponentially increases with the number of instances in the die and the functional yield of the cell. Mathematically,

$$F_{cell} = 1 - [1 - F_{die}]^{\frac{1}{N}}$$

Where:  $F_{cell}$  = *Failure probability of the bit – cell*

$F_{die}$  = *Failure probability of the die*

$N$  = *Number of instances the die has of the cell*

For instance, a chip yield of 99% and an SRAM array with only 1Kbit (1024 cells) requires a cell failure probability below 0.000009814733 and that is translated to a standard deviation of 5 ( $\sigma = 5$ ) and more than 100,000 simulation runs.

### 2.3.3 SRAM Design Approaches

The literature shows several approaches and design techniques proposed to improve the performance metrics of the SRAM and overcome its, previously mentioned, challenges. Upon careful inspection of these design methods,

this research opts to categorize them into four categories, as entitled by the next four subsections. This categorization benefits this research during the stage of improving the SRAM performance metrics.

### **2.3.3.1 Bit-Cell Based Techniques**

The well known design conflict between the read-stability and write-ability (was explained in section 2.3.2), which is essential in the 6T bit-cell, in addition to several other challenges were behind an approach of abandoning this bit-cell and directing all efforts towards developing new bit-cells. Towards that aim, several bit-cells were proposed by adding/deleting one/more transistors to/from the 6T bit-cell. Figure 2.13 lists the most important proposed realizations, which were introduced to solve one or more issues of the 6T bit-cell at the expense of some design metrics. Starting from the cells with the minimum number of transistors, the text below discusses the main features and limitations of each one.

The load-less 4T and the 5T cell were proposed for the purpose of increasing the density of the SRAM array [34-36] as the main objective. Their area is 34% and 23% smaller than the conventional 6T cell respectively and their overall stability and characteristics are acceptable in the old CMOS generation, 180nm. However, their essential design requirements are hard to satisfy in the submicron technologies due to increasing process variations and leakage current [15].

Enabling ultra-low energy applications was behind introducing the single ended 6T cell [37, 38], which is able to work robustly below the sub-threshold region. This robustness came at the cost of area overhead, i.e. 42% increase in the cell area plus short bit-lines, and several circuits to assist the operation, which is described in the next section.

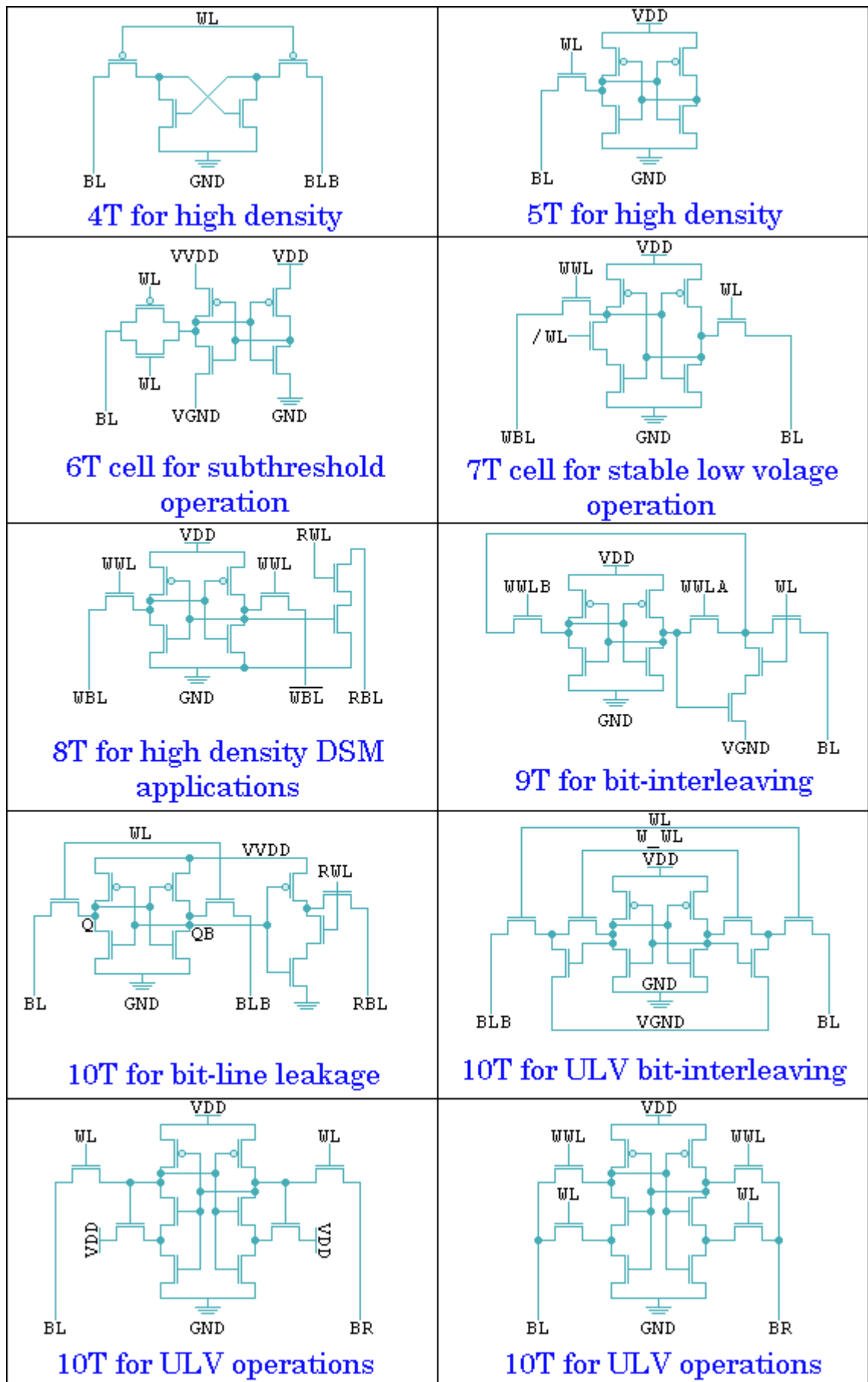


Figure 2.13 Published SRAM bit-cells.

The authors of [39] exploited the intuitive observation that SRAM operation time is determined by the slowest cell and that is usually the furthest cell from peripheral circuitry in the block due to the interconnect delay. Accordingly, it is proposed to slow down all other bit-cells which are faster than the slowest cell by replacing some/all of their normal  $V_{th}$  transistors with high  $V_{th}$  transistors in order to decrease the leakage. The replacing is accomplished via an algorithm to guarantee that the swapping process will not result in reliability degradation while optimizing the leakage reduction. The method was extended later in [40] to cover dual  $T_{ox}$  along with dual  $V_{th}$ , both of which showed a leakage reduction ranging from 30%-40% for small size SRAM bank. The drawbacks of this technique include changing the design flow to include hybrid cells and decreasing the manufacturing yield due to adding mask layer for the high  $T_{ox}$  and  $V_{th}$ .

The single ended asymmetrical 7T cell with triple word-lines allowed reducing the active power via decreasing the VDD while maintaining the reading stability. To enable an active operation fairly above the threshold voltage, the cell incurs 13% area overhead per cell and its layout forms an L-shape, which results in a useless gap, enough to accommodate two transistors, for each two abutted cells [41, 42].

The single ended 8T cell [23] aims to resolve the fundamental design conflict in the 6T cell via adding two more transistors dedicated for reading to prevent it from upsetting the stored data. This isolation gives the opportunity to optimize the cross-coupled inverter along with the access transistors for write-ability and hold-stability. This bit-cell has demonstrated its full functionality for a medium size memory system, 256kb, implemented using submicron technology, 65nm, down to the sub-threshold region [31]. However, the cell is 30% bigger than the conventional cell and its single ended sensing decreases the area efficiency from 70% to 50% [15, 23].

A triple word-lines and a bit-line single ended 9T cell was proposed in [43], which incurs 97% area overhead and requires several operational assist techniques to enable safe sub-threshold operation.

Published papers and their citations indicate that ten transistors are almost the maximum acceptable number of transistors per cell, accordingly several 10T bit-cells were proposed as described in the following paragraphs.

The motivation for the proposed 10T cell in [44] was to minimize the energy per operation via working in the sub-threshold regime and cut down the bit-line leakage, which saves more power and allows increasing bit-line size. The main constraints of this design are 66% area overhead, and the need of adding assisting technique in order to make the cell writeable.

Another differential dual word-line 10T cell was proposed in [45] to provide efficient bit-interleaving scheme for the purpose of mitigating soft errors and enhancing ultra-low voltage operations. Real silicon proved that this design is able to work down to 180mV for 32kb array implemented in 90nm technology, a remarkable feat. Nonetheless, the cell suffers from an area penalty of 61% comparable to the single ended 8T cell and the essential need of 30% boosted supply voltage for writing operation, which significantly deteriorates the area.

The last two cells described here abandoned the cross-coupled inverters and replaced them with cross-coupled Schmitt Trigger (ST) based inverters [46-48], they are called ST-1 and ST-2. These two designs were proposed in light of the fact that Schmitt trigger employs a built-in feedback mechanism to mitigate process variations and improve the noise margin of the cell. ST-1 and ST-2 incurs more than 100% area overhead. Nevertheless, they are skilful at enabling ultra-low voltage/power applications via operating the memory system in the deep sub-threshold regime while save safe operations [15].

Meaningful comparison between these cells cannot be concluded because each one was proposed for different application and was tested in different technology node. Finally, it is worth highlighting that in all of the previously proposed cells, improving the robustness of the cell allows decreasing the supply voltage during reading, writing, or holding state, which is reflected upon the active and leakage power dissipation of the whole memory system.

Accordingly, improving the robustness of SRAM cuts down its energy consumption.

### **2.3.3.2 Voltage Level Based Techniques**

The second category of approaches, for improving SRAM performance parameters, involves designing auxiliary circuits to play with the voltage level of one or more signals in the SRAM system. Designers have the choice of whether to combine this technique with the previous one, new bit-cell [31, 44, 49, 50], or serve it separately based on the 6T cell [51-57]. Importantly, this technique requires redesigning the timing control circuitry in order to adjust the timing of the manipulated signals. Nevertheless, the challenge here is to guarantee the correct operation of the added timing circuits across the complete operational range of the application [31, 44, 49-55, 57]. The following text in this section discusses the most important voltage level design techniques employed in the SRAM, each in a separate paragraph. The text starts by explaining the theory behind each design method, followed by some noticeable examples from the literature, and ended by the main limitations of that method.

As described earlier, successful writing must involve decreasing the voltage of the node storing one below the trip point of the opposite inverter during the time when word-line signal is high. Based on that, write-ability improves as that voltage node decreases or trip point increases during the specified time. The voltage divider between access transistor and pull-up transistors determines the minimum voltage at the node storing one, hence increasing the relative strength of the access transistor to pull-up transistors, i.e. pull-up ratio, enhances the write-ability. Based on that, the adaptive increasing of the differential voltage between word-line and VDD decreases write failure. At the same time, trip point of the opposite inverter increases as its ground voltage rises, accordingly raising the cell ground voltage enhances the write-ability as well. Recent works proposed several circuit realizations to implement the described assisting technique differently. In [44, 49] cell VDD is floated using a gated transistor while the word-line signal is kept at its nominal value to improve the pull-up ratio. In con-

trast, it was proposed in [49, 51-53] to decrease the cell VDD instead of just floating it as the write-ability of the relevant cell is a challenging problem. All these write-ability enhancement circuit techniques incur performance degradation and area overhead per bit-cell for switching and routing the other supply voltage respectively. In addition to that, they require an accurate timing circuit for swapping the VDDs as it is compulsory to raise the cell supplied voltage to an acceptable level before closing the access transistors in order to allow new data settle inside the cell. The area overhead of the assist technique in 10T cell is less than that in 6T, since the latter require two global power supplies supplied externally, however, the former suffer from the process variations of the gated transistor. In [57], the other cell voltage is globally generated via an on-chip regulator, which requires a reference voltage and has an amplifier.

Similarly, a sufficient level of stability during reading requires that the pre-charged bit-line does not raise the voltage of the node storing zero above the trip point of the opposite inverter during the time when the access transistors are enabled. Based on that, stability improves as that voltage node decreases or the trip point increases during the specified time. The bit-line precharged voltage divided between the access transistor and pull-down transistor determines the maximum voltage at the node storing zero. Hence, increasing the relative strength of the access transistor to the pull-down transistor, i.e. cell ratio, or decreasing the precharged voltage of the bit-lines enhances the reading stability. At the same time, the trip point of the opposite inverter increases as supplied voltage rises, accordingly, raising the cell supplied voltage enhances the stability of the cell. Again, several circuit realizations are implemented to adaptively control the cell ratio, differently. It was proposed in [51, 52] to connect the read cell to a higher voltage supplied externally while in [53] a dynamic analogue circuit was implemented for playing with the level of word-line signal. The authors of [58] found that for maximum read margin,  $V_{DD} - V_{th}$  is the optimum voltage value for pre-charging the bit-lines. As before, the main limitations of these designs include area and performance overhead.

Virtual ground is able to limit the off current of un-accessed cells, however, it involves a design conflict since the virtual ground should be able to block as much leakage current as possible from un-accessed rows while sink as much  $I_{read}$  current as possible from the accessed row. This concern can be addressed by controlling the virtual ground inverter with a charge pump as in [31, 49].

Dynamic Voltage Scaling (DVS) is an approach that adjusts the system VDD to conserve energy at the expense of performance [59]. It was shown in [54] that 35% energy efficiency can be acquired in 64 Mb SRAM implemented in 65nm by employing DVS between 0.7V and 1.2V. However, the overall design, which contains sophisticated programmable circuits for timing, references, and WL modulation [18], is dedicated for dual-supply voltage applications [54]. The previous working range has been extended to between 0.3V and 1.2V for the same technology and 64kb SRAM, which was entitled by the authors of [49] Ultra DVS SRAM, to increase the energy efficiency. For that design, decreasing the voltage from 0.8V to 0.4V is able to save more than half of the total energy consumption. Nevertheless, the design required several reconfigurable assist circuits for widening the statistical operating margin as described above. Generally, DVS requires stalling the system between switching modes to allow transient voltage to settle on an acceptable level unless the system is able to adapt itself for variable voltage operation. The other issue in DVS is that low voltage operation time should be, at least, enough to compensate energy loss during charging/discharging the large capacitances required for operation mode swapping [49]. Other noticeable contributions in the area of multi-mode SRAM operations appear in [50, 55, 56], which employ assist circuits in order to improve the operation robustness at low voltage.

As explained earlier, the strong dependences of the SRAM parametric failures upon the threshold voltage variations from one side and the threshold voltage upon the body-bias from the other side, made a clear opportunity to employ the body-bias calibration for increasing the SRAM parametric yield [60-62]. The technique involves a method to determine the corner of the chip



using a sensor, then based on that corner, either a Reverse-Body-Bias (RBB) or Forward-Body-Bias (FBB) is applied in order to decrease the parametric failure. The sensor detects the chip corner from its leakage current, which means that it has to be insensitive to temperature and process variations. Nevertheless, this technique suffers from area overhead for routing the body-bias terminal in addition to the testing overhead for the calibration.

Decreasing the rail-to-rail voltage of the array during the standby mode is one of the effective energy saving techniques since it decreases the leakage linearly. In order to preserve the memory content, the rail-to-rail voltage has to be larger than the Data Retention Voltage (DRV) of the memory, which is significantly affected by the global and local process variations along with the system temperature. It was proven in [63] that for leakage reduction in SRAM, raising GND is more effective than lowering VDD. According to the literature, this technique was implemented differently in an open loop manner [56, 63-69] in different process technologies. The implementation involves placing intuitive circuits (e.g. nMOS or pMOS diodes) or smart circuits (e.g. programmable diodes or voltage regulators) between the array and the rail voltage in order to decrease one/both of rail voltages to such a level where preserving the data is guaranteed under all operational conditions of the system. This rail-to-rail voltage value is set during the design time and it includes excessive margins to accommodate the process variations and other reliability concerns, accordingly, it is not the optimum rail-to-rail value and further reduction and saving is possible. While this method shows significant savings in leakage power, it suffers from moderate to marginal area and performance overhead. Closed loop techniques outperform open loop ones in terms of leakage reduction but require more adaptive and clever circuit designs. Its implementation might involve adding replica bit-cells [70-72] (e.g. canary cell or DRV sensor), which are required to match the array cells. The closed loop algorithm recursively decreases the voltage of the replica cells, tests its content, and reflects that voltage to the main array as far as the replica contents are safe. The algorithm also provides a method of adding an adaptive safe margin to accommodate any reliability concerns. It was shown in [72] that a sophisticated off-chip algorithm

can be employed in order to determine the actual DRV of the real array without corrupting its content.

Gating power from SRAM is the most effective way of leakage reduction in the ideal case, however, it erases all memory contents [73, 74]. Hence, a smart technique is needed in order to determine if a specific portion of data is no longer useable [74]. The literature does not show comprehensive studies of power gating for SRAM including: its susceptibility to PVT and ageing variations, its area and performance overhead, and its ability to preserve the data as far as that is required.

### **2.3.3.3 Timing Circuit Based Techniques**

Memory designers know that most of SRAM performance metrics manifest themselves as timing issues. While that is clear for operation performance and energy, it needs more clarifications for other metrics like failures and yield, which can be explained as follows.

SRAM, normally, operates based on timing assumptions where the timing control block is in charge of organizing the timing relationship between all blocks in the memory system in order to guarantee safe and successful operations. The workhorse of the timing control block is the basic gates, e.g. inverter, where the functions and latencies depend upon the switching of both the nMOS and pMOS devices [75]. In contrast, the operation of the bit-cell mainly depends on either the nMOS device during reading or the pMOS device during writing as described above, which results in timing mismatch between the bit-cell and the circuitry controlling its time. This mismatch is compounded by other SRAM challenges, which do not exist in basic gates, e.g. the bit-line leakage. Importantly, the overall situation is deteriorated under PVTA variations. The mentioned timing discrepancy between the actual timing and that generated from the control circuit is reflected back upon the correct operation of the SRAM as follows. Opening the access transistors of a cell during either reading or half-selecting upsets its contents, where the failure probability depends upon the time during which the word-line signal is high [17]. Writing failure happens if the word-line enabling time is not sufficient to discharge the voltage of the node storing one below

the trip point of the opposite inverter. Similarly, if the access transistors signal is withdrawn before adequate charging/discharging voltage is built-up on the bit-lines, the reading operation ends up with an access time failure. Moreover, all assist circuit techniques require timing circuits for controlling the timing of manipulated signals. The aforementioned facts directed some of the research towards analysing SRAM timing mismatch and proposing new circuits to address its design challenges from the timing point of view.

It was found in [75] that even for old technologies, i.e. 250nm, and under stable VDD the mismatch between bit-line delay and inverter delay might vary by a factor of two over all process corners and high and low temperatures. Accordingly, the authors proposed a new timing circuitry, which employs a replica bit-line with dummy bit-cells to generate the sense amplifier and word-line enable signals. Despite the ability of this timing control block to outperform its inverter chain based counterpart in terms of delay matching, it still requires several delay matching elements to match the delay of other components (e.g. decoder), which is likely to suffer from timing mismatch owing to increasing the random process variations in the scaled technology.

As the design in [75] does not cope with a wide range of VDD, nor does it address the timing discrepancy results from data-dependent bit-line leakage, the authors of [32] had an aim to fill up this gap. The proposed design is based on a replica column with two types of dummy cells, which requires a reference voltage and that is assumed to be adjustable for all operational conditions.

Both of the designs in [32] and [75] addressed the timing issue of the SRAM during reading operation only, leaving the writing timing hazard problems open.

Dual-rail completion detection for reading operation was built in [33] and [76] for the 6T and 10T bit-cell respectively, in order to match the exact time of the operation under wide range of operational conditions. However, their

writing operation still relies on timing assumptions of delay matching elements, which does not guarantee safe and successful operation under all operational conditions.

#### **2.3.3.4 Peripheral Circuit Based Techniques**

As described in section 2.3.1, the responsibility of the correct operation is shared between the bit-cells, timing circuits, and peripheral circuits. Peripheral circuits contain decoders, multiplexers, write drivers, prechargers, read buffers/sense amplifiers. The literature showed many previous works attempting to improve the characteristics of one or more of these components in order to improve some of the SRAM performance metrics, below are some examples of that.

Rather than decoding address bits in a single stage, a two stage decoding scheme was proposed in [77], coined Divided Word Line (DWL), for the purpose of improving the power and performance efficiency of SRAM, especially those beyond 64Kb SRAM at the cost of a little area penalty. SRAM larger than 4Mb was analyzed in [78] and it was found that it requires an additional level of decoding in order to optimize its delay time and power consumption to end up with what is called Hierarchical Word Decoding (HWD). Generic models for the SRAM access time were proposed in [79], which analytically combine the array hierarchical architecture with the wire length and fan-outs along the decoding and sensing critical paths. The models enable optimizing the array architecture for total access time. Several sense amplifier designs were proposed in [80-88] in order to improve SRAM performance metrics.

### **2.4 Summary**

Powering microelectronic systems via batteries liberate them from the main supply, however, maintaining and replacing batteries is a challenging task, and in numerous cases, they are impossible, inconvenient, costly, and/or hazardous. In addition, power consumption of SoCs doubles every couple of years, following Moore's Law, while power density of batteries doubles every ten years, which creates a considerable gap between SoCs and batteries. At the same time, the advances in the field of micro-generators made a clear

opportunity to employ them for powering SoCs. While the battery could be regarded as having unlimited power at any time, but limited energy in the long run, energy harvesters are the opposite scenario, which has an unlimited supply of energy in the long run, but limited power at any time. Although, the general idea is not new, the context is totally novel and it involves countless challenges.

Importantly, it is worth starting investigations from SRAM rather than any other component in SoC because it occupies the majority of chip area, its design challenges are more complicated than any other component, and it is vital for all computation logics. SRAM challenging story begin with a fundamental design conflict between optimizing the cell for reading or writing. It inherited a high-replication property, which puts pressures on minimizing its size and accordingly made it more susceptible to reliability concerns. Other main challenges include, but are not restricted to, bit-line leakages, standby leakage versus stability and EDA tool limitations. This thesis categorized all circuit design techniques proposed in literature, to improve one or more SRAM performance metrics, into four categories as follows. Bit-cell is the workhorse and it requires special attention during the design process. Peripheral circuits determine the architecture of the SRAM systems and they are controlling the bit-cells during both the operation and standby states, hence it is worth optimizing them in order to improve the SRAM performance metrics. If the application requires more than what the combination of bit-cells and peripheral circuits can provide, auxiliary circuits can be added for further improvement. Finally, timing is an effective knob for optimizing SRAM performance metrics, despite that fairly little research used that knob due to the high risks involved.

## 2.5 References

1. T. J. Kaźmierski and S. Beeby, *Energy Harvesting Systems: Principles, Modeling and Applications*: Springer London, Limited, 2011.
2. G. Nicolescu, I. O'Connor, and C. Piguet, *Design Technology for Heterogeneous Embedded Systems*: Springer London, Limited, 2012.
3. R. J. M. Vullers *et al.*, "Micropower Energy Harvesting," *Solid-State Electronics*, vol. 53, pp. 684-693, 2009.
4. S. Bandyopadhyay and A. P. Chandrakasan, "Platform Architecture for Solar, Thermal, and Vibration Energy Combining With MPPT and Single Inductor," *Solid-State Circuits, IEEE Journal of*, vol. 47, pp. 2199-2215, 2012.

5. M. Raju and M. Grazier, <http://www.ti.com/lit/wp/slyy018a/slyy018a.pdf>, Texas Instruments white paper.
6. Z. Wang et al., "Micromachined Polycrystalline SiGe-Based Thermopiles for Micropower Generation on Human Body," in *Design, Test, Integration and Packaging of MEMS/MOEMS (DTIP), 2007 Symposium on*, 2007.
7. L. Cortez et al., "Progress on the Problems of the Study in the Performance of a Solar Module under Conditions of Random Changes of Radiation," *International Journal of Energy*, vol. 3, pp. 17-24, 2009.
8. Y. Tadesse, Z. Shujun, and S. Priya, "Multimodal Energy Harvesting System: Piezoelectric and Electromagnetic," *Journal of Intelligent Material Systems and Structures*, vol. 20, pp. 625-632, March 1, 2009.
9. S. Hanson et al., "Exploring Variability and Performance in a Sub-200-mV Processor," *Solid-State Circuits, IEEE Journal of*, vol. 43, pp. 881-891, 2008.
10. J. Kwong et al., "A 65nm Sub- $V_t$  Microcontroller with Integrated SRAM and Switched-Capacitor DC-DC Converter," in *Solid-State Circuits Conference, 2008. ISSCC 2008. Digest of Technical Papers. IEEE International*, 2008, pp. 318-616.
11. Columbia University, *Energy-Harvesting Active Networked Tags (EnHANTs)* [online]. Available: <http://enhants.ee.columbia.edu/>
12. University of Southampton, *Next Generation Energy-Harvesting Electronics: A Holistic Approach* [online]. Available: <http://www.holistic.ecs.soton.ac.uk/>
13. A. Pavlov, and M. Sachdev, *CMOS SRAM Circuit Design and Parametric Test in Nano-scaled Technologies: Process-Aware SRAM Design and Test*: Springer London, Limited, 2008.
14. E. Seevinck, F. J. List, and J. Lohstroh, "Static-noise margin analysis of MOS SRAM cells," *Solid-State Circuits, IEEE Journal of*, vol. 22, pp. 748-754, 1987.
15. J. P. Kulkarni and K. Roy, "Ultralow-Voltage Process-Variation-Tolerant Schmitt-Trigger-Based SRAM Design," *Very Large Scale Integration (VLSI) Systems, IEEE Transactions on*, vol. 20, pp. 319-332, 2012.
16. B. H. Calhoun and A. P. Chandrakasan, "Static Noise Margin Variation for Sub-Threshold SRAM in 65-nm CMOS," *Solid-State Circuits, IEEE Journal of*, vol. 41, pp. 1673-1679, 2006.
17. S. Mukhopadhyay, H. Mahmoodi, and K. Roy, "Modeling of Failure Probability and Statistical Design of SRAM Array for Yield Enhancement in Nanoscaled CMOS," *Computer-Aided Design of Integrated Circuits and Systems, IEEE Transactions on*, vol. 24, pp. 1859-1880, 2005.
18. M. Qazi, M. E. Sinangil, and A. P. Chandrakasan, "Challenges and Directions for Low-Voltage SRAM," *Design & Test of Computers, IEEE*, vol. 28, pp. 32-43, 2011.
19. H. Iwai, "CMOS Technology-Year 2010 and Beyond," *Solid-State Circuits, IEEE Journal of*, vol. 34, pp. 357-366, 1999.
20. E. Grossar et al., "Read Stability and Write-Ability Analysis of SRAM Cells for Nanometer Technologies," *Solid-State Circuits, IEEE Journal of*, vol. 41, pp. 2577-2588, 2006.
21. N. H. E. Weste and D. M. Harris, *CMOS VLSI Design: A Circuits and Systems Perspective*: Addison Wesley, 2011.
22. V. G. Oklobdzija, *Digital Design and Fabrication*: CRC Press, 2007.
23. L. Chang et al., "Stable SRAM Cell Design for the 32 nm Node and Beyond," in *VLSI Technology, 2005. Digest of Technical Papers. 2005 Symposium on*, 2005, pp. 128-129.
24. J. Singh, S. P. Mohanty, and D. K. Pradhan, *Robust Sram Designs and Analysis*: Springer, 2012.
25. F. Boeuf et al., "0.248 $\mu\text{m}^2$  and 0.334 $\mu\text{m}^2$  Conventional Bulk 6T-SRAM Bit-Cells for 45nm Node Low Cost - General Purpose Applications," in *VLSI Technology, 2005. Digest of Technical Papers. 2005 Symposium on*, 2005, pp. 130-131.
26. A. Singhee and R. A. Rutenbar, *Extreme Statistics in Nanoscale Memory Design*: Springer, 2010.
27. M. J. M. Pelgrom, A. C. J. Duinmaijer, and A. P. G. Welbers, "Matching Properties of MOS Transistors," *Solid-State Circuits, IEEE Journal of*, vol. 24, pp. 1433-1439, 1989.
28. The International Technology Roadmap for Semiconductors, *ITRS Home* [online]. Available: <http://www.itrs.net/>
29. S. G. Narendra and A. P. Chandrakasan, *Leakage in Nanometer CMOS Technologies*: Springer, 2006.
30. A. Grove, [http://www.intel.com/pressroom/archive/speeches/grove\\_20021210.pdf](http://www.intel.com/pressroom/archive/speeches/grove_20021210.pdf), *IEDM2002 Key-note Luncheon Speech*.
31. N. Verma and A. P. Chandrakasan, "A 256 kb 65 nm 8T Subthreshold SRAM Employing Sense-Amplifier Redundancy," *Solid-State Circuits, IEEE Journal of*, vol. 43, pp. 141-149, 2008.
32. C. Meng-Fan, Y. Sue-Meng, and C. Kung-Ting, "Wide  $V_{DD}$  Embedded Asynchronous SRAM with Dual-Mode Self-Timed Technique for Dynamic Voltage Systems," *Circuits and Systems I: Regular Papers, IEEE Transactions on*, vol. 56, pp. 1657-1667, 2009.

33. J. Dama and A. Lines, "GHz Asynchronous SRAM in 65nm," in *Asynchronous Circuits and Systems, 2009. ASYNC '09. 15th IEEE Symposium on*, 2009, pp. 85-94.
34. K. Noda et al., "An Ultrahigh-Density High-Speed Loadless Four-Transistor SRAM Macro with Twisted Bitline Architecture and Triple-Well Shield," *Solid-State Circuits, IEEE Journal of*, vol. 36, pp. 510-515, 2001.
35. K. Noda et al., "A Loadless CMOS Four-Transistor SRAM Cell in a 0.18- $\mu$ m Logic Technology," *Electron Devices, IEEE Transactions on*, vol. 48, pp. 2851-2855, 2001.
36. I. Carlson et al., "A High Density, Low Leakage, 5T SRAM for Embedded Caches," in *Solid-State Circuits Conference, 2004. ESSCIRC 2004. Proceeding of the 30th European*, 2004, pp. 215-218.
37. Z. Bo et al., "A Sub-200mV 6T SRAM in 0.13 $\mu$ m CMOS," in *Solid-State Circuits Conference, 2007. ISSCC 2007. Digest of Technical Papers. IEEE International*, 2007, pp. 332-606.
38. Z. Bo et al., "A Variation-Tolerant Sub-200 mV 6-T Subthreshold SRAM," *Solid-State Circuits, IEEE Journal of*, vol. 43, pp. 2338-2348, 2008.
39. B. Amelifard, F. Fallah, and M. Pedram, "Low-Leakage SRAM Design with Dual  $V_t$  Transistors," in *Quality Electronic Design, 2006. ISQED '06. 7th International Symposium on*, 2006, pp. 6 pp.-734.
40. B. Amelifard, F. Fallah, and M. Pedram, "Leakage Minimization of SRAM Cells in a Dual- $V_t$  and Dual  $T_{ox}$  Technology," *Very Large Scale Integration (VLSI) Systems, IEEE Transactions on*, vol. 16, pp. 851-860, 2008.
41. K. Takeda et al., "A Read-Static-Noise-Margin-Free SRAM Cell for Low-VDD and High-Speed Applications," *Solid-State Circuits, IEEE Journal of*, vol. 41, pp. 113-121, 2006.
42. K. Takeda et al., "A Read-Static-Noise-Margin-Free SRAM Cell for Low- $V_{dd}$  and High-Speed Applications," in *Solid-State Circuits Conference, 2005. Digest of Technical Papers. ISSCC. 2005 IEEE International*, 2005, pp. 478-611 Vol. 1.
43. T. Ming-Hsien et al., "A Single-Ended Disturb-Free 9T Subthreshold SRAM with Cross-Point Data-Aware Write Word-Line Structure, Negative Bit-Line, and Adaptive Read Operation Timing Tracing," *Solid-State Circuits, IEEE Journal of*, vol. 47, pp. 1469-1482, 2012.
44. B. H. Calhoun and A. Chandrakasan, "A 256kb Sub-Threshold SRAM in 65nm CMOS," in *Solid-State Circuits Conference, 2006. ISSCC 2006. Digest of Technical Papers. IEEE International*, 2006, pp. 2592-2601.
45. C. Ik Joon et al., "A 32 kb 10T Sub-Threshold SRAM Array with Bit-Interleaving and Differential Read Scheme in 90 nm CMOS," *Solid-State Circuits, IEEE Journal of*, vol. 44, pp. 650-658, 2009.
46. J. P. Kulkarni, K. Kim, and K. Roy, "A 160 mV Robust Schmitt Trigger Based Subthreshold SRAM," *Solid-State Circuits, IEEE Journal of*, vol. 42, pp. 2303-2313, 2007.
47. J. P. Kulkarni, K. Keejong, and K. Roy, "A 160 mV, Fully Differential, Robust Schmitt Trigger Based Sub-Threshold SRAM," in *Low Power Electronics and Design (ISLPED), 2007 ACM/IEEE International Symposium on*, 2007, pp. 171-176.
48. J. P. Kulkarni et al., "Process Variation Tolerant SRAM Array for Ultra Low Voltage Applications," in *Design Automation Conference, 2008. DAC 2008. 45th ACM/IEEE*, 2008, pp. 108-113.
49. M. E. Sinangil, N. Verma, and A. P. Chandrakasan, "A Reconfigurable 8T Ultra-Dynamic Voltage Scalable (U-DVS) SRAM in 65 nm CMOS," *Solid-State Circuits, IEEE Journal of*, vol. 44, pp. 3163-3173, 2009.
50. M. Yabuuchi et al., "A 45nm 0.6V Cross-Point 8T SRAM with Negative Biased Read/Write Assist," in *VLSI Circuits, 2009 Symposium on*, 2009, pp. 158-159.
51. K. Zhang et al., "A 3-GHz 70MB SRAM in 65nm CMOS Technology with Integrated Column-Based Dynamic Power Supply," in *Solid-State Circuits Conference, 2005. Digest of Technical Papers. ISSCC. 2005 IEEE International*, 2005, pp. 474-611 Vol. 1.
52. Z. Kevin et al., "A 3-GHz 70-mb SRAM in 65-nm CMOS Technology with Integrated Column-Based Dynamic Power Supply," *Solid-State Circuits, IEEE Journal of*, vol. 41, pp. 146-151, 2006.
53. S. Ohbayashi et al., "A 65-nm SoC Embedded 6T-SRAM Designed for Manufacturability With Read and Write Operation Stabilizing Circuits," *Solid-State Circuits, IEEE Journal of*, vol. 42, pp. 820-829, 2007.
54. M. Khellah et al., "A 4.2GHz 0.3mm<sup>2</sup> 256kb Dual- $V_{cc}$  SRAM Building Block in 65nm CMOS," in *Solid-State Circuits Conference, 2006. ISSCC 2006. Digest of Technical Papers. IEEE International*, 2006, pp. 2572-2581.
55. M. Yamaoka et al., "A 300MHz 25 $\mu$ A/Mb Leakage on-Chip SRAM Module Featuring Process-Variation Immunity and Low-Leakage-Active Mode for Mobile-Phone Application Processor," in *Solid-State Circuits Conference, 2004. Digest of Technical Papers. ISSCC. 2004 IEEE International*, 2004, pp. 494-542 Vol.1.

56. M. Yamaoka *et al.*, "A 300-MHz 25- $\mu$ A/Mb-Leakage on-Chip SRAM Module Featuring Process-Variation Immunity and Low-Leakage-Active Mode for Mobile-Phone Application Processor," *Solid-State Circuits, IEEE Journal of*, vol. 40, pp. 186-194, 2005.
57. H. Pilo *et al.*, "An SRAM Design in 65-nm Technology Node Featuring Read and Write-Assist Circuits to Expand Operating Voltage," *Solid-State Circuits, IEEE Journal of*, vol. 42, pp. 813-819, 2007.
58. A. Bhavnagarwala *et al.*, "Fluctuation Limits & Scaling Opportunities for CMOS SRAM Cells," in *Electron Devices Meeting, 2005. IEDM Technical Digest. IEEE International*, 2005, pp. 659-662.
59. P. Macken *et al.*, "A Voltage Reduction Technique for Digital Systems," in *Solid-State Circuits Conference, 1990. Digest of Technical Papers. 37th ISSCC., 1990 IEEE International*, 1990, pp. 238-239.
60. M. Yamaoka *et al.*, "65nm Low-Power High-Density SRAM Operable at 1.0V under  $3\sigma$  Systematic Variation Using Separate  $V_{th}$  Monitoring and Body Bias for NMOS and PMOS," in *Solid-State Circuits Conference, 2008. ISSCC 2008. Digest of Technical Papers. IEEE International*, 2008, pp. 384-622.
61. S. Mukhopadhyay, H. Mahmoodi, and K. Roy, "Reduction of Parametric Failures in Sub-100-nm SRAM Array Using Body Bias," *Computer-Aided Design of Integrated Circuits and Systems, IEEE Transactions on*, vol. 27, pp. 174-183, 2008.
62. S. Mukhopadhyay *et al.*, "Design of a Process Variation Tolerant Self-Repairing SRAM for Yield Enhancement in Nanoscaled CMOS," *Solid-State Circuits, IEEE Journal of*, vol. 42, pp. 1370-1382, 2007.
63. Y. Takeyama *et al.*, "A Low Leakage SRAM Macro with Replica Cell Biasing Scheme," *Solid-State Circuits, IEEE Journal of*, vol. 41, pp. 815-822, 2006.
64. K. Zhang *et al.*, "SRAM Design on 65-nm CMOS Technology with Dynamic Sleep Transistor for Leakage Reduction," *Solid-State Circuits, IEEE Journal of*, vol. 40, pp. 895-901, 2005.
65. A. J. Bhavnagarwala *et al.*, "A Pico-Joule Class, 1 GHz, 32 KByte $\times$ 64 b DSP SRAM with Self Reverse Bias," in *VLSI Circuits, 2003. Digest of Technical Papers. 2003 Symposium on*, 2003, pp. 251-252.
66. W. Yih *et al.*, "A 1.1 GHz 12 $\mu$ A/Mb-Leakage SRAM Design in 65 nm Ultra-Low-Power CMOS Technology with Integrated Leakage Reduction for Mobile Applications," *Solid-State Circuits, IEEE Journal of*, vol. 43, pp. 172-179, 2008.
67. F. Hamzaoglu *et al.*, "A 3.8 GHz 153 Mb SRAM Design with Dynamic Stability Enhancement and Leakage Reduction in 45 nm High-k Metal Gate CMOS Technology," *Solid-State Circuits, IEEE Journal of*, vol. 44, pp. 148-154, 2009.
68. Q. Hulfang *et al.*, "SRAM Leakage Suppression by Minimizing Standby Supply Voltage," in *Quality Electronic Design, 2004. Proceedings. 5th International Symposium on*, 2004, pp. 55-60.
69. K. Nii *et al.*, "A 90-nm Low-Power 32-kB Embedded SRAM with Gate Leakage Suppression Circuit for Mobile Applications," *Solid-State Circuits, IEEE Journal of*, vol. 39, pp. 684-693, 2004.
70. W. Jiajing and B. H. Calhoun, "Canary Replica Feedback for Near-DRV Standby VDD Scaling in a 90nm SRAM," in *Custom Integrated Circuits Conference, 2007. CICC '07. IEEE*, 2007, pp. 29-32.
71. W. Jiajing, A. Hoefler, and B. H. Calhoun, "An Enhanced Canary-Based System with BIST for SRAM Standby Power Reduction," *Very Large Scale Integration (VLSI) Systems, IEEE Transactions on*, vol. 19, pp. 909-914, 2011.
72. M. Qazi, K. Stawiasz, L. Chang, and A. P. Chandrakasan, "A 512kb 8T SRAM Macro Operating Down to 0.57 V With an AC-Coupled Sense Amplifier and Embedded Data-Retention-Voltage Sensor in 45 nm SOI CMOS," *Solid-State Circuits, IEEE Journal of*, vol. 46, pp. 85-96, 2011.
73. H. Chung-Hsien, C. Tung-Shuan, and H. Wei, "Distributed Data-Retention Power Gating Techniques for Column and Row co-Controlled Embedded SRAM," in *Memory Technology, Design, and Testing, 2005. MTDT 2005. 2005 IEEE International Workshop on*, 2005, pp. 129-134.
74. S. Kaxiras, H. Zhigang, and M. Martonosi, "Cache Decay: Exploiting Generational Behavior to Reduce Cache Leakage Power," in *Computer Architecture, 2001. Proceedings. 28th Annual International Symposium on*, 2001, pp. 240-251.
75. B. S. Amrutur and M. A. Horowitz, "A Replica Technique for Wordline and Sense Control in Low-Power SRAM's," *Solid-State Circuits, IEEE Journal of*, vol. 33, pp. 1208-1219, 1998.
76. S. Vincent Wing-Yun, C. Chiu-sing, and C. Cheong-Fat, "A Four-Phase Handshaking Asynchronous Static RAM Design for Self-Timed Systems," *Solid-State Circuits, IEEE Journal of*, vol. 34, pp. 90-96, 1999.
77. M. Yoshimoto *et al.*, "A Divided Word-Line Structure in the Static RAM and its Application to a 64K Full CMOS RAM," *Solid-State Circuits, IEEE Journal of*, vol. 18, pp. 479-485, 1983.
78. T. Hirose *et al.*, "A 20-ns 4-Mb CMOS SRAM with Hierarchical Word Decoding Architecture," *Solid-State Circuits, IEEE Journal of*, vol. 25, pp. 1068-1074, 1990.



79. A. J. Bhavnagarwala, S. Kosonocky, and J. D. Meindl, "Interconnect-Centric Array Architectures for Minimum SRAM Access Time," in *Computer Design, 2001. ICCD 2001. Proceedings. 2001 International Conference on*, 2001, pp. 400-405.
80. A.-T. Do, Z.-H. Kong, and K.-S. Yeo, "Hybrid-Mode SRAM Sense Amplifiers: New Approach on Transistor Sizing," *Circuits and Systems II: Express Briefs, IEEE Transactions on*, vol. 55, pp. 986-990, 2008.
81. L. Ya-Chun and H. Shi-Yu, "A Resilient and Power-Efficient Automatic-Power-Down Sense Amplifier for SRAM Design," *Circuits and Systems II: Express Briefs, IEEE Transactions on*, vol. 55, pp. 1031-1035, 2008.
82. P. Nasalski *et al.*, "SRAM Voltage and Current Sense Amplifiers in sub-32nm Double-Gate CMOS Insensitive to Process Variations and Transistor Mismatch," in *Circuits and Systems, 2009. ISCAS 2009. IEEE International Symposium on*, 2009, pp. 3170-3173.
83. E. Seevinck, "A Current Sense-Amplifier for Fast CMOS SRAMs," in *VLSI Circuits, 1990. Digest of Technical Papers., 1990 Symposium on*, 1990, pp. 71-72.
84. M. E. Sinangil, N. Verma, and A. P. Chandrakasan, "A 45nm 0.5V 8T Column-Interleaved SRAM with on-Chip Reference Selection Loop for Sense-Amplifier," in *Solid-State Circuits Conference, 2009. A-SSCC 2009. IEEE Asian*, 2009, pp. 225-228.
85. D. Anh-Tuan *et al.*, "A Full Current-Mode Sense Amplifier for Low-Power SRAM Applications," in *Circuits and Systems, 2008. APCCAS 2008. IEEE Asia Pacific Conference on*, 2008, pp. 1402-1405.
86. B. Wicht, T. Nirschl, and D. Schmitt-Landsiedel, "A Yield-Optimized Latch-Type SRAM Sense Amplifier," in *Solid-State Circuits Conference, 2003. ESSCIRC '03. Proceedings of the 29th European*, 2003, pp. 409-412.
87. K. Sasaki *et al.*, "A 7-ns 140-mW 1-Mb CMOS SRAM with Current Sense Amplifier," *Solid-State Circuits, IEEE Journal of*, vol. 27, pp. 1511-1518, 1992.
88. I. Arsovski and R. Wistort, "Self-Referenced Sense Amplifier for Across-Chip-Variation Immune Sensing in High-Performance Content-Addressable Memories," in *Custom Integrated Circuits Conference, 2006. CICC '06. IEEE*, 2006, pp. 453-456.

## Chapter 3. Truly Self-Timed SRAM

### 3.1 Introduction

This chapter is the first core chapter of this study, which benefits from the background summarized in the previous chapter, and it is divided into five sections. The second section digs out the research gap and states the problem statement of this research based on evidence. The third section tries to find out any solution in the literature to address the found problem, and then it proposes the researcher's methodology and design technique for such type of issue along with his novel design. The fourth section investigates the introduced design and highlights its main features and overheads. The next to last section employs the analysis included in the fourth section to propose a new version of the proposed design, which possesses some features. The last section summarizes and concludes the chapter. The main results appearing in this chapter was published in [1, 2].

### 3.2 Problem Statement: Timing Variations in Non-Deterministic Environments

Exploring the published works along with the ITRS reports enhance the understanding of the microelectronic systems roadmap. This roadmap explains from where these systems came from and where it is anticipated they go together with design strategies involved in each era (e.g. high performance era, low power era, portable devices era). The clear understanding of the mentioned roadmap does help not only in pointing out the hidden gaps but also in picking out the best techniques to address them.

Currently, microelectronic system design is becoming more energy conscious. This is mainly because of limited energy supply (scavenged energy or bat-

tery) and excessive heat with associated thermal stress and device wear out. At the same time, the high density of devices per die and the ability to operate with a high degree of parallelism, coupled with environmental variations, create almost permanent instability in voltage supply (cf. VDD droop), making systems highly power variant. When systems are subjected to varying environmental conditions, with voltage and thermal fluctuations, timing tends to be the first affected issue. Most systems are still designed with global clocking and the design is often made overly pessimistic to avoid failures due to VDD (timing) variations. Along with the advent of the nanometre CMOS technology, the continuation of the scaling process is vital to the future development of the digital industries. ITRS predicts poorer scaling for wires than transistors in future technology nodes [3]. This makes the above worst timing assumption even worse along with power supply voltage drooping [4]. The following sub-section investigates this issue for the chosen case study, SRAM.

### **3.2.1 SRAM Latency under Different VDDs**

Normally, memory works based on timing assumptions and energy harvester supplies a wide range of non-deterministic voltages. Accordingly, it is necessary to understand how the timing assumptions of memory behave under different voltages. So, this research started by investigating the difference between the latency on SRAM including a bit-line driver and its corresponding timing controllers, typically implemented in an inverter chain kind of delay elements, under different voltages. This potential timing mismatch between SRAM and the mentioned type of controller has already been pointed out in a previous work [5] but in the context of process and temperature corners not in the context of variable VDD. Emerging energy harvesting systems necessitates investigating this delay mismatch in the context of non-deterministic VDD.

The experiment bundles an SRAM cell with an inverter chain, both operating under the same value of VDD as shown in Figure 3.1. A start signal then triggers reading/writing operation in the SRAM together with the inverter

chain and when the SRAM operation finishes, the number of inverters the start signal has passed is counted.

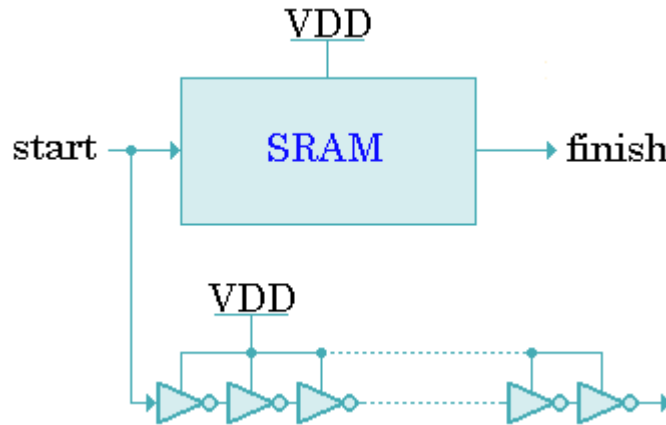


**Figure 3.1** A method to investigate timing discrepancy between SRAM and inverter chain.

This is repeated for the whole range of supply voltages where both SRAM and inverter chain work, which was found to be from 1V down to 0.19V for 90nm technology, and the results are plotted in Figure 3.2. The graph shows the number of inverters required to bundle the SRAM timing for different voltages.

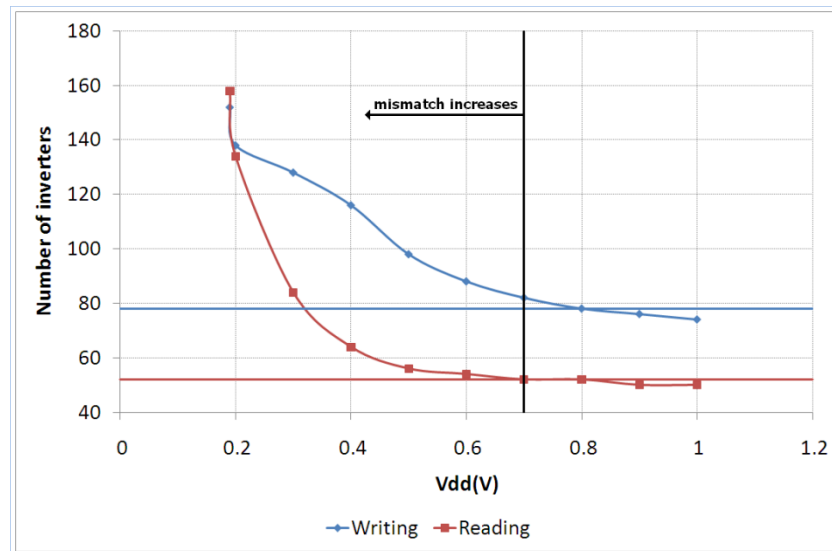


**Figure 3.2** Timing mismatch between SRAM and its bundling delay element.

Using the inverter delay as a measurement unit, the results confirm that under the lowest supply voltage the writing operation is about two times slower than under the nominal voltage and that difference increases to more than three times for the reading operation. Interestingly, this mismatch is quite small when the supplied voltage is above 0.7V, which coincidentally

was the lowest voltage investigated in some of the previous work (e.g. [6]) for the same technology node. In other words, both reading from and writing to memory become slower at a much higher rate than inverter chains when the VDD is reduced below 0.7V. Moreover, delay elements, implemented based on inverters, do not track memory operation delays when both are operating under the same value of supply voltage. This demonstrates that for the case of wide ranges of VDD, employing standard inverter chains for memory delay bundling would require precise design time delay characterization and conservative worst case provisions, which could be above three times more wasteful.

After these results were published [1], similar research appeared (e.g. [7]). The case considered in [7] is only the reading operation in 65nm node and it augmented the experiment here by expanding the bit-lines to include 128 cells, where the data stored in the cells reflect the worst case bit-line leakage described in the second chapter. The reading operation in [7] requires one clock cycle, which assumed to equate the delay of 20 inverters. For such a case, the clock frequency varies from more than 0.8GHz at 1.2V to 200kHz at 0.2V, which means the difference is more than eight orders of magnitude.

In conclusion, this experiment [1] confirms that when the VDD varies a great deal, the most vulnerable metric of memory system is its timing. In that case, delay bundling cannot benefit from simple chain of basic gates without sacrificing more than two times of the system resources. Based on that, the next section discusses the ideal design technique for this challenge and then tries to find the right solution to address it.

### **3.3 Methodology and Design Strategy: Power Adaptive Computing**

In the not so long past low power design was targeted merely at the reduction of capacitance, VDD, and switching activity, whilst maintaining the required system performance. In many current applications, the design objectives changed to maximizing the performance within the dynamic power constraints from energy supply and consumption regimes. Such systems can no longer be simply regarded as low power systems, but rather as power

adaptive or power resilient systems. Normally, this kind of system has two main properties, which are being power efficient not just low power, and has the ability to work under non deterministic supply voltage (probably with known range, which tends to be low) that varies over time. Recently, a possible solution is proposed for this kind of system, coined energy modulated systems, which takes power and energy as dynamic resources [8]. That is, when power is not enough, some of the subsystems could either be powered off or be executed under lower power supplies and whenever power is adequate, systems can provide high performance. This means that all tasks in a system are managed based on the power resources, performance requirements, and thermal constraints. In the scope of this vision, the next subsection tries to find the right answer to the raised research question.

### **3.3.1 Self-Timed SRAM**

According to the categorization of SRAM circuit design approaches mentioned in the previous chapter, the timing issue has to be addressed by a timing circuit based approach. Hence, the researcher's methodology for such a challenge, which agrees with his understanding of the microelectronic systems roadmap, is to employ handshaking protocols in order to release the memory system from any timing assumptions and regulate the circuit operation based on the actual speed of the data flow rather than on any worst case timing assumptions [9]. In addition, having such a design gives the management unit of the whole system the opportunity to swap between different operational modes (e.g. high performance, minimum energy, etc.) while guaranteeing that SRAM will adapt itself for any mode.

Unfortunately, as described in the second chapter, exploring the literature shows that fully SRAM operation (reading and writing) has not yet benefited from completion detection. While reading completion detection was implemented in [10, 11], all works either overlooked writing completion detection [11] or claimed that it is difficult and impractical [10]. Some works require a reference voltage, to operate the SRAM under wide range of supply voltage, and assume it is adjustable for different operational conditions [12]. However, in the energy harvesting environment, there might be no stable

reference voltages at all as almost everything is non-deterministic. So anything based on comparators will not work. Other works require a reference voltage in an indirect way by employing adjustable delay elements for different operational conditions, which again requires a voltage reference for the case of different ranges of supply voltages [10]. Finally, despite that this problem is a timing issue, some works tried to address it via bit-cell based techniques by adding several transistors to the 6T cell to allow it acknowledge the end of writing operation [11, 13]. However, they do not clearly justify why they migrate from the 6T cell to others, is the 6T not suitable for writing completion detection, is that impossible as claimed in [10]? These questions are still open.

In summary, SRAM has a challenging timing problem, especially if it is supplied from a non-deterministic energy source. This challenge cannot be addressed by the prevalent techniques based on a simple chain of basic gates and certainly it requires defined handshaking protocols. Until the date of proposing the design in this thesis, 6T SRAM had not yet benefited from completion detection and even was believed it is difficult and impractical.

Here this research proposes a fully self-timed SRAM operate based on handshaking protocols, where each stage of the operation is acknowledged once it is completed. The block diagram of the proposed memory system is shown in Figure 3.3, which contains two main blocks, the memory system and its timing control block. The writing and reading operations are as follows.

During writing operation, the timing controller receives the WReq signal, which initiates the writing operation and accordingly the Precharge signal is taken down, that opens the pMOS transistors of the prechargers and starts precharging the bit-lines. While precharging, the controller monitors the bit-lines and once it detects that both bit-lines were fully precharged, it raises the Precharge signal to stop the precharging. Following that, the controller generates the WL signal to open the access transistors of the cell in charge, which results in discharging one of the bit-lines based on the stored data. The timing controller detects the discharging, since it monitors the bit-lines, and then it issues the WE signal to enable the write drivers. Enabling

the write drivers results in withdrawing one of the bit-lines to the ground based on the input data. If that bit-line is in the same side as the node storing high voltage, that node will be discharged below the trip point of the other inverter and the cell flips, which results in charging the other node to high voltage and hence monitoring the bit-lines can detect the writing completion. However, if the node storing low voltage is in the same side as that bit-line, which was taken down, then there is no actual writing and the other bit-line is already at high voltage, hence the completion is detected faster. Once the controller detects the end of writing operation, it raises the WAck signal. Then the computational logic responds to that by withdrawing the WReq signal and upon that, the controller takes WL, WE and WAck down respectively.

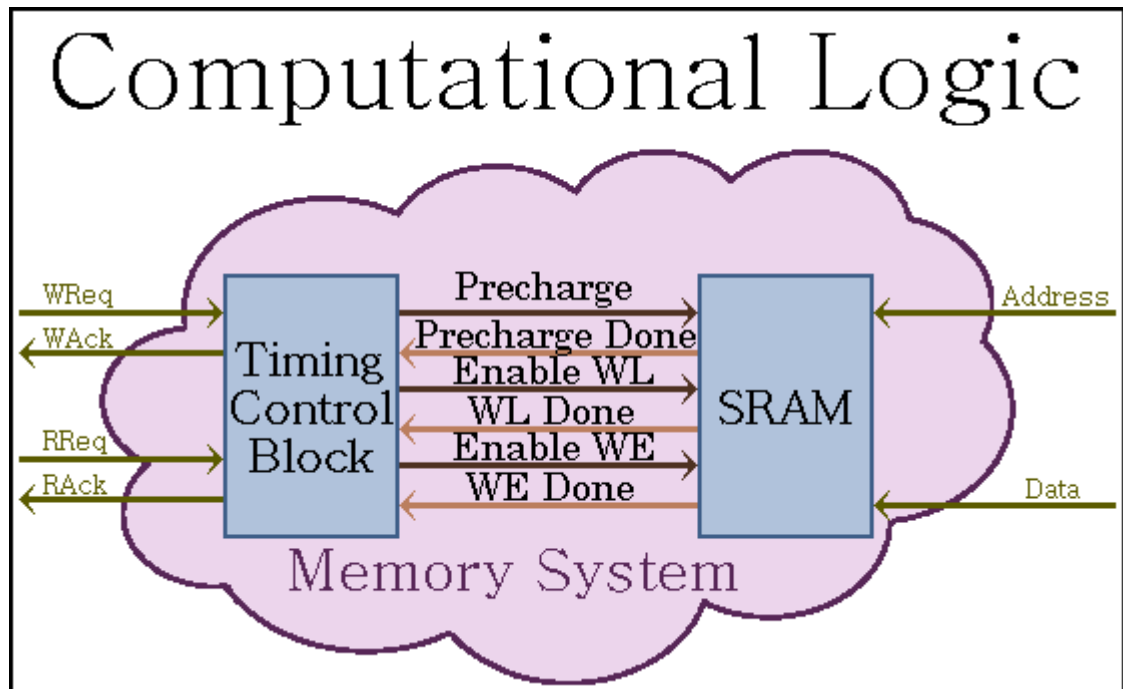


**Figure 3.3 Block diagram of the proposed self-timed memory system.**

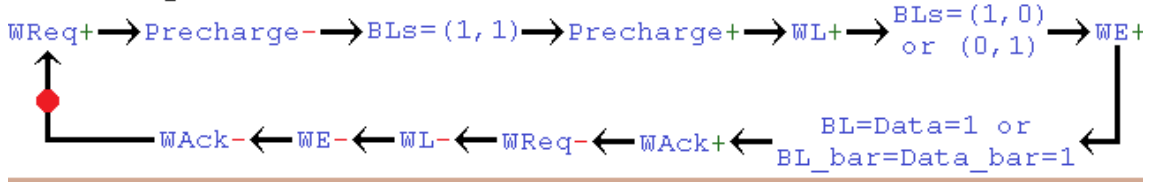
Reading is a replica of part of the writing process, it starts by raising the RReq signal followed by taking down the Precharge signal to start the precharging stage and then rising it to stop the precharging once it is completed. After that, the controller issues the WL signal to open the nMOS access transistors of the cell in charge. Consequently, one of the bit-line is discharged according to the stored data, which acknowledges the end of the reading operation by raising the RAck signal. After the reading acknowl-



edgment, the RReq signal is withdrawn by the environment and upon that, the controller takes the WL and RAck signal down respectively.

These proposed protocols are able to detect the completion of the writing and reading operation as well as detect the completion of each stage during writing and reading. For instance, the protocol can inform the surrounding environment whether the precharging phase finishes or not, whether the access transistors are opened or not, and so on. The Signal Transition Graph (STG) specifications of the previously described reading and writing operation are depicted in Figure 3.4.

### Writing STG:



### Reading STG:

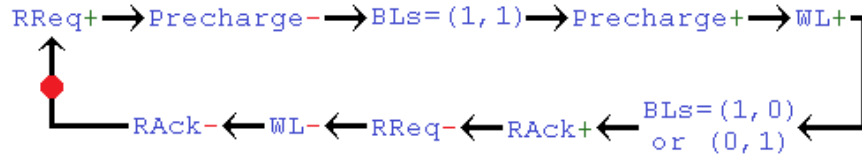


Figure 3.4 STG specifications of the reading and writing operations in the 6T cell.

Different circuit design techniques can be employed to implement the STGs in Figure 3.4. The safest asynchronous circuit is the Delay Insensitive (DI) one, where the operation works correctly irrespective of latency behaviours of any component, including logic and wires. Such systems should in general work correctly under nondeterministic supply voltage variations with average case performance. However, DI techniques usually require complex coding (e.g. dual-rail), and have power and size disadvantages [14]. For memory such as on-chip SRAMs, even small unit penalties will be multiplied to intolerable scales. Moreover, for many applications, DI solutions cannot be found [15]. Various approximations to true DI have been proposed. For instance, if the delays on wires are assumed to be zero or negligible, systems can be designed so that any delay variations in the gates do not compromise correctness. Systems designed in this way are known as Speed Independent (SI). SI systems tend to be easier and cheaper to design and implement than

DI ones, hence, the research's choice went with this next best option. The timing controller realisation shown in Figure 3.5 is obtained from optimizing the Petrify [16] solution of the combined STG specifications shown in Figure 3.4. This circuit diagram represents one of the possible implementation to the described STGs, where the operation is described as follows.

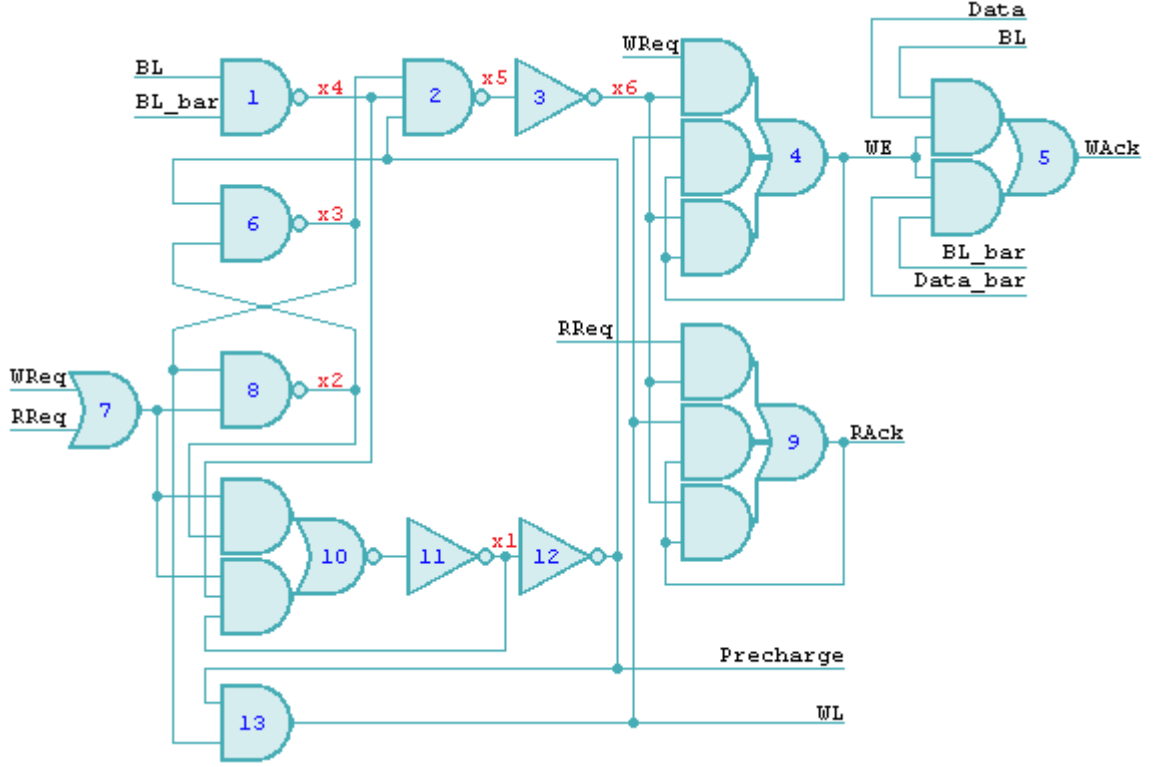


Figure 3.5 Possible implementation of the STG's in Figure 3.4.

Initially, WReq, RReq, x2, and x3 are 0, 0, 1, 0 respectively. Consequently WAck, RAck, Precharge, WL, WE, x1, x5, and x6 are 0, 0, 1, 0, 0, 0, 1, 0 respectively. The x4 is in a “don't care” value initially.

As an example, writing operation is used to show how the controller works. After the address and data are ready, the WReq signal is issued. WReq goes through gate 7 and then through to gate 10. As x2 is 1, so x1 is 1 and then it makes Precharge equal to 0. The low Precharge signal opens the pMOS transistors in precharge drivers. The Precharge also goes to the SR latch formed by gates 6 and 8 to reset the latch when Precharge is low. After both bit-lines are 1 and the SR latch is reset, x1 is changed to 0, and then Precharge signal is removed. Following that, gate 13 is triggered to generate WL and that opens the pass transistors in the 6T cell. Consequently, the da-

ta stored in the cell is read to the bit lines, which makes  $x_4$  equal to 1. As the SR latch was reset,  $x_6$  will be 1 and accordingly WE goes to 1 to open the write driver. If the new data is the same as the data stored in the cell, either  $(Data, BL)=(1, 1)$  or  $(Data\_bar, BL\_bar)=(1, 1)$ , WAck is generated to notify the computational unit that the data has already been written into the cell. However, if for instance, new data is 1 and the stored data is 0, the following happens. After the write driver is opened,  $BL\_bar$  is low, which discharges  $Q\_bar$ , flips the cell, and charges  $Q$  to 1. That 1 will transfer to BL to trigger gate 5 to acknowledge the end of the writing operation. After WAck is generated, WReq is removed and then only after the controller is returned to the initial states, WAck is withdrawn to wait for a new reading/writing operation. This design assumes that data is only allowed to change after WAck is removed.

Inspecting the timing controller shows that RAck is generated by gate 9, which has similar structure to gate 4 except that it is connected to RReq instead of WReq. Accordingly, RAck is issued by the same signal sequences of that of WE.

As for a memory bank, gate 1 is replicated. The number of the duplicated gates equals to the number of bits the memory word has. The inputs of each gate are a pair of bit-lines corresponding to each bit of the memory word. All outputs of the duplicated gates are collected in a C-element. The output of the C-element replaces  $x_4$ . Gate 5 is also replicated. All outputs of the duplicated gates are collected in a C-element and the output of the C-element is the new WAck signal.

### 3.4 Investigations on the Proposed SI SRAM

This section contains analysis and computations of the introduced design in order to judge its ability to address the raised SRAM timing issue in addition to concluding its advantages and overheads. Three subsections do this job, the first one investigates the behaviour of the introduced design under variable supply voltage, a typical case in an energy harvesting environment. The second subsection has the important time and energy computations of

the self-timed SRAM. The last section examines the energy overhead of the timing controller.

### 3.4.1 Behaviour of SI SRAM under Variable VDD

Firstly, an SI SRAM is investigated under variable supply voltage, a raw harvester's output. In this experiment, the SRAM along with its peripheral components and timing circuitry are all powered by a sinusoidal voltage with a frequency of 700kHz and minimum and maximum value of 0.3V and 1V respectively. The experiment consists of writing 0 to the SRAM followed by a reading operation, then writing 1 to flip the cell followed by a reading operation. The timing diagrams of all controllers' critical signals are plotted in Figure 3.6 in order to examine the functionality. The names in the graph are the same conventional names employed above.



**Figure 3.6 Critical waveforms of self-timed SRAM under variable VDD.**

As the VDD changes, the same operation takes different times according to the voltage at that time. The red and green boxes bound the timing of writing operation at low and nominal voltages respectively. On the one hand, the former takes longer time than the latter and at the same time, it runs faster as the voltage increases. On the other hand, the latter operation generates the acknowledgement in next to no time and does the task at the maximum speed of the circuit.

The key achievement of this experiment is demonstrating the ability of the truly and fully self-timed SRAM to remove the timing assumptions required to operate the circuit at a predefined level of performance. Accordingly, the circuit adapt itself to regulate the data flow based on the maximum speed it can provide at each operational condition. Importantly, reflecting upon that shows a clear opportunity to enable the scheme discussed above, power adaptive computing. In that scheme, the system has to finish the required task within the supplied amount of energy even if the performance is very low and at the same time, it must give the maximum performance whenever the harvested energy is enough to serve it. Moreover, voltage stability is the last concern to consider in this scheme as confirmed above.

### **3.4.2 Timing and Energy Computations**

This subsection consists of several experiments, which have the purpose of measuring the performance and energy of the proposed self-timed SRAM. Firstly, an SRAM chip is designed in a full-custom manner, by tiling 1024 6T bit-cells in 64 rows and 16 columns to form a bank. Then, the following peripheral circuits are added, 6x64 decoder, write drivers, prechargers, and SI-latches. The timing of all included components is managed by the SI controller proposed above.

The memory chip is then tested under a wide range of variable supply voltage and found to be fully functional from as low as 0.19V all the way up to 1V. The full functionality here means safe and correct reading, and successful writing. After verifying the functionality of the whole SRAM chip, the performance and energy calculations are recorded for each value of VDD. The graphs in Figure 3.7 and Figure 3.8 depict the operation's delay and its consumed energy respectively, for different voltage values, where the calculated metric is for one memory word 16 bits long. Each figure has two graphs, one for reading coloured in dark red, and one for writing, which is coloured in green.

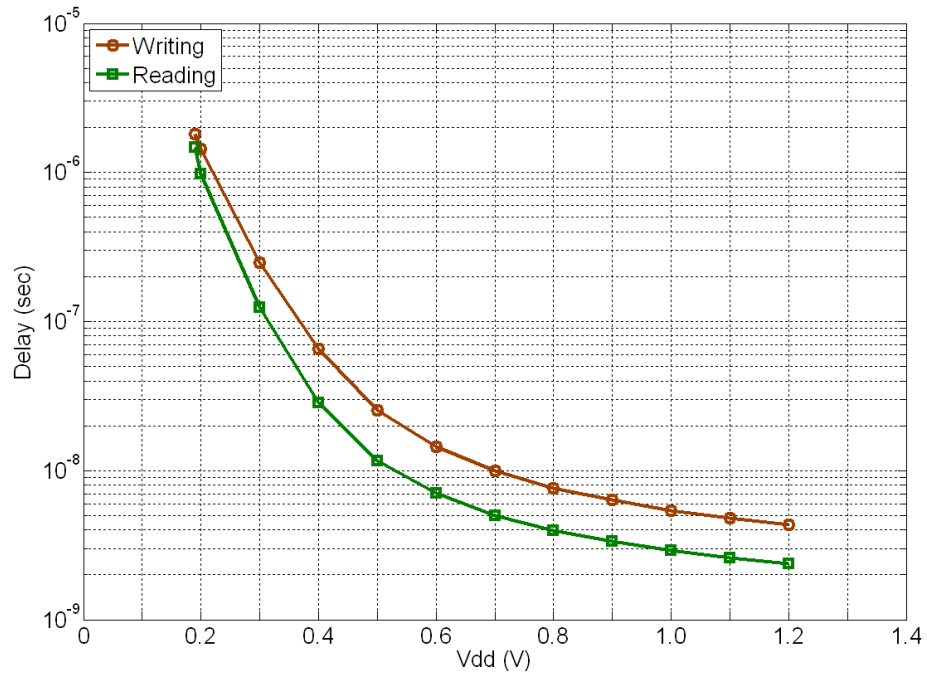


**Figure 3.7 Operation delay of the proposed self-timed SRAM.**

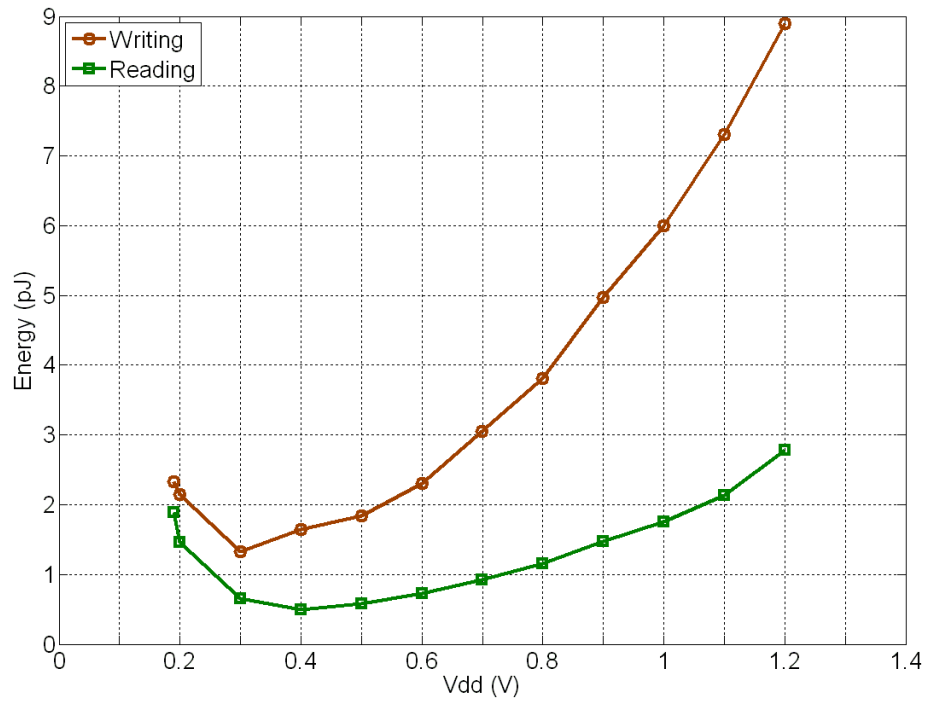


**Figure 3.8 Energy consumptions of the proposed self-timed SRAM.**

Examining both graphs shows that the writing operation takes more time and consumes more energy than reading and that was expected since the writing protocol of the proposed controller includes reading as described above. The energy consumption graph depicts that the Minimum Energy Region (MER) for this design seems to be between 0.3V and 0.5V.

### 3.4.3 Energy Overhead

At present, energy consumption of any new circuit component is a crucial metric and the first property the designer considers, especially those designed to operate in an energy conscious environment as the one proposed here. Hence, it is important to calculate the energy consumption of the proposed controller, moreover, how much this amount occupies from the total consumed energy. For this purpose, this subsection is dedicated.

Basically, the previous experiment is repeated with an aim of measuring the energy consumed by the self-timed memory system including bit-cells and all peripheral components on the one hand, and that of the timing controller only on the other hand. Then, the percentage of the latter to the former is calculated and bar charts representing both are plotted in Figure 3.9 and Figure 3.10 for writing and reading operation respectively.

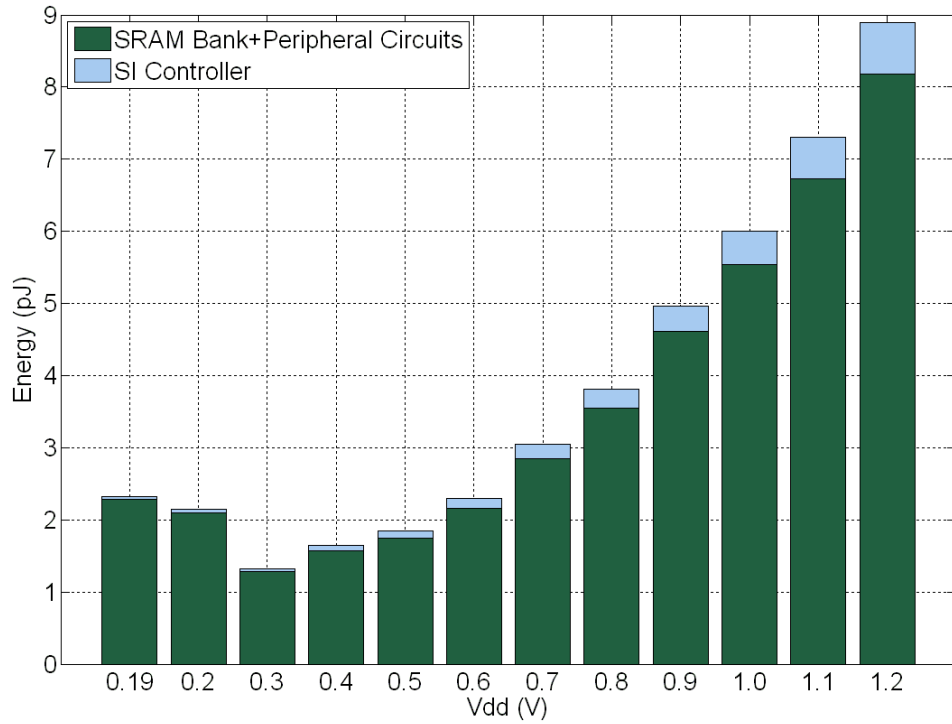


**Figure 3.9 Energy overhead of the proposed timing controller during writing.**

The green part of each bar represents the energy consumed by the SRAM bank along with all peripheral circuitry, while the light blue part illustrates that of the SI timing controller only. Certainly, the sum of both is the total energy consumption of the memory chip, which is exactly equal to the plots in Figure 3.8.

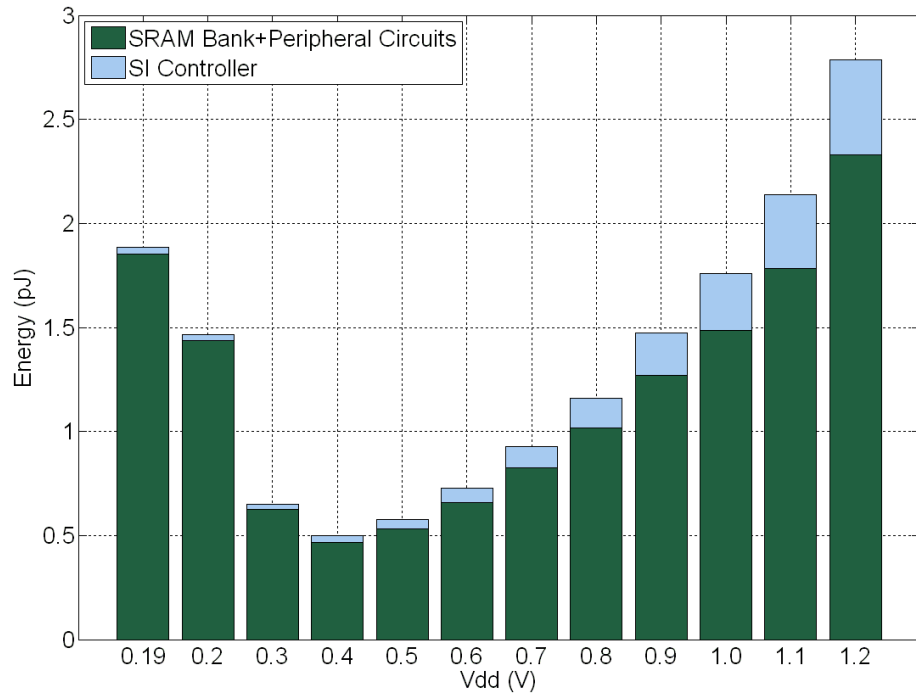


**Figure 3.10** Energy overhead of the proposed timing controller during reading.

Both bar charts show that at the lowest supply voltage, the timing controller consumes no more than 2% of the total energy consumptions and this percentage increases as the supply voltage rises. At the nominal supply voltage, the controller consumes around 8% of the total energy consumptions during writing and slightly above 16% of the total energy during reading. Comparing these figures with the portion of energy consumption the clock dissipates in synchronous SRAM demonstrates that the asynchronous SRAM is more energy efficient than its synchronous counterpart. Typically, most of the clocked systems power is dissipated in clock generation and distribution and it roughly reaches up to 50% of the total switching power [17, 18].

### 3.5 More Efficient Design Technique: Smart Latency Bundled Self-Timed SRAM

According to the results gained from previous experiments, the proposed fully SI solution is able to address the challenging timing problem in self-powered systems while it provides an acceptable level of delay and energy calculations. However, for large memory comprising several banks/arrays the fully SI solution might be expensive in terms of area, performance and energy as consequences of replicating gates 1 and 5, of the controller, for each bit-line and combining the output of all replicated gates by C-elements.



Therefore, this section proposes a more efficient design for large memory system, which trades off a marginal level of operation safety in order to save system's resources. The trade-off involves adding several timing assumptions to the circuitry, hence, reducing the complexity level of completion detections.

### 3.5.1 Bundling Techniques in Self-Timed SRAM

The asynchronous bundled data design method [9] is the usual alternative for cases where a large number of similar components execute together, such as the reading/writing of memory. In general, for bundled data designs, the timing control circuits, which provides the latency bundling, tend to be much smaller than the bundled logic, otherwise the designer might as well choose to implement the main logic directly in SI or even DI. Conventional latency bundling elements are therefore usually based on the lightest possible logic.

In the context of SRAM, reading and writing operations usually involve multiple cells each time along an entire row. This can be bundled using a single memory cell in that row using the same timing control block. Normally, this cell should have the worst case timing among its colleagues under all application's operational conditions. This is schematically shown in Figure 3.11. In this scheme, although the timing control block in addition to bundling cell is heavier than one regular memory cell, it is much lighter than the entire row, with reasonable word lengths, fully controlled by SI circuits.

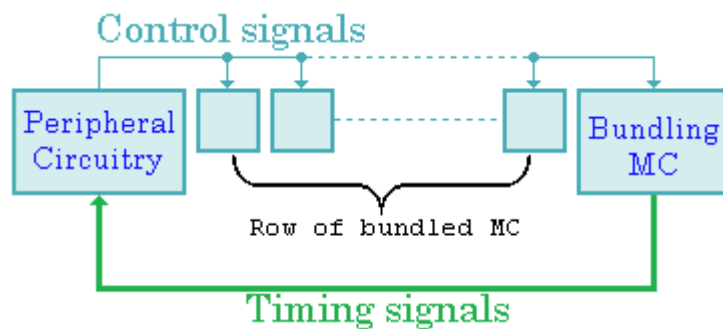


Figure 3.11 Bundling scheme in self-timed SRAM.

In practice, a bank of such SRAM bundled with SI cells will include one bundling cell in each row. For consistent implementation, layout practicality, and to compensate for the effect of leakage currents through the bit lines, these timing control cells should be put to the same position in each row. In other words, in a bank of such memory, one of the columns should be designated the timing control or latency bundling column. The delays of cells in this column must correctly bundle the delays of the whole memory bank under all working modes of the targeted application. In scope of this condition, what is the optimum position for this bundling column? According to [19], the furthest column from the decoder and other peripheral circuitry is the slowest column owing to interconnect latencies. This fact guided this study to implement the last column with SI cells to serve both as the far end bits of memory words and as the timing control units (exactly as shown in Figure 3.11). This approach is valid in purely timing assumption based design, as timing assumptions can be made data independent.

However, in self-timed design, data independence cannot be assumed and needs to be verified. Intuitively, in the context of SRAM, the worst case, where writing takes the longest time, is when the data in the memory cell needs to be flipped. Accordingly, an experiment is designed to clarify this matter. In this experiment, one normal SRAM column is compared with a fully SI one. The latency between writing start and data fully settling in the normal SRAM and the latency between writing request and writing acknowledgement in the SI SRAM are compared. In the bundling approach in the form of scheme in Figure 3.11, the writing acknowledgement in the SI SRAM is used to indicate the completion of writing, thus implying that data has settled in the row, including other “bundled” cells. Experiments across all process corners (TT, SS, FF, SNFP, and FNFP) were conducted for all data combinations and all voltage values from 1V down to 0.2V. Unfortunately, it was obtained from these experiments that when any bundled cell has a bit flipping in writing and its corresponding SI one does not, the writing acknowledgement signal from the SI cell comes before the written bit in the regular cell settled at some process corners. Moreover, that timing discrepancy cannot be covered by the additional interconnect delay of the long-

est wires. This means that bundling may fail when the SI cell used for bundling does not experience bit flipping under writing. These experiments have also shown that when the SI cell experiences bit flipping, its acknowledgement signal always comes a safe distance after the data in the regular cell has settled. This bundling failure is mainly caused by the low power design techniques used in the proposed SI SRAM design, in which if the new data is the same as the data stored in the targeted cell, no actual writing is executed and the acknowledgment signal is generated directly. This saves power as well as reduces the writing latency, however, it makes the writing operation data dependent.

In the scope of the acquired results, this study touches on an important issue in the philosophy of bundling techniques. The proposal of Figure 3.11 specifies that the bundling unit should be structurally equivalent to the bundled units. Nevertheless, in actual fact it has to exhibit behavioural equivalence in addition to structural equivalence. As a result, so long as at least one of the cells in a word flips, the bundling cell must display this behaviour and flip too. Importantly, this is unlikely if the bundling cell belongs to the data word.

Accordingly, this research’s solution is to construct the entire data memory from regular cells, and append an additional column of “professional” latency bundling SI cells to the far side of the furthest data column in the bank, where the bundling column will have the longest interconnect from the peripheral circuitry. In other words, the structure remains that of Figure 3.11 but now with the data word stopping just before the bundling cell, which no longer represents the last digit of the data word. The concept of this idea itself is not new and was previously introduced in [5, 12], however, the design techniques are totally novel, where the differences between the previous and the proposed one are:

1. The redundant column of other techniques contains non-real cells internally connected in a special way to reflect some worst cases timing while the proposed replica column contains real cells. Consequently, timing signals generated from the proposed technique reflects real

operation in real cells while timing signals generated from other designs reflected worst case timing generated from dummy cells.

2. The timing circuitry employed in other methods is constructed entirely from basic gates, acting as delay elements, triggered by dummy cells [5] or controlled by reference voltage [12] while the proposed one has fully SI circuit monitors real cells during real operations.

These two fundamental differences between the design proposed here and the previous ones indicate the ability of the former method to provide full and secure bundling, which matches the actual timing of all other columns and even outperforms other methods in terms of tolerating the randomness of the supplied voltage. This latency bundling method is “smart” or “intelligent” because it is based on extracting the relevant latencies in the most accurate possible manner, from components of exactly the same type as the bundled component and through a secure (SI) circuit that monitors real operations of real components that have real data.

With the data in the timing control column having no operational functionality, alternating bit values can always be written to the SI SRAM cells to ensure that bit flipping happens in every write. To do that the design needs to read the data from the column, invert it, and then write the inverted result back to the column. Fortunately, the asynchronous controller proposed in the previous section incorporates a reading action in its writing process as discussed in section 3.3.1. Therefore, there is no need to change the main part of the controller, but the writing STG specification must be modified from the shape in Figure 3.4 to that shown in Figure 3.12 for reasons already alluded to earlier.

#### Modified Writing STG:

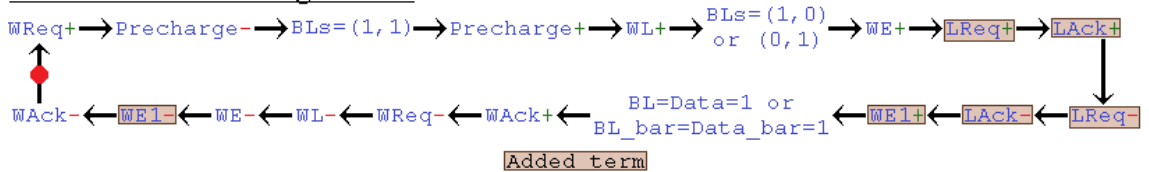


Figure 3.12 Modified writing STG for latency bundled SRAM.

The STG in Figure 3.4, although correct for use in a system where all cells are SI, is not suitable for a bundling cell. For instance, if the data being written into a memory cell is the same as the data already stored in the cell, according to the STG specification in Figure 3.4, as a round of reading is included in the writing process, so the (BL, BL\_bar) presents the data stored in memory. Consequently, the WAck signal will be generated as quickly as possible, and then the other control signals, such as WL, WE, will be withdrawn. This maximizes speed and reduces energy consumption, as the actual writing of a bit into the cell is not performed in such a case, but for a bundling cell, this speed up is inappropriate. As a result, the specification for a bundling cell timing controller is derived from Figure 3.4 and shown in Figure 3.12. Here a forced writing of a different data bit is used to eliminate temporal inconsistencies. After the reading action in the writing process has been completed (indicated by WE+), the data just read (the current stored data in the memory) is written into a storage, i.e. an SI-latch, by LReq+, and after this writing to a latch is completed, LAck+ is generated. The resets of LReq and LAck immediately follow to let the data settle in the storage, and afterward the complementary of the bit settled in the SI-latch, which is the inverse of the original data bit, is written back to the cell as new data. This makes the data being written permanently different from the data previously stored in the cell. It is worth highlighting that as the data being written into the latch needs to be stable during write back, the LReq and LAck signals should be reset before data writing. This is shown in Figure 3.12, as LAck+ followed by LReq-, and LAck-.

Based on this new STG, the controller must be updated as shown in Figure 3.13 with additional components. As the augmented requirements do not affect the main part of the controller, rather than re-synthesizing completely from Figure 3.12, the researcher chose to retain the design in Figure 3.5 and manually introduce the additional components to cover the difference between Figure 3.4 and Figure 3.12. The added logic include a D-element (sometimes also known as a “sequencer”) to manage the handshakes and an SI-latch to store and invert the bit data. For the D-element, {WE, WE1} is the master handshake and {LReq, LAck} is the slave one. The

D-element is in charge of implementing the  $WE+ \rightarrow LReq+ \rightarrow LAck+ \rightarrow LReq- \rightarrow LAck- \rightarrow WE1+ \rightarrow WE- \rightarrow WE1-$  handshake sequence.

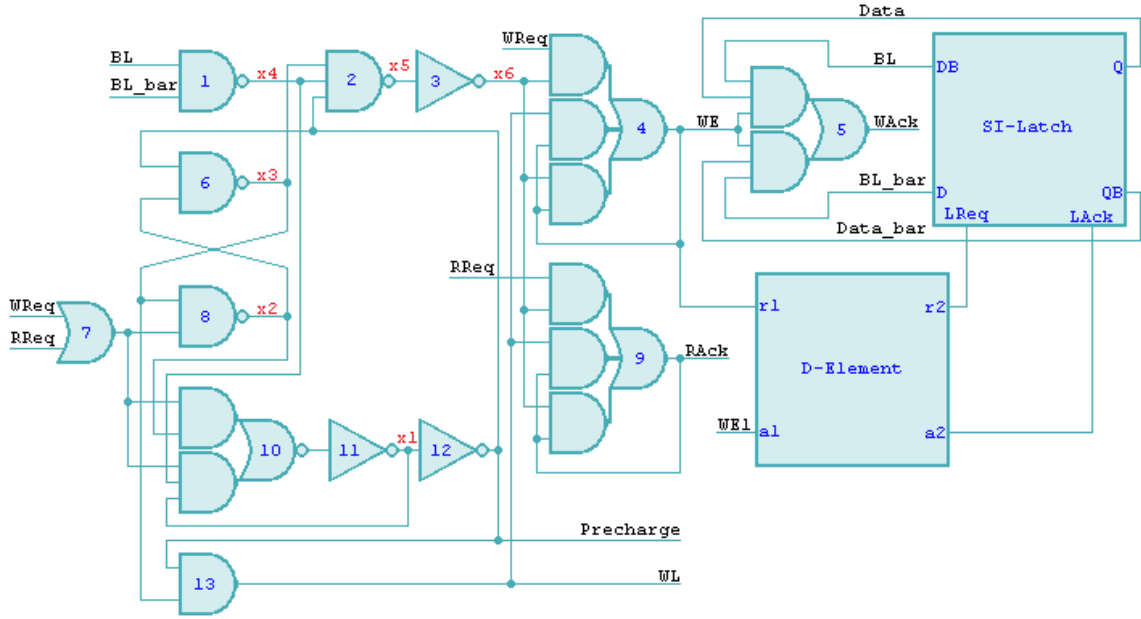


Figure 3.13 Modified timing circuit based on the modified STG.

The scheme of Figure 3.11 is designed for a bundling cell with a controller to manage the timing of a single row. In a multi-row bank, where only one row can be written or read per a request, only a single bundling cell may be working at any time. This means that, whilst the bundling 6T cell should reside next to the row bundled by it for best layout consistency in latency, the timing controller in Figure 3.13 does not need to be replicated for every row and one SI circuit is enough to serve one bank.

It is worth noting that the ability of the proposed design to reuse a previously built and tested component as a main part contributes to the coined name “Smart” along with the other features mentioned above.

### 3.5.2 Timing and Energy Comparisons

In order to study the advantages and disadvantages of the proposed smart latency bundling and guarantee that the gained improvement of performance metrics are worth the sacrificed level of safety, experiments must be carried out, for which this subsection is dedicated. The experiments here involve comparing a bundled SRAM system with a fully SI one in terms of energy and latency per operation. Both designs have exactly the same bank,

decoder, write drivers, prechargers, and SI-latches. However, the SI one uses the previous timing controller connected to all bit lines while the bundled one has a redundant column controlled by the last proposed timing circuitry, both of which as described earlier. After the full-custom implementation of both designs, each of them was tested separately and its full functionality is verified across a wide range of variable VDD, that is from as low as 0.19V all the way up to 1V. The full functionality means safe and correct reading, and successful writing. After verifying the functionality of both SRAMs, the performance and energy calculations are recorded at each value of VDD during reading and writing.

The experiments results are plotted in Figure 3.14, Figure 3.15, Figure 3.16, and Figure 3.17 for writing and reading latencies and energy consumptions respectively. Each calculated value represents an operation of reading or writing a 16 bits word. In each graph two bars are plotted at each voltage level, one is dark blue and the other is light one, both the former and latter illustrate the performance metrics corresponding to the fully SI and smartly bundled SRAM respectively.

The obtained results confirm that despite the bundled design having a redundant column, which means more area and switching, it is still able to save an acceptable amount of energy and timing of the operation across the whole range of voltage. The graphs conclude that the savings in performance metrics during reading is more than that during writing, which occurred because both the latency and energy of writing were worsened by adding two more components to the controller and an extra stage, as described above. The experiments also show that the latency saving decreases as the supplied voltage increases owing to the fact that as the voltage increases the overhead of combining completion signals from all bit-lines decreases. In contrast, the saving in energy increases as the supply voltage increases and that proves the efficiency of the proposed bundling technique in any energy conscious environment. Certainly, the bigger the bank the more saving the bundling technique achieves.

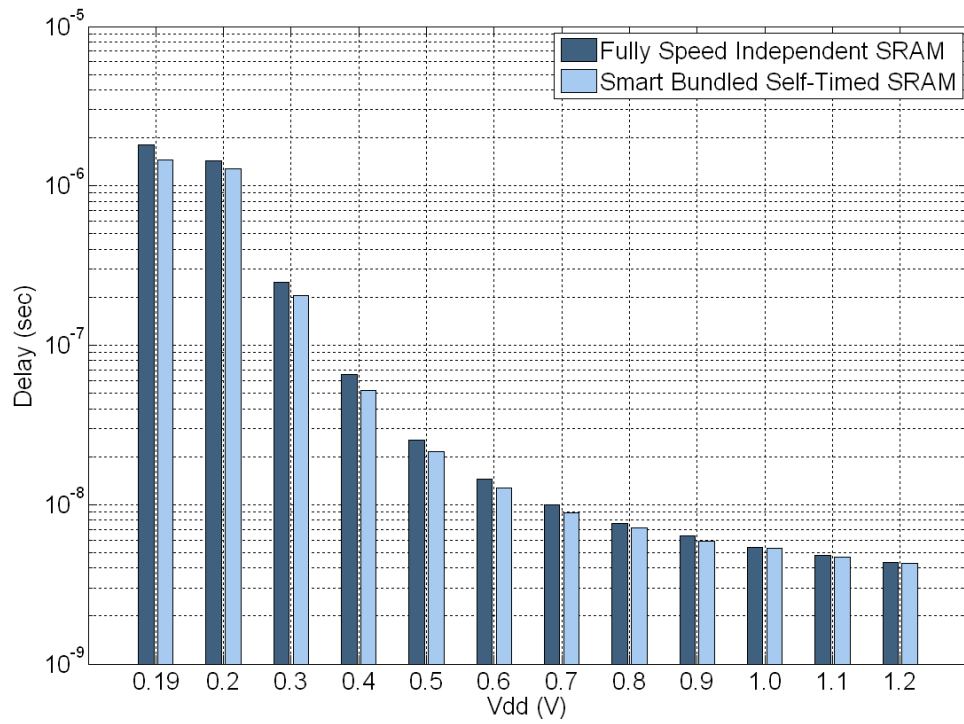


**Figure 3.14 Writing latency comparison between fully SI and smartly bundled SRAM.**

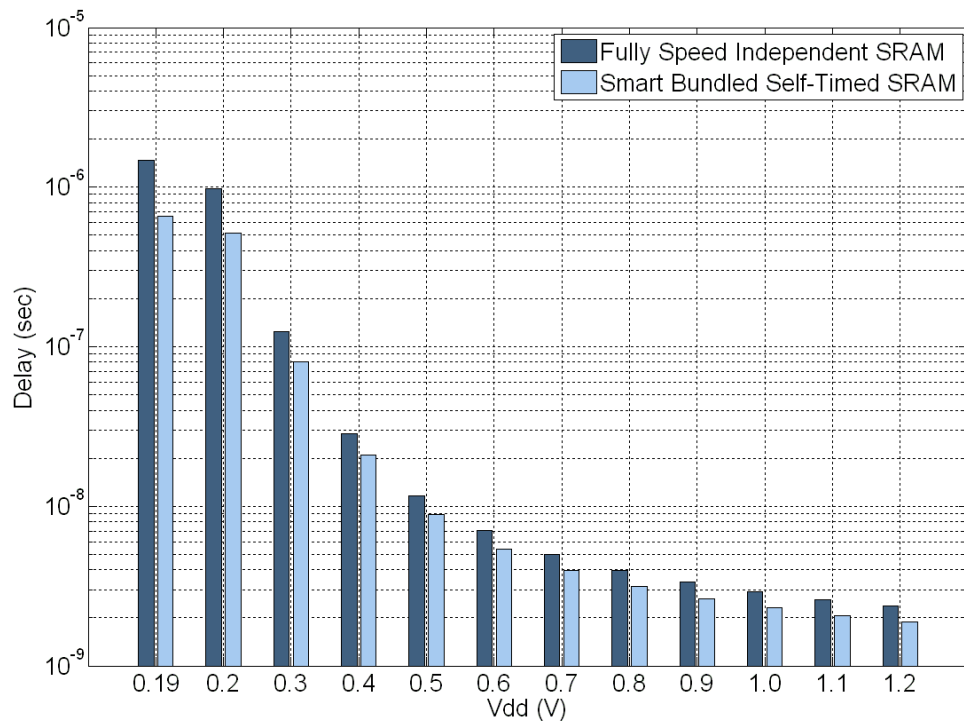


**Figure 3.15 Reading latency comparison between fully SI and smartly bundled SRAM.**



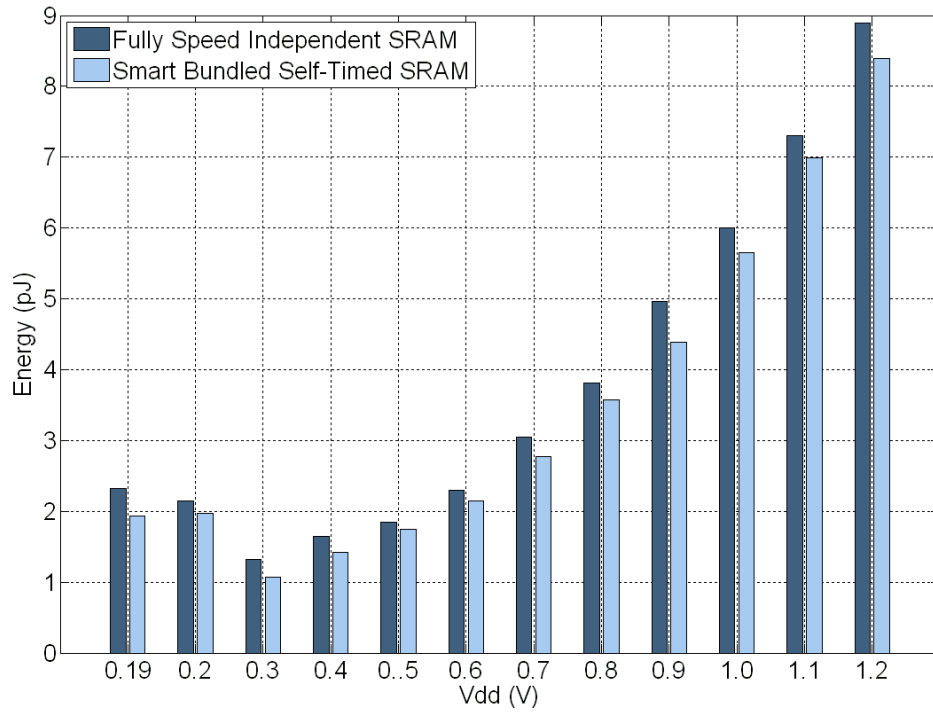


Figure 3.16 Writing energy comparison between fully SI and smartly bundled SRAM.

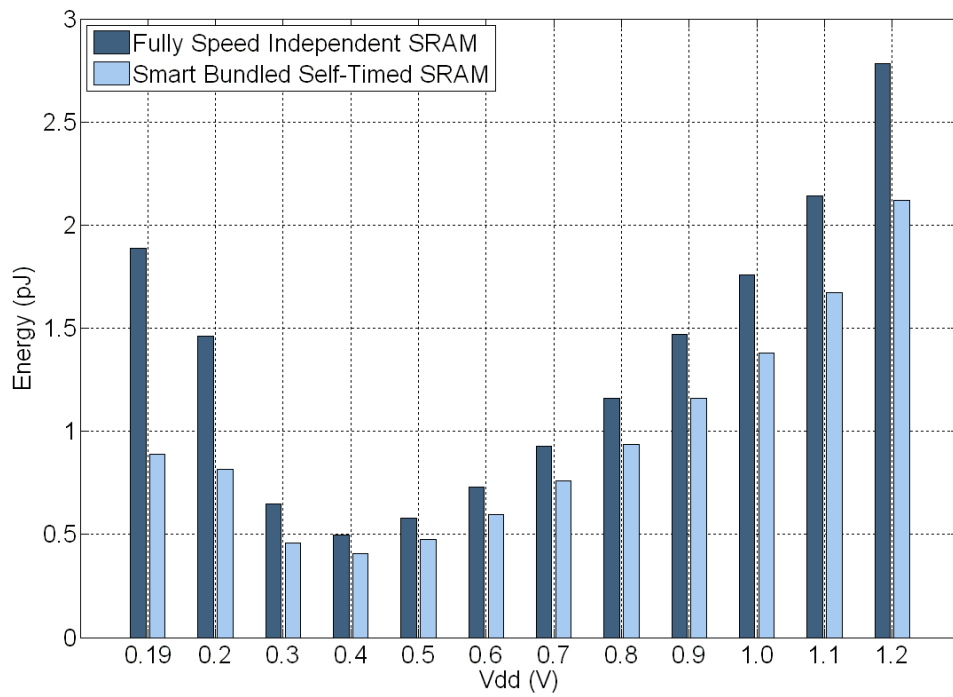


Figure 3.17 Reading energy comparison between fully SI and smartly bundled SRAM.

### 3.6 Conclusion

The aggressive scaling of transistor dimensions increases its process variations, hence considerably varies its threshold voltage, moreover, energy

scavengers supply nondeterministic voltage to their load. These two main factors in addition to other reliability issues significantly affect circuit timing and make it a fuzzy metric during the design time.

Nonetheless, the prevalent techniques of controlling SRAM timing are via the signals generated from a chain of basic gates. Commonly, in case of a wide range of operational conditions, reference voltage is generated and employed to control different delay elements. In both cases, delay elements are designed according to the worst case cell timing [19], moreover, it is compulsory to add a safe margin, during the design time, in order to accommodate any reliability concerns after fabrication. Unfortunately, this technique tends to waste a significant portion of system energy and performance, which exceeds more than twice the required resources, in case of wide range of supply voltage in the context of SRAM. Furthermore, reference voltage is impossible to be generated in a nondeterministic environment.

After pointing out the aforementioned issue, this research attempted to provide a proof of concept of enabling power adaptive computing in the context of energy harvesting microelectronic systems. Practically, the study suggests regulating the data flow in SRAM based on the actual speed of the circuits by employing handshaking protocols. This should cancel all timing assumptions and allow the load to adapt itself for whatever is supplied to it. Importantly, the proposed idea follows the recent ITRS prediction that asynchrony will increase with the complexity of on-chip systems. Unfortunately, until this research proposed its contribution, SRAM had not yet benefited from fully completion detections operations owing to the challenging involved in asynchronous design and the belief of some memory designers that fully and truly handshaking is difficult and impractical for SRAM.

Accordingly, this study provided a method of generating the acknowledgment after completing both reading and writing operation of the SRAM as well as synthesized that behavioural model in an SI circuits.

The beauty of the synthesized timing controller resides in its ability to report the completion of the whole operation (reading/writing) as well as each

stage during the whole operation (precharging, opening access transistors, enabling write drivers). A basic NAND gate, called Gate 1 (Figure 3.5), is used to monitor the bit-lines and report the bit-cell activity to the controller. Therefore, whenever a deadlock happens or the system stops operating, examining the timing circuits tells what the current state is and what the existing problem is. Moreover, the ability of this timing controller to operate the memory under variable VDD highlights the unprecedented feature of changing the operational modes of the SRAM, i.e. DVS, while it is working without the need of stopping the operation nor waiting the supply voltage to settle down. Furthermore, everything is related to and controlled by the voltage knob only. That is whenever the computing logic requires high performance and does not care about the energy, voltage knob should be rotated towards high values while the opposite direction means please complete the task within the supplied amount of energy. In contrast, a synchronous memory system requires two knobs, voltage and clock, which must be rotated in opposite directions and with a predefined amount, otherwise, the whole system fails. Finally, just ignoring the acknowledgment signal of the timing controller means synchronous SRAM, but with high robustness.

Testing the proposed design showed its ability to address the pointed out research gap with acceptable timing and energy calculations. Following that, the study proposed another design based on bundling techniques which is less safe than the fully SI design but lighter as well, a feature making it suitable for large banks.

### 3.7 References

1. A. Baz, D. Shang, F. Xia, and A. Yakovlev, "Self-Timed SRAM for Energy Harvesting Systems," in *Integrated Circuit and System Design. Power and Timing Modeling, Optimization, and Simulation*. vol. 6448, R. Leuken and G. Sicard, Eds., ed: Springer Berlin Heidelberg, 2011, pp. 105-115.
2. A. Baz, D. Shang, F. Xia, and A. Yakovlev, "Self-Timed SRAM for Energy Harvesting Systems," *Journal of Low Power Electronics*, vol. 7, pp. 274-284, 2011.
3. The International Technology Roadmap for Semiconductors, *ITRS Home* [online]. Available: <http://www.itrs.net/>.
4. V. J. Reddi *et al.*, "Voltage Emergency Prediction: Using Signatures to Reduce Operating Margins," in *High Performance Computer Architecture, 2009. HPCA 2009. IEEE 15th International Symposium on*, 2009, pp. 18-29.
5. B. S. Amrutur and M. A. Horowitz, "A Replica Technique for Wordline and Sense Control in Low-Power SRAM's," *Solid-State Circuits, IEEE Journal of*, vol. 33, pp. 1208-1219, 1998.
6. M. Yamaoka *et al.*, "90-nm Process-Variation Adaptive Embedded SRAM Modules with Power-Line-Floating Write Technique," *Solid-State Circuits, IEEE Journal of*, vol. 41, pp. 705-711, 2006.

7. J. P. Kulkarni and K. Roy, "Ultralow-Voltage Process-Variation-Tolerant Schmitt-Trigger-Based SRAM Design," *Very Large Scale Integration (VLSI) Systems, IEEE Transactions on*, vol. 20, pp. 319-332, 2012.
8. A. Yakovlev, "Energy-modulated computing," in *Design, Automation & Test in Europe Conference & Exhibition (DATE), 2011*, 2011, pp. 1-6.
9. S. Jens and S. Furber, *Principles of Asynchronous Circuit Design: A Systems Perspective*: Springer, 2001.
10. S. Vincent Wing-Yun, C. Chiu-sing, and C. Cheong-Fat, "A Four-Phase Handshaking Asynchronous Static RAM Design for Self-Timed Systems," *Solid-State Circuits, IEEE Journal of*, vol. 34, pp. 90-96, 1999.
11. J. Dama and A. Lines, "GHz Asynchronous SRAM in 65nm," in *Asynchronous Circuits and Systems, 2009. ASYNC '09. 15th IEEE Symposium on*, 2009, pp. 85-94.
12. C. Meng-Fan, Y. Sue-Meng, and C. Kung-Ting, "Wide  $V_{DD}$  Embedded Asynchronous SRAM with Dual-Mode Self-Timed Technique for Dynamic Voltage Systems," *Circuits and Systems I: Regular Papers, IEEE Transactions on*, vol. 56, pp. 1657-1667, 2009.
13. L. S. Nielsen and J. Staunstrup, "Design and Verification of a Self-Timed RAM," in *Design Automation Conference, 1995. Proceedings of the ASP-DAC '95/CHDL '95/VLSI '95., IFIP International Conference on Hardware Description Languages. IFIP International Conference on Very Large Scale*, 1995, pp. 751-758.
14. H. Saito *et al.*, "What is the Cost of Delay Insensitivity?," in *Computer-Aided Design, 1999. Digest of Technical Papers. 1999 IEEE/ACM International Conference on*, 1999, pp. 316-323.
15. J. M. Alain, "The Limitations to Delay-Insensitivity in Asynchronous Circuits," presented at the Proceedings of the sixth MIT conference on Advanced research in VLSI, Boston, Massachusetts, USA, 1990.
16. J. Cortadella *et al.*, "Petrify: A Tool for Manipulating Concurrent Specifications and Synthesis of Asynchronous Controllers," *IEICE TRANSACTIONS on Information and Systems*, vol. E80-D, pp. 315-325, 1997.
17. V. G. Oklobdzija, *Digital Design and Fabrication*: CRC Press, 2007.
18. V. G. Oklobdzija *et al.*, *Digital System Clocking: High-Performance and Low-Power Aspects*: Wiley, 2005.
19. B. Amelifard, F. Fallah, and M. Pedram, "Leakage Minimization of SRAM Cells in a Dual- $V_t$  and Dual  $T_{ox}$  Technology," *Very Large Scale Integration (VLSI) Systems, IEEE Transactions on*, vol. 16, pp. 851-860, 2008.

## **Chapter 4. Design, Fabrication and Testing of HoliSRAM**

### **4.1 Introduction**

After proposing a novel design that is able to successfully address the SRAM timing challenge under nondeterministic power supply, it is the time now to prove this functionality on real silicon. Accordingly, this chapter is dedicated for the design, fabrication and testing of the proposed SI SRAM in a chip, coined HoliSRAM. This name was elected by the research supervisor as a proof of concept of employing the holistic approach of the project in developing such a power adaptive SRAM. It is worth highlighting that, while this chapter tries to cover comprehensively the design and fabrication of the HoliSRAM chip, it, at the same time, avoids reporting some details regarding the employed technology or the used EDA/CAD tools, which break the Non Disclosure Agreement (NDA) of using these technologies and/or tools. These details include but are not limited to cells structures and measurements, particular design rules and almost all screenshots of the tools. The current chapter consists of four main sections, where the next one describes the chip architecture and the reasons behind designing each of its main components. The third section discusses the design flow of the chip together with the involved challenges. Following that, chip testing and measured results appeared in the fourth section. Finally, the last section concludes the chapter and highlights the key achievements.

### **4.2 Chip Architecture**

HoliSRAM is a chip designed for the aim of demonstrating the ability of the self-timed SRAM to work under nondeterministic variable VDD (i.e. Fig-

ure 3.6). Unfortunately, this kind of operation for such an application is very limited in literature, hence, the researcher mainly started from his thoughts. Furthermore, the problem does not only reside in the design phase but in the testing as well. This is because the design is new and accordingly the full functionality has to be guaranteed, which means running a huge amount of testing to cover all combinations of data and addresses across the targeted range of VDD. Based on that, the researcher decided to add testing circuitry around the SRAM on chip and control that from outside the chip. These testing components aim to autonomously test and check all operations of the self-timed SRAM by almost all combinations of data and addresses, especially those combinations reflect the worst case bit-line leakage. The aforementioned reasons resulted in the chip structure shown in Figure 4.1. The general function of this circuitry is to write, read, and compare the written data with the read ones in an asynchronous and autonomous manner, without any interactions from the user or environment.

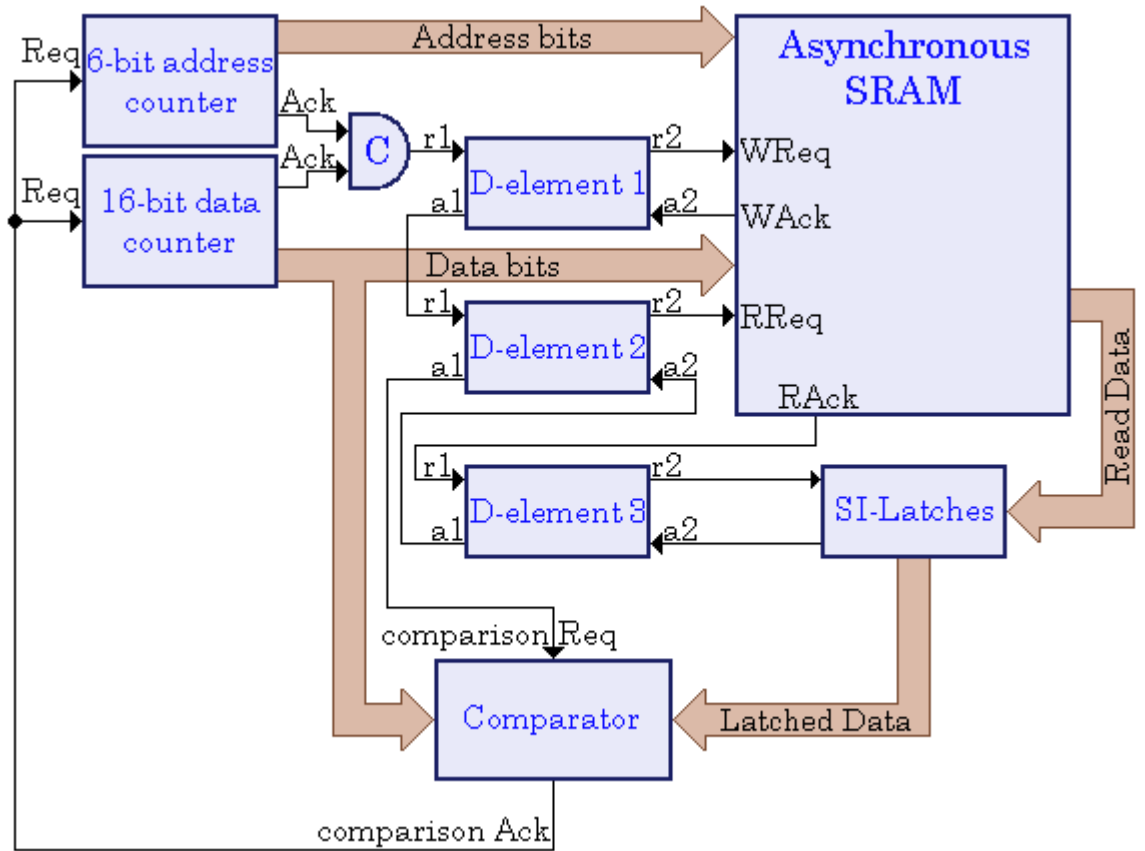


Figure 4.1 Main part of the HoliSRAM chip.

This structure contains two asynchronous counters to generate address and data and three D-elements to manage the write and read cycle handshakes. The D-element is a popular asynchronous handshake interface circuit, which encloses a slave handshake inside a master one [1]. The self-timed counters are based on the design found in [1]. There is also a comparator, based on an XOR logic triggered by the a1 signal of the second D-element, which determines the consistency or the lack thereof between the written and read data. The outputs of all XOR gates are combined by a C-element to provide the consistency confirmation signal. If there is at least a single bit of disagreement, a negative result is returned.

The signal flow of the chip is as follows: The first counter generates the address and sends its acknowledgement signal to the C-element. Asynchronously, the second counter generates the data and sends its acknowledgement signal to the C-element. Once both counters settle, the C-element sends its acknowledgement signal to the first request (r1) of the first D-element. That D-element works as a writer and sends the WReq signal to the controller inside the asynchronous SRAM to request writing. Once writing finished, the memory replies with the WAck signal to D-element 1. Accordingly, D-element 1 withdraws the WReq signal to rest the SI controller and then sends a request signal to the second D-element, which as a reader sends an RReq signal to the SRAM to request reading. Once reading is completed, the SRAM responds with the RAck signal to the third D-element, which acts as a downloader, to download the read data to the SI-latches. Upon latching the data, D-element 3 resets the buffers and acknowledges that to the second D-element, which in turn withdraws the RReq signal to reset the memory controller, and after that it requests the comparator to compare the read data with the written ones. It is compulsory to guarantee both compared data are stable before starting the comparison, which occurs here since the data counter is stable and the SI-latches are ideal. Consequently, the comparator starts to judge whether the read data is the same as the written ones or not, in a bitwise manner. If and only if all corresponding bits of both data do match, the comparator acknowledges that to both counters to start another round. This means that a round of writing follow-





erate properly. Accordingly, several configuration registers are added to the chip for the purpose of turning on/off the closed loop in the circuitry of Figure 4.1. If the closed loop is deactivated, the configuration registers allow the user to access both data and address counters and assign them specific values before requesting the operation. Consequently, the chip ended up with two main testing modes:

1. Fully autonomous mode, in which the user sends a start signal and accordingly the entire circuitry enters an infinite loop of generating address and data, write, read, and comparing the written data with the read data. This loop continues so long as the compared data are consistent. Moreover, the included configuration bits allow the user to configure both counters independently to start from zero or a specific value and increment every turn or halt at a defined value. This feature gives the opportunity of testing the SRAM under all combinations of address and data, as well as, concentrating in a specific range of values for troubleshooting.
2. Off the chip mode, in which the user uploads both the data and address to the data and address counter respectively, and then initiates the operation.

These testing modes increased the challenges involved in designing such a chip. In order to safely configure the testing modes and guaranteeing the settlement of configuration bits, all registers containing the configuration information should be powered by the nominal voltage all the time while the entire self-timed SRAM (DUT) has to be tested under variable VDD. Therefore, the chip ended up combining dual power domains supplied externally. Nevertheless, it is worth highlighting that one power domain is sufficient to operate the proposed self-timed SRAM, however, the need for another one is imposed by the targeted testing modes. Since the circuitry in both domains exchange information before and after testing, a proper signal communication technique between domains is required. Signal communication cannot be conducted via level shifters, as one of the domains is completely variable. Challenges do not stop at dual power domain nor at the communications be-

tween them. Moreover, the lack of standard cells to support some essential components in SRAM and asynchronous design (e.g. prechargers, write drivers, C-elements, multiplexers), forced the researcher to lay these circuits out using full-custom designs. Accordingly, the whole design ended up in a chip requiring dual power domains (nominal voltage for testing circuitry and variable voltage for DUT) and dual cell design (standard library and full-custom cells). The next couple of sub-sections are responsible for covering the design of each part separately together with the integration between them.

#### 4.2.1 Dual Power Domain Design Phase

Figure 4.3 shows another view of the HoliSRAM chip, it contains two main parts, which are the variable power domain part and stable power domain part. The former mainly contains the block diagram in Figure 4.1 in addition to some auxiliary circuits for buffering and latching.

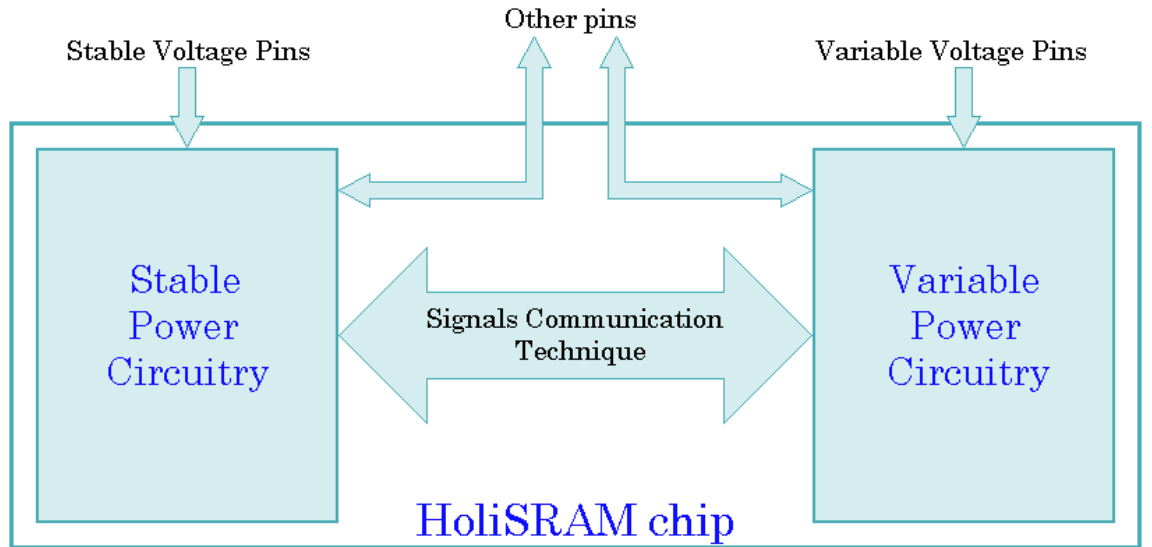


Figure 4.3 Power domain view of the HoliSRAM chip.

The stable part is much smaller than the variable one and it comprises other testing facilitating circuitry, which is designed outside the scope of this thesis, and its main purposes are to allow the user:

1. Configure the chip for a specific testing mode, i.e. full autonomous mode or off the chip mode.

2. Set up the mode and the starting state of the address and data counters.
3. Select the type of the operation within the chosen testing mode (e.g. single reading/writing, recursive reading/writing, same address reading/writing, same data reading/writing, etc).
4. Download the data from the SRAM bank.

The voltage rails of all circuit components in each power domain are connected together and the signal communications between the two domains are achieved by means of transmission gates, designed according to the results obtained from the following experiment.

A straightforward experiment was conducted here to investigate the suitable way to exchange signals between the involved power domains. The experiment compared between two methods, normal logic design method based on logic gates and logic design based on transmission gates as shown in Figure 4.4.

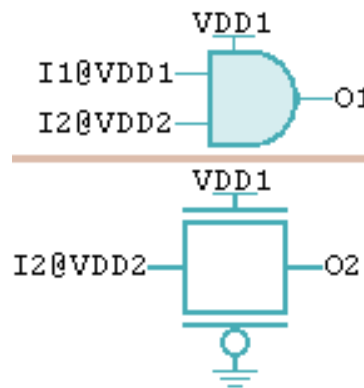


**Figure 4.4 A method to investigate suitable way of signal communications.**

On the top, a basic AND gate is powered from a single power domain and required to communicate a signal from a different domain (I2). Similarly, the transmission gate in the lower part of the figure carries out the same task. Different combinations of inputs and supply voltages are tried in these two designs, where the results confirm that the latter outperforms the former via communicating the signal faster and without any distortion as

shown in Figure 4.5 for one of the cases. Moreover, a transmission gate requires fewer transistors.



**Figure 4.5 Waveforms of the signal communication experiment.**

#### 4.2.2 Dual Cell Design Phase

Unfortunately, standard cells do not support all kinds of cells and circuits, hence, some components employed by the HoliSRAM chip are required to be laid out using full-custom design techniques. These components include bit-cell/bank, C-elements, write drivers, multiplexers, de-multiplexers, and pre-chargers. According to the number of instances the chip has of each component and whether the instances are directly connected to other standard cells or not, these components are categorized into two main categories as follows.

The former category includes C-element, multiplexer, and de-multiplexer, which are all required by the design metrics to reside as nearest as possible to the connected standard cells for high efficiency in terms of power, area, signal propagation delay and layout consistency. This, however, requires to design all these cells according to the design rules of standard cells and Place and Route (P&R) them via the automatic P&R tool. Standard cell design rules are a complete set of rules, which include grid dimensions, cell-width, cell-height, pin text, boundary rules, cell structure, etc. Obeying these rules add a level of difficulty to layout the mentioned cells because it

requires combining the design rules of the standard cell with those of the employed technology itself.

The latter category includes bit-cell, bank, precharger and write driver. All these cells are either not directly connected to the standard cells or connected but are repeated a few times. This design condition gives those cells more freedom about where to reside in the design and the required design technique.

### **4.3 Chip Design Flow**

The previous section discussed how the researcher shaped up the chip architecture and structure according to the testing modes he targeted along with the design techniques and rules involved in each part of the chip. Therefore, it is the time now to start the real design flow, towards that this section is dedicated.

Firstly, the researcher started by designing the transistor level of the full-custom cells, following that, he combines the cells he designed with other standard cell components to form the main circuitry of the chip (e.g. decoder, SI timing controller, etc.). After that, he compiled all circuits and components into one schematic file that contains two main parts each powered separately as described earlier.

Before laying out the layers of the obtained schematic file, it is crucial to examine the operation of the whole chip under the nominal operational conditions as well as under the effect of process variations. This step would help in guaranteeing the functionality of the chip after fabrication along with its operational limits. The following subsection covers the experiments and obtained simulation results in more details.

#### **4.3.1 Results of Chip Simulation**

Simulating the design in Figure 4.1 confirms its functionality according to the design goals and testing strategies as depicted in Figure 4.6. The timing waveforms show that the internal circuits issue the WReq signal, after generating the address and data as requested, and then hand the job over to the SI timing controller. The timing controller achieves its job by generating the

Precharge, WL, WE, and finally WAck signals according to the internal operation in SRAM. Following that, the control is returned back to the main circuits, which withdraws the WReq, to reset the controller, and then issues the RReq. Consequently, the controller starts the reading round and at its end, it returns with the Rack signal, to the main circuits, which ends the reading round, resets the controller, and starts the comparison. After each successful comparison, another complete handshake cycle starts again. Generated data and address along with the comparison signals are hidden in Figure 4.6, where the detailed timing relationships can be shown in Figure 3.6.

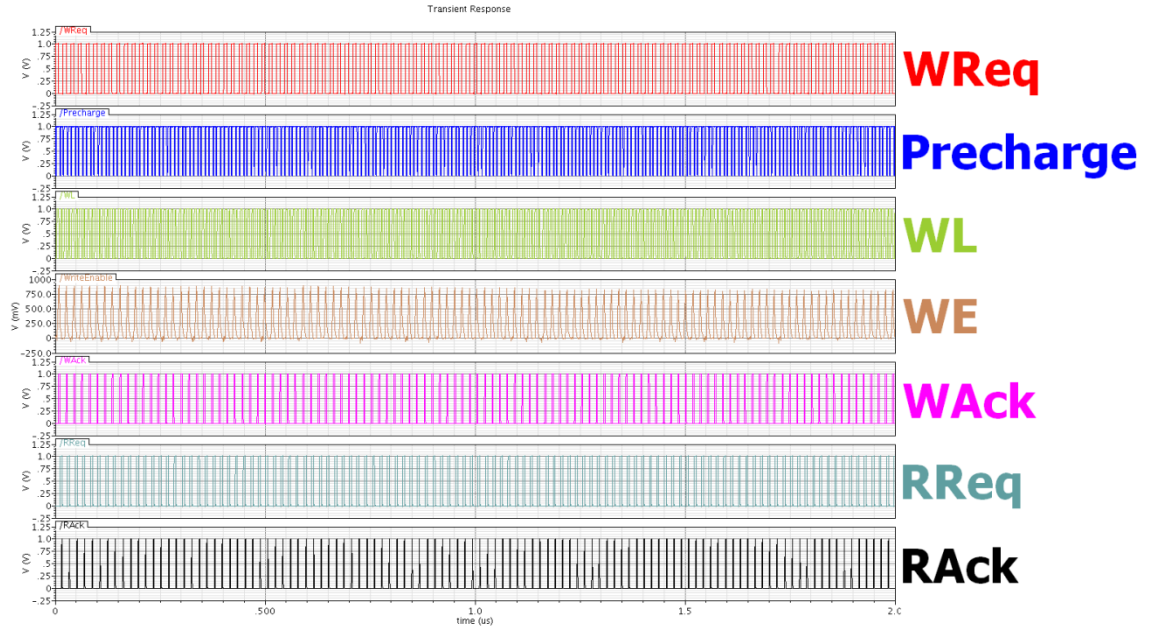


**Figure 4.6 Timing waveforms of the closed loop self-timed SRAM.**

The previous experiment is repeated again for the purpose of investigating the susceptibility of the chip core to process variations. This experiment involves 45 simulations, each with different operational conditions, which in total cover all process corners (SS, FF, TT, SNFP, and FNFP), and VDD between 0.2V and 1V. The experiment results are plotted in Figure 4.7 and that shows the time required for the design in Figure 4.1 to complete writing, reading, and checking the whole SRAM, row by row, across different process corners and voltages. The results gained from this experiment confirm that below 0.4V, the closed loop of the handshaking cycle stops working at some corners, this reflects upon the graph as no values were plotted be-

low this voltage value. Further investigation was conducted to figure out the reasons behind this issue, which was found to be that 0.4V is the working limit of the address and data counter under process variations.

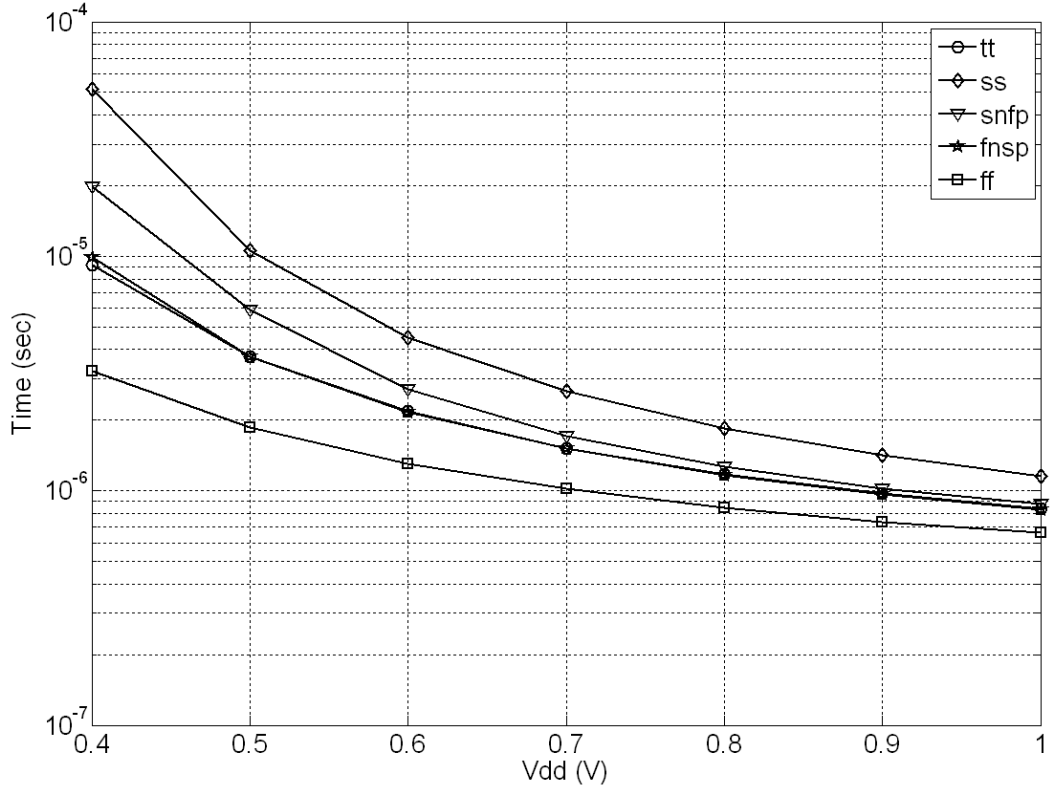


**Figure 4.7** Corner analysis of the HoliSRAM core.

As the corner analysis only captures the worst/best/typical timing case of the fabricated devices, more analysis is required in order to determine the failure rate of the core chip. Therefore, the researcher employed Monte-Carlo analysis to investigate the functional yield of an SI SRAM cell, including the proposed timing controller. The experiment tested the SRAM along with its controller using a thousand samples drawn from a space covering 99.9% of the variation distributions ( $\sigma = 6$ ). Functional yield is defined as the ratio of successful simulations to the total number of simulations, where successful operation has to satisfy the following four mandatory conditions:

1. After receiving the request signal, the timing controller has to generate the signals in the order depicted in Figure 3.4.

2. If the operation is writing, it has to end up with flipping the cell and the cell has to hold the new data until withdrawing the acknowledgment signal.
3. If the operation is reading, it has to end up with latching the data in the SI-latches and the cell has to stay settled until withdrawing the acknowledgment signal.
4. After taking down the request signal, the timing controller has to reset itself by withdrawing all signals in the order described in ure 3.4.

The results of the Monte-Carlo simulation are listed in Table 4.1, which concludes that the SI SRAM has an acceptable functional yield of 99% for all voltages ranging from 1V down to 0.3V and 0.5V for reading and writing respectively. The results also show that for the considered case of process variations, the SI SRAM starts to experience failures as the voltage decreases below 0.5V.

**Table 4.1 Functional yield of the SI SRAM.**

VDD (V)	Functional Yield %	
	Writing	Reading
1.20	99.9	99.9
1.10	99.9	99.9
1.00	99.9	99.9
0.90	99.9	99.9
0.80	99.9	99.9
0.70	99.9	99.9
0.60	99.9	99.9
0.50	99.7	99.9
0.40	97.6	99.9
0.30	87.9	99.9
0.20	72.8	94.8
0.19	71.8	86.2

Nevertheless, this functional yield does not mean that the circuitry will completely stop working below 0.5V, however, it shows what is most likely to happen if the fabricated chips experience a high level of process variations.



In conclusion, the proposed chip circuitry confirmed the ability to meet the design goals and testing strategies with an acceptable yield and worst case analysis and that means full functionality between 100% and 42% of the nominal voltage and partial functionality below that. This result suggests taping the chip out, accordingly, the next subsection covers the process of converting the final schematic developed in this section to real silicon layers, fully described in the Graphic Database System II (GDSII) file and ready for fabrication [2].

#### **4.4 Chip Testing**

After receiving the chip, the researcher started to prepare for testing according to his testing goals explained above. It is the aim of the researchers to test the fabricated chip in different environments each one was called stream. Stream I involved examining the functionality of the chip using all possible testing modes and procedures via an FPGA. Stream II includes demonstrating the functionality in a portable board by the means of a microcontroller, in which the user can interact with the SI SRAM via a developed program interface. It is worth mentioning that stream II is the one involved in this thesis, more information about the demonstration can be found in the project website: <http://www.holistic.ecs.soton.ac.uk/>

##### **4.4.1 Stream II Demonstration: a Portable HoliSRAM Box**

The main aim of the stream II demonstration is to demonstrate the full functionality of the self-timed SRAM without equipping any testing instruments, only a laptop suffices.

Figure 4.8 depicts the system diagram of stream II demonstration, which involves designing the required logic to demonstrate the functionality of the HoliSRAM chip in a portable box the size of A5 paper.

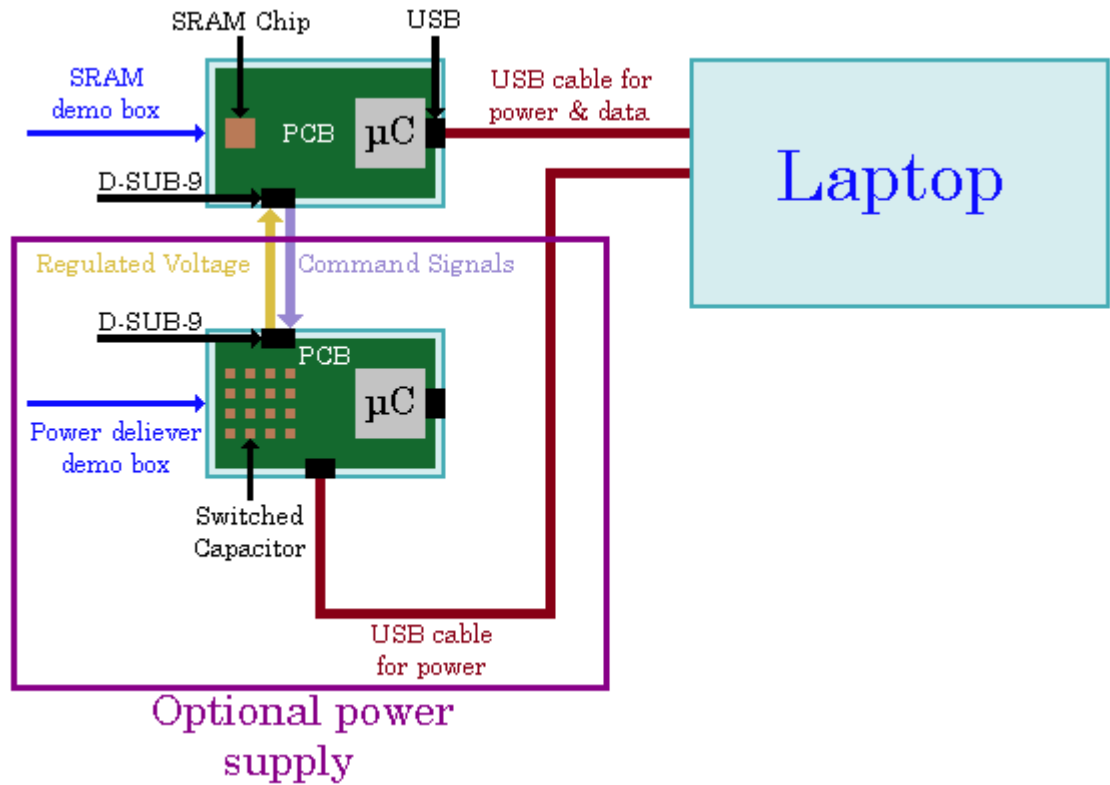


Figure 4.8 Stream II demonstration system diagram.

The entire demonstration box is required to accommodate the SI SRAM chip together with a microcontroller connected via a USB cable to a personal computer. It is the responsibility of the researcher to develop the program together with the interface required to allow the user to interact with the microcontroller, which accordingly interact with the HoliSRAM chip. Due to the low power design methods involved in designing the SRAM chip, it is found that only one USB cable is sufficient to serve both data and power to the chip, microcontroller, and all logic in the box. It is intended to add an important feature to this portable box, which allows it to power its components either from an in-box regulator or a D-Subminiature-9 connector supplied externally. This feature would help future demonstrations of this research.

Drawing the block diagram of the demonstration box is the first step towards developing it from scratch. This step strongly depends upon the type of the employed microcontroller, since the electrical characteristics of it along with those of the HoliSRAM chip will determine the other logics required inside the box. For the purpose of this demonstration, it is found that

PIC32MX795F512L (abbreviated PIC32 thereafter) is sufficient, which is one of the most recent microcontroller developed by Microchip Technology Inc. ([www.microchip.com](http://www.microchip.com)). This PIC32 is a 100-pin package operating at 80MHz and 3.3V, and provides almost all functions of most  $\mu$ Cs. Unfortunately, the voltage level of the chosen  $\mu$ C is completely different from those voltages required by the HoliSRAM chip, but that would happen with any other type of off the shelf  $\mu$ C. Precisely, the chip requires three voltages, which are 1.2V for the stable power domain part, 2.5V for the I/O cells, and unstable voltage between 0.4V and 1.2V for the DUT. To address such a circumstance, the researcher needs to add some Low DropOut (LDO) regulators to the board in order to convert the voltages from the  $\mu$ C domain to the HoliSRAM domain. Just now, the block diagram of the demo system can be drawn, which is shown in Figure 4.9. It comprises the  $\mu$ C, HoliSRAM chip, three LDO regulators, two banks of Level Shifter (LS) and a digital POTentiometer (POT). Two of the LDO regulators convert the 3.3V to 1.2V and 2.5V. The last LDO is an adjustable one controlled by the included POT to supply a variable voltage in the range between 0.4V and 1.2V, which is abbreviated Var\_VDD thereafter. The digital POT itself is set up via the Serial Peripheral Interface (SPI) via the microcontroller.

For the reasons explained earlier, all configuration registers are accessed at 2.5V while data, address, request, and acknowledgment signals are communicated at a variable voltage ranging between 0.4V and 1.2V. Accordingly, it is required to have a means of signal communication between these power domains. For this purpose, the box will accommodate two different banks of LS, the upper one communicates the configuration bits while the one in the middle communicates the signals of the DUT. The former is supplied by the 3.3V from the  $\mu$ C and 2.5V from the LDO, while the latter is supplied by 3.3V from the  $\mu$ C and Var\_VDDV from the other LDO.

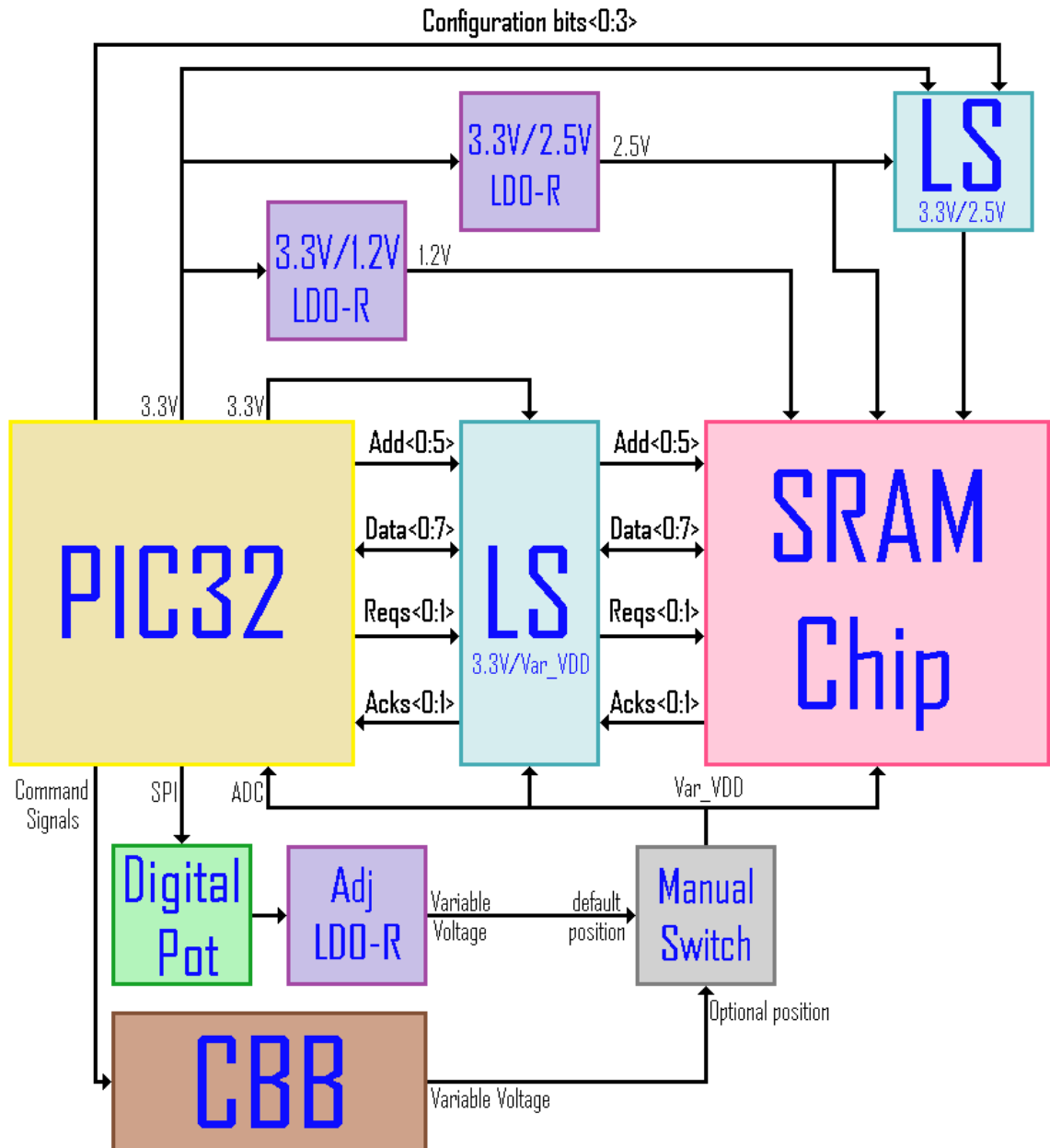


**Figure 4.9 Block diagram of the SRAM demonstration box.**

Following completing the jigsaw puzzle of the block diagram, it is now ready for the swapping stage, in which each block is replaced with the proper off the shelf component that fits the purpose of it. Certainly, this phase required searching the database of the IC's suppliers like FARNELL, RS, TI, etc., reading the datasheets of the available components, and conducting numerous experiments in the lab to check out the ability of the chosen components to suffice its purpose. The main challenge faced here was the disappearance of the some components from the stock after verifying their suitability. This forced the designer to replace the out of stock component with

the next best available one. Finally, the components ended up as shown in Table 4.2.

**Table 4.2 Components list of the portable demonstration box.**

Block	Real Component	
	Manufacturer Part No	Manufacturer
$\mu$ C	PIC32MX795F512L	Microchip Technology Inc.
LS	TXB0304	Texas Instruments Inc.
LDO	MCP1726	Microchip Technology Inc.
Digital Pot	MCP4162	Microchip Technology Inc.

Despite that the chosen components are the best available that suffices its purpose, yet, some of them do not fully fit their purposes. For instance, the LS TXB0304 is able to convert signals between 0.9V and 3.6V, which is the widest range available in the market. However, the demo requires conversion below 0.9V, for that purpose the in-lab experiment confirms that below 0.9V, TXB0304 can convert signals but the operation strongly depends upon the gap between the high and low supplied voltages. Accordingly, all DUT signals are converted by the means of two stages of LS to allow them to communicate information down to 0.4V. The first stage, from the side of  $\mu$ C, converts between 3.3V and 1.2V while the next stage converts between 1.2V all the way down to 0.4V.

In addition to defining each component in the block diagram, the testing board requires the knowledge of what port in the  $\mu$ C are connected to which component. Accordingly, the designer determines all ports needed for the purpose of the demo, which are all listed in Table 4.3 along with the port type and its duty. The next to last step is designing the required logic around each component and testing the whole demonstration system in a breadboard. Following successful testing, it is the time to draw the final schematic of the PCB and send it for fabrication and components installation. For this purpose, a couple of circuit design tools were employed, Multisim and Ultiboard, both of which are provided by National Instruments Corporation ([www.ni.com](http://www.ni.com)).

**Table 4.3  $\mu$ C ports employed during the demonstration.**

Purpose	$\mu$ C ports	
	Port name	Type
SRAM address	RB8-RB13	Output
SRAM data	RB0-RB7	Input/Output
WReq	RC1	Output
RReq	RC2	Output
WAck	RF0	Input
Rack	RF1	Input
Configuration bits	RE0-RE3	Output
Secondary supply setting bits	RE5-RE8	Output
SPI for POT	SPI2	Output/Input
ADC for Var_VDD	RB15	Input

#### 4.4.2 Interactive Interface for Interactive Demonstration

After receiving the fabricated board with all components installed, it was tested for any manufacturing defects and all of them were correctly fixed. Following that, the researcher started to compile and complete all codes, employed during testing, under a single interactive interface to enable the user interacting with the self-timed SRAM via the  $\mu$ C. For the purpose of developing the interface, MPLAB was employed, which is an Integrated Development Environment (IDE) tool provided by Microchip Technology Inc. ([www.microchip.com](http://www.microchip.com)). The following paragraph briefly describes the general duty of the program while all details together with the codes are listed in Appendix A.

The program was developed in an interactive way that allows it to exchange the data, measurements, and information extracted from the HoliSRAM chip with the user. Moreover, the tool enables the user to control and command the SRAM by the all possible means. Starting from powering the SRAM, the user can power the SRAM either from the built-in adjustable regulator or a Capacitor Bank Block (CBB) [3]. In both options, the user can enter a specific value to generate stable voltage or a range of values to generate variable voltages in that range. The user can also play with the self-timed SRAM by either reading from it or writing to it, in both cases he has the option of accessing the whole SRAM or alternatively accessing any randomly selected address. Once the  $\mu$ C receives all the required information, it starts dealing with the request and informs the user, via the interface, with

what is happening inside the SRAM. More specifically, the user is briefed with the current VDD value, the working address, the accessed data, whether the operational condition allows the SRAM to complete the task and generate the acknowledgment signal or not, and whether the SI controller can be reset or not.

#### 4.4.3 Measurements and Testing Results

After successfully completing all the previous stages, it is plug and play time, where everything is put together and tested under a single framework. The portable demonstration box is pictured from all sides, to show the components involved in each one and the whole picture appears in Figure 4.10.

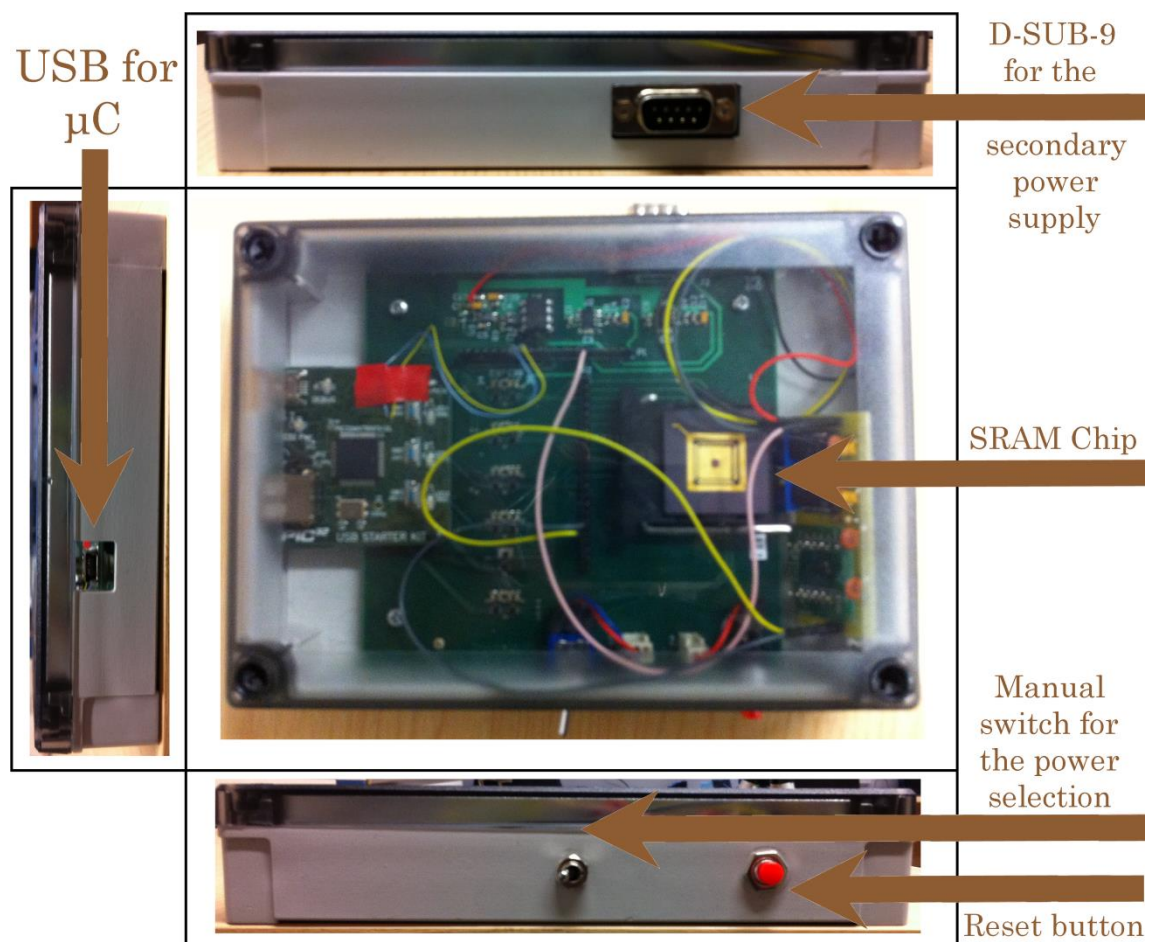


Figure 4.10 Portable demonstration box pictured from all sides.

Upon running the program, the HoliSRAM chip shows full functionality that matches the design aim. Firstly, the SRAM was tested under the nominal stable voltage by exploiting all combinations of addresses and data during both reading and writing. For all cases, the SRAM affirms the safe and cor-

rect reading and successful writing, where writing is tested by a subsequent reading. Figure 4.11 and Figure 4.12 show the oscilloscope snapshot for one of the reading and writing cases respectively. Both figures have the request signal at the top, vertically followed by acknowledgment, MSB of address and LSB of data respectively.

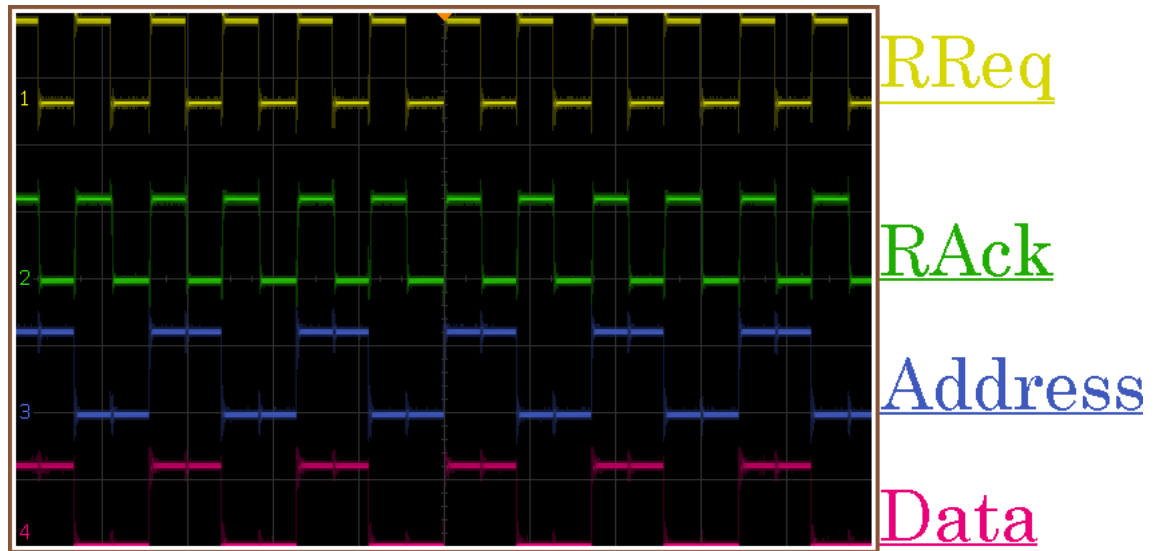


Figure 4.11 Oscilloscope screenshot for the HoliSRAM critical signals during reading.

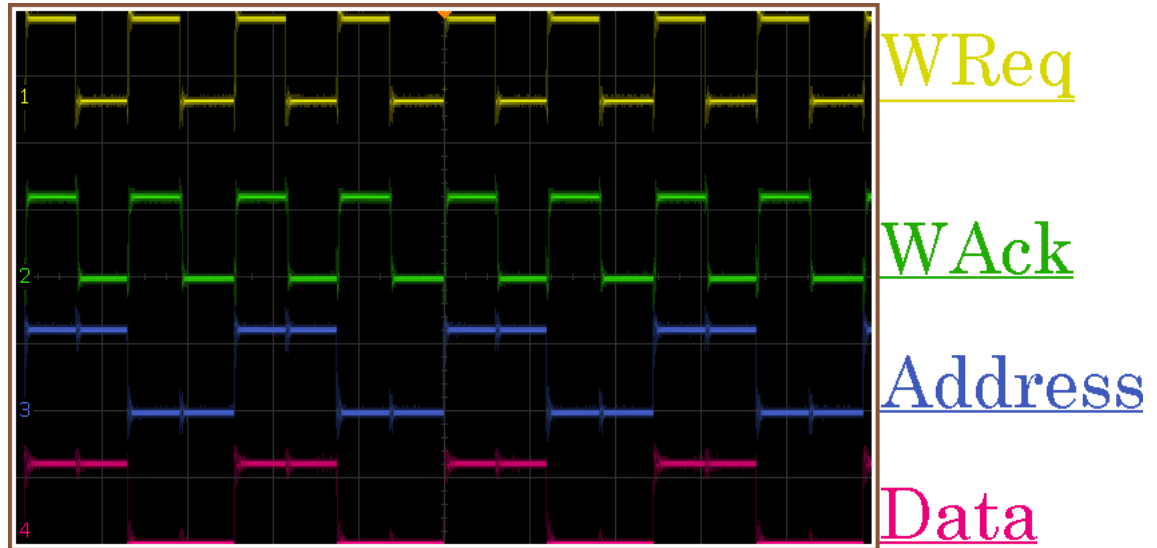


Figure 4.12 Oscilloscope screenshot for the HoliSRAM critical signals during writing.

Afterwards, the chip was tested under a variable supply voltage, a typical scenario in an energy harvesting system. The range of variable voltage started to vary between 1.2V and 1.0V, and then the range increased gradually to cover all voltages between 1.2V and 0.4V. Two signal types of variable voltage were employed in the testing, the former is a sawtooth, which



appears in Figure 4.13, while the latter is a sinusoidal and it appears in Figure 4.14. Both figures have the VDD signal at top vertically followed by WReq, WAck, RReq and RAck signals respectively. The experiment involves recursive writing, followed by recursive reading, where the data is compared via the developed tool. The obtained waveforms show two regions of operations, one between 1V and 0.75V and the other between 0.75V and 0.4V. The former reflects correct and full functionality of the chip while the latter reflects an ambiguous region, where the acknowledgment signals hardly appear denoted by the gaps in Figure 4.13 and Figure 4.14.

Importantly, these genuine signals, which are extracted from a real piece of silicon, confirm the ability of the proposed asynchronous SRAM to tolerate supply voltage variations up to 64% of the nominal value in addition to the embedded process variations in 90nm technology. This high level of robustness is acquired via regulating the data flow inside the SRAM according to the actual speed of the circuit, which has a deep gratitude to the proposed smart completion detection technique. The proposed SI timing controller is acknowledged as well for its ability to tolerate the delay variations inside its component in order to generate hazard free signals. In terms of Data Retention Voltage (DRV), the HoliSRAM chip confirms preserving the data down to 0.4V at room temperature.

Notably, the real signals highlight an important philosophy behind the proposed design technique of this study, which states that only one knob (i.e. the supply voltage) is sufficient to control everything. If that knob is rotated towards high values, it means do the job with the highest performance regardless of the energy consumption. However, if the knob is spun in the opposite direction, that means complete the task within the supplied amount of energy and do not concern the performance. In contrast, in the synchronous counterpart, two knobs are required (i.e. the supplied voltage and clock) where both must be rotated in the opposite direction with a sensible amount, which is pre-defined based on the worst case scenario, otherwise the whole system would certainly fail. The above highlighted philosophy is a

proof of concept of enabling power adaptive computing in the context of energy harvesting systems.

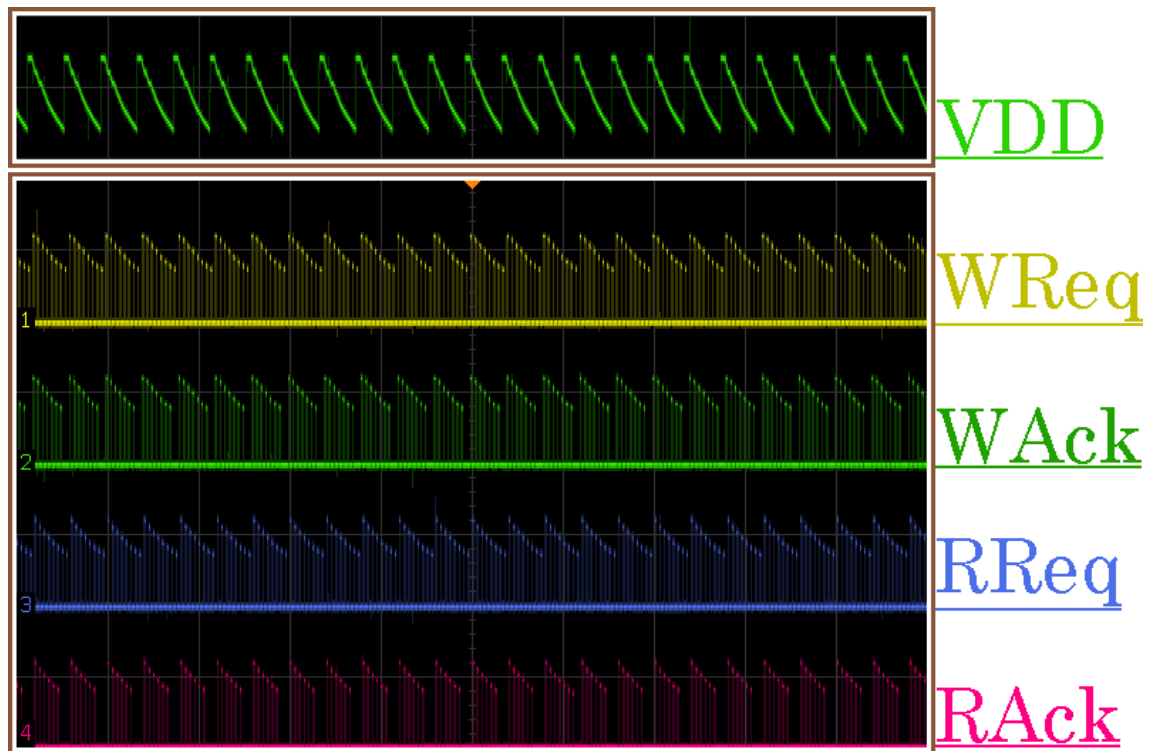


Figure 4.13 Oscilloscope screenshot of the HoliSRAM chip under a sawtooth voltage.

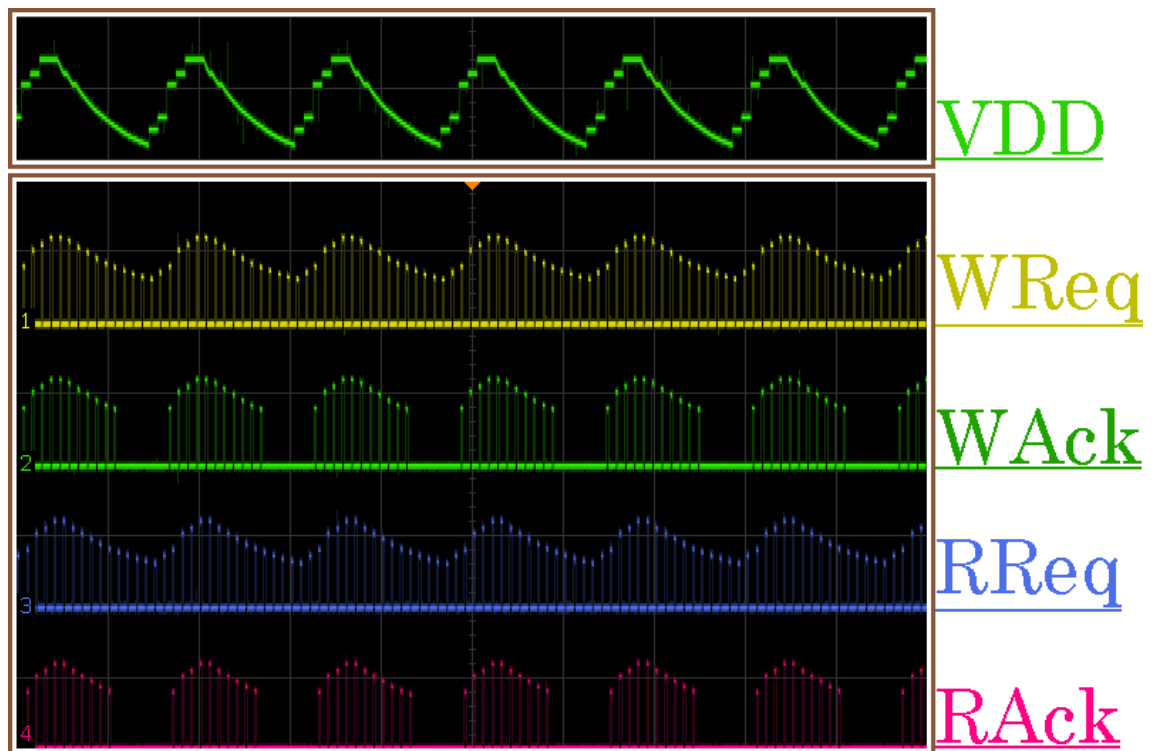
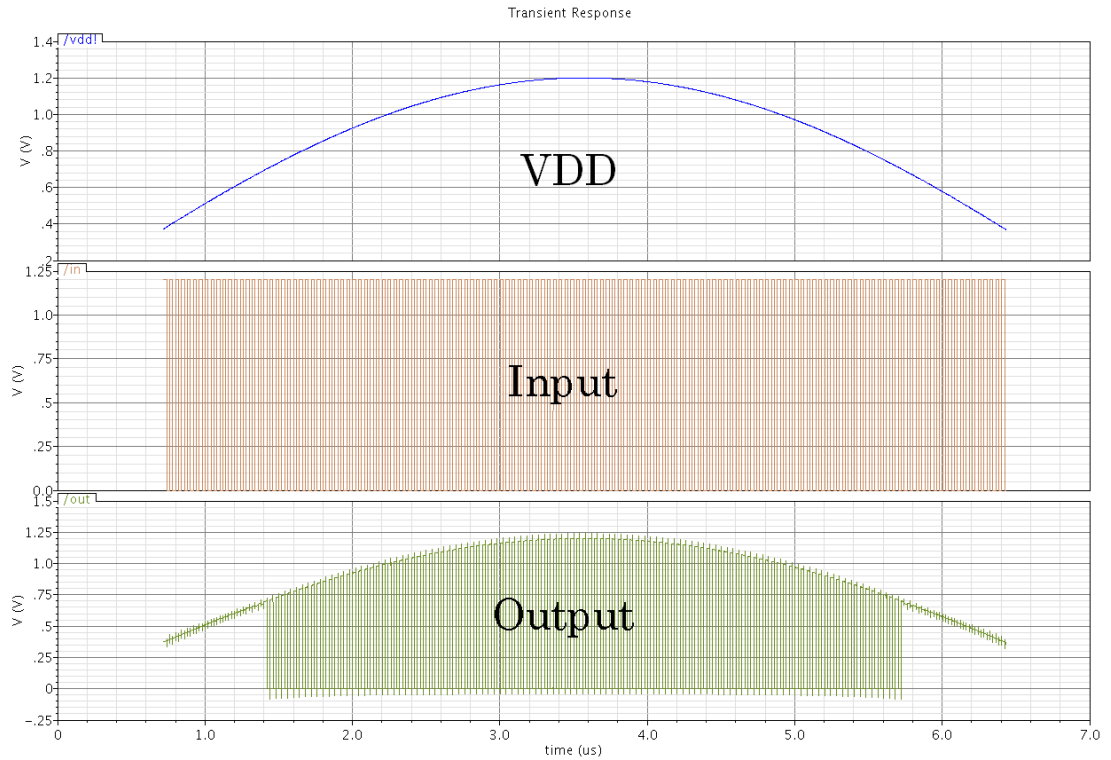


Figure 4.14 Oscilloscope screenshot of the HoliSRAM under a sinusoidal voltage.

Unfortunately, as stated above decreasing the VDD below 0.75V causes the SRAM to stop working, more precisely, the internal timing controller suddenly halts at its current state. Certainly, increasing the supplied voltage again above this critical value restores the operation back from the same point it stopped at. This disadvantage highlights another feature behind the self-timed SRAM. This feature resides in the ability of the design to restore its operation from exactly the same states it stopped at before halting. Synchronous SRAM cannot achieve that, whenever it stops for whatever reason the operation must restart from beginning again.

Nevertheless, it was the aim of the researcher to operate the proposed self-timed SRAM near the sub-threshold boundary and the ability of that was proven via simulation under a wide range of process variations. According to the foundry documents, which cannot be revealed here, such a big mismatch in operational range between the simulation and real silicon is unlikely to be caused by errors in the simulation models nor manufacturing defects. This fact guided the researcher towards more investigation in the fabricated chip along with the demonstration board. After long investigations, simulations and testing, the problem was found, which resides in one of the components that was updated just before taping out the chip. At that time, the designer thought this modification will optimize the overall functionality, however, it causes the mentioned mismatch.

Figure 4.15 shows the waveforms obtained from simulating the circuit in charge. First waveform is the VDD, second one is the circuit input, and last one is the circuit output. The experiment mimics the same case faced during testing by supplying a voltage varies between 0.4V and 1.2V. The waveforms confirm that this circuit stops operating at around 0.73V. Just now, the mismatch in operational range between the simulation (0.73V) and real silicon (0.75V) can be interpreted, where the most likely reasons for the mismatch can be error in device modelling, manufacturing defects, lack of buffering, or wire delay.



**Figure 4.15 Waveforms of the circuits causing the mismatch.**

Fortunately, this circuit gives the researcher an opportunity to design new type of circuits, which are clever enough to operate only within certain level of VDD and stop working elsewhere. Such a kind of circuits can be called “reference free voltage sensor”, nowadays, there is a high demand for them.

## 4.5 Conclusions

This chapter covers the design, fabrication, and testing of the HoliSRAM chip with the aim of demonstrating, in real silicon, the ability of the proposed design techniques to tolerate the high variations in VDD, which is one of the challenging problem in the energy harvesting systems.

Firstly, the researcher defined what the chip is required to demonstrate and accordingly the testing circuitry was designed and embedded around the self-timed SRAM. Consequently, it was found that the chip has to accommodate multiple power domains and multiple cell libraries, which increases the challenges of the design and testing. After completing the whole design, numerous simulations are conducted to guarantee the correct functionality under a wide range of process variations. Following that, the final single schematic file is converted to a GDSII file, which is the only format the

foundry understands, via a very long process and by employing several tools.

After sending the chip for fabrication, the process of testing preparation started. It was planned to involve the chip in several testing and demonstration streams. This thesis concentrates on only one of them, which is called stream II. This stream aims to design a portable demonstration system for the HoliSRAM chip that allows interacting with the self-timed SRAM without equipping any other testing instruments, only a laptop suffices. The demonstration involves circuit design, fabrication, and testing of PCB,  $\mu\text{C}$  programming, and numerous measurements.

The genuine signals obtained from real silicon demonstrate the ability of the proposed design technique to tolerate VDD variations of up to 64% of its nominal value at 90nm technology. Variable voltage outside this range causes the internal timing controller to halt at its current state, however, the controller acts as a memory where the normal operation is restored from the same point once the voltage is increased above the critical value. Moreover, DRV of the chip was found to be 0.4V. A tiny mistake occurred during the layout causes limiting the operational range of the SRAM, nevertheless, it makes a clear opportunity to design a reference free voltage sensor, an idea has already been proven in real silicon in this chapter.

## 4.6 References

1. V. V. I. Varshavskii, *Self-Timed Control of Concurrent Processes: The Design of Aperiodic Logical Circuits in Computers and Discrete Systems*: Kluwer Academic Pub, 1990.
2. E. Brunvand, *Digital VLSI Chip Design with Cadence and Synopsys CAD Tools*: Addison-Wesley, 2009.
3. X. Zhang, D. Shang, F. Xia, and A. Yakovlev, "A Novel Power Delivery Method for Asynchronous Loads in Energy Harvesting Systems," *ACM Journal on Emerging Technologies in Computing Systems (JETC)*, vol. 7, pp. 1-22, 2011.

## **Chapter 5. Improving the Robustness of Self-Timed SRAM**

### **5.1 Introduction**

The results obtained from simulations and real silicon in the last chapter encouraged the researcher to improve the robustness of the self-timed SRAM to variable VDD using additional SRAM design techniques. The second chapter categorized all SRAM design techniques into four categories, which are bit-cells based techniques, voltage level based techniques, timing circuit based techniques, and peripheral circuit based techniques. This categorization helps this study to clearly understand the advantages and disadvantages of each technique along with when and where to employ each of them, which allows choosing the best solution to address the found issue. It is worth highlighting that improving SRAM robustness has a twofold role as it enables enhancing the area density and/or decreasing the minimum operational voltage. This chapter includes five sections, the first one contains primary analysis to figure out the main limitation behind operating the self-timed SRAM under a wide range of supply voltage. The following three sections propose three design techniques to address the found issues while the last one concludes the chapter.

### **5.2 Preliminary Analysis**

The simulation results obtained in the previous chapters showed that the self-timed SRAM is fully functional down to the sub-threshold region in the ideal case, nevertheless, under high process variations, it stops working below 0.4V. However, there was no clear indication why does it stop, whether the controller stops to operate or the cell fail to work?

This section investigates the mentioned issue in order to benefit other sections to provide the solution. The first conducted experiment had the aim of finding the reasons why SRAM stops working below 0.4V under high process variations. The experiment involves testing an SRAM column controlled by the SI timing controller both experiencing high level of process variations. During the experiment, one of the common failure cases was captured and the corresponding critical timing waveforms are plotted in Figure 5.1, with the same conventional signal names. The obtained waveforms are for writing operation, which confirm that the actual writing happened, however, the bit-line voltage level is not high enough to trigger the gate in the timing controller that is responsible for generating the acknowledgment signal. Consequently, the operation landed in a deadlock state where the actual operation finished but the acknowledgment cannot be issued. In conclusion, the bit-line signal strength is vital for the SI controller in order to report the actual bit-cell status, nevertheless, process variations weaken that strength and obfuscate the transparency between the controller and the bit-cell.

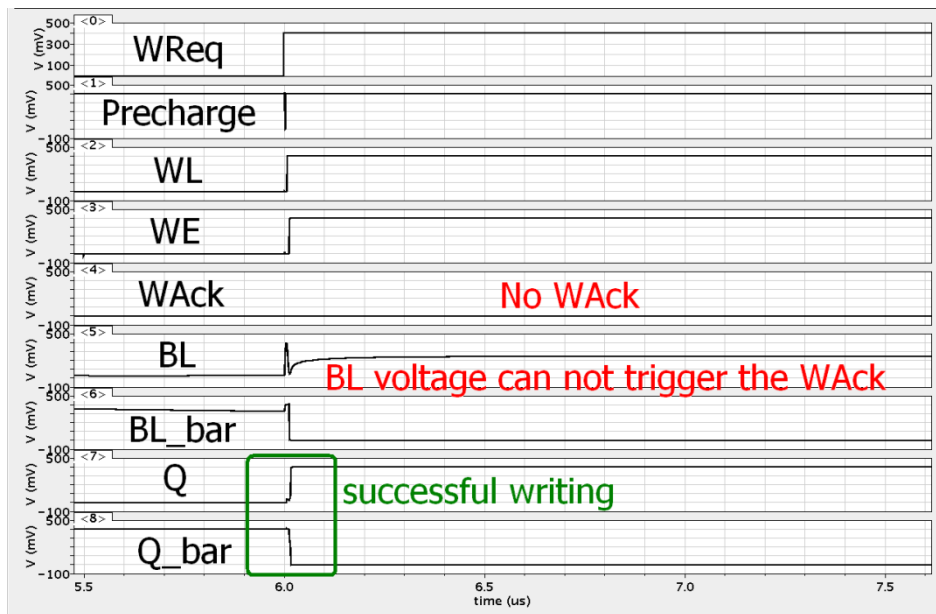


**Figure 5.1** Timing waveforms of a typical failure case in self-timed SRAM.

It is the fact that process variations escalate the problem but does not cause it, the issue is initiated by both the leakage from un-accessed cells, and the nature of the nMOS access transistor being unsuitable to propagate logic

one. Leakage current itself is affected by several factors, where the most important of them are the number of cells per bit-line, the threshold voltage variations, the cell data, and the temperature variations. The next experiment investigates several bit-lines with different sizes, each combines the worst case process for leakage with worst case data scenario to highlight how the leakage limits SRAM density and/or minimum operational voltage.

To recap, the worst case process for leakage happens when the variations decrease the threshold voltage of all transistors (nMOS and pMOS) to its limit to make the devices as fast as possible and consequently increase their leakage and driving current. On the other hand, the worst case cell data happens when all cells in the same column store the same data and the writing operation involves flipping one of them. Accordingly, after successful writing, the written cell tries to charge the bit-line, while the leakage currents from all un-accessed cells try to discharge it.

Figure 5.2 shows the simulation results of the maximum bit-line voltage, after successful writing, under the worst case process for leakage and worst case cell data scenario for different number of cells per column. The brown, blue, and green lines are for 64, 128, and 256 cells per bit-line, while the red line represents the minimum bit-line voltage required to trigger that gate in charge of issuing the acknowledgment signal. The results illustrate that increasing number of cells per column linearly degrades the bit-line voltage and consequently increase the minimum operational voltage for that size of column. The results obtained here confirm those obtained in the previous chapter from corner and Monte-Carlo analysis.

As a summary, in the 6T self-timed SRAM, the reading completion detection is generated once one of the bit-lines is discharged according to the stored data, while the writing is acknowledged after the written cell charges one of the bit-lines. Both charging and discharging have to exceed the threshold voltage of the transistor in order to trigger that gate responsible of the acknowledgment signal. While this is completely achievable during reading, however, as the SRAM cell is normally designed based on minimum or near minimal feature size devices, charging the whole bit-line is a challenging



task. Cell data and leakage from un-accessed cells make this problem even harder while process variations escalate it to a terminal level. The following three sections propose three different design techniques to address this issue.

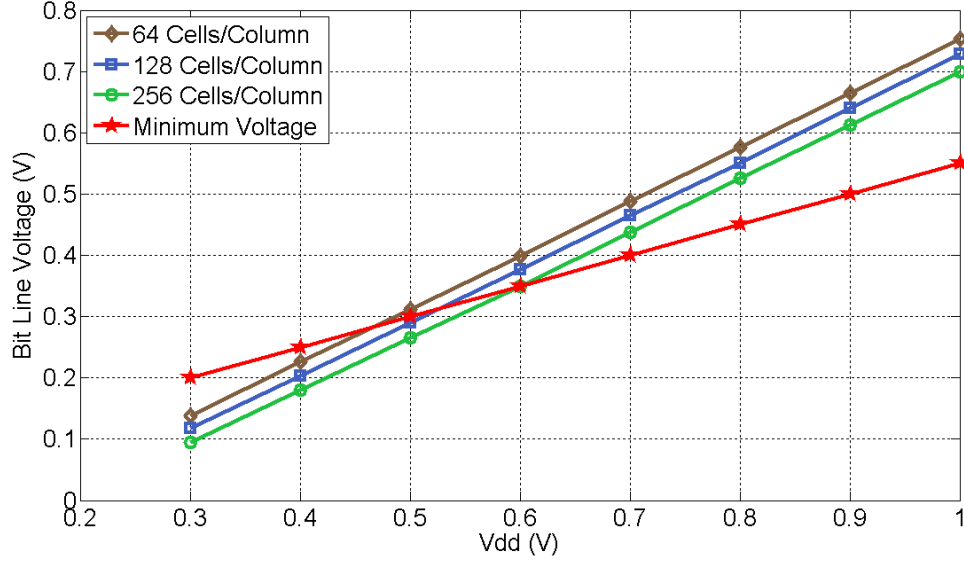


Figure 5.2 Bit-line voltage after successful writing for different bit-line sizes.

### 5.3 New Robust Self-Timed SRAM: a Bit-Cell Based Technique

As stated in the previous section, the issue is fundamentally caused by the nature of the nMOS access transistor being unsuitable to propagate logic one to trigger the completion gate during writing. Accordingly, the idea proposed here is based on changing the mechanism of sensing the completion, rather than charging one of the bit-line via the weak cell, discharging it is easier. Nevertheless, in this case, neither of the bit-lines can be used for completion detection because one will be used by the write driver to flip the cell and the other one cannot be discharged by the cell. Therefore, the bit-cell requires an additional pair of bit-lines for completion detection, while the original one will be reserved for writing only.

After adding the new bit-lines and arranging their controlling transistors, the 10T bit-cell in Figure 5.3 is obtained. By coincidence, after designing the bit-cell, the researcher noticed that this cell is exactly the same as the one previously proposed by the authors of [1]. However, their design aim was to

separate the reading ports from the storage in order to tolerate noise. This property is inherited here in addition to two more features. The former is employing the added transistors to dynamically build a path to ground based on the stored value to discharge one of the bit-lines for completion detection, while the latter is reducing the bit-line leakage by the two stacked transistors at each side of the added bit-line.

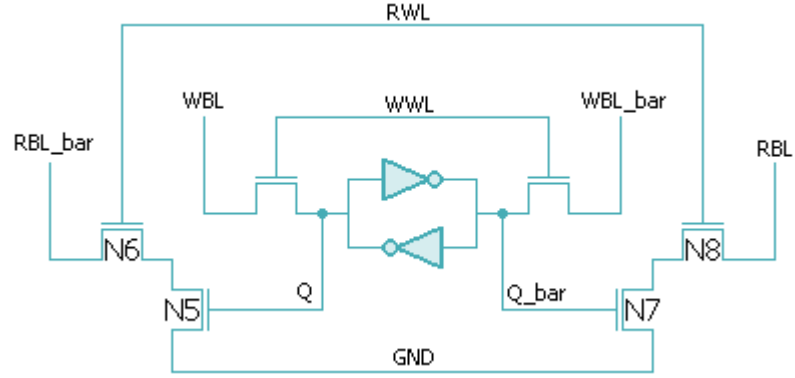


**Figure 5.3 Proposed 10T SRAM cell.**

The size of the 10T cell is about 67% bigger than the 6T. Its write-ability and holding stability are similar to the 6T's while it has no reading disturbance [1]. Hereafter, the name of RWL & WWL and (RBL & RBL\_bar) & (WBL & WBL\_bar) are reading and writing word-lines, and reading and writing bit-lines respectively.

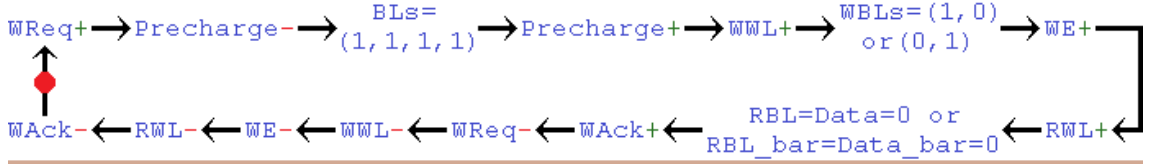
Similar to the self-timed 6T, reading operation is arranged in two consecutive events, the first is precharging the bit-lines and the second is asserting RWL to enable the (N6 & N8) access transistors, which discharges one of the reading bit-lines according to the stored data. The discharged bit-line indicates that data is ready for collection.

In contrast to the 6T, writing is arranged in four events. By assuming that the cell stores zero and the writing involves flipping it, the steps are as follows. 1) Precharging the bit-lines. 2) Opening the writing word-line (i.e. WWL), which discharges one of the writing bit-lines (WBL in this case) according to the stored data. 3) Enabling the write driver to discharge WBL\_bar and consequently flip the memory cell. 4) Enabling RWL, which results in discharging RBL\_bar provided that the cell is flipped and one is

generated from the other side to open the transistor N5, hence guaranteeing the completion of writing operations.

As before, the STG specifications of the aforementioned events are in Figure 5.4, for writing and reading.

### Writing STG:



### Reading STG:

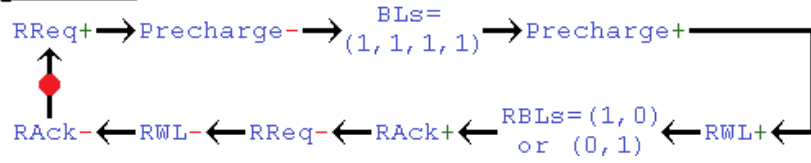


Figure 5.4 STG specifications for writing and reading in self-timed 10T SRAM.

Delay-Insensitive (DI) solution is the safest asynchronous logic as they work correctly regardless of how much delay both wires and gates have [2]. However, DI is hard to implement or even impossible in some cases and the next best option is the Quasi-Delay-Insensitive (QDI) or Speed Independent (SI) circuits [3]. Figure 5.5 shows an SI solution mapped from the combined STG specifications above. The circuit is designed by Petrify [4] and optimized manually.

Figure 5.6 shows the waveforms obtained from the controller for reading (a) and writing (b). The numbers 1 to 4 in the timing diagram are associated with the reading and writing steps mentioned above.

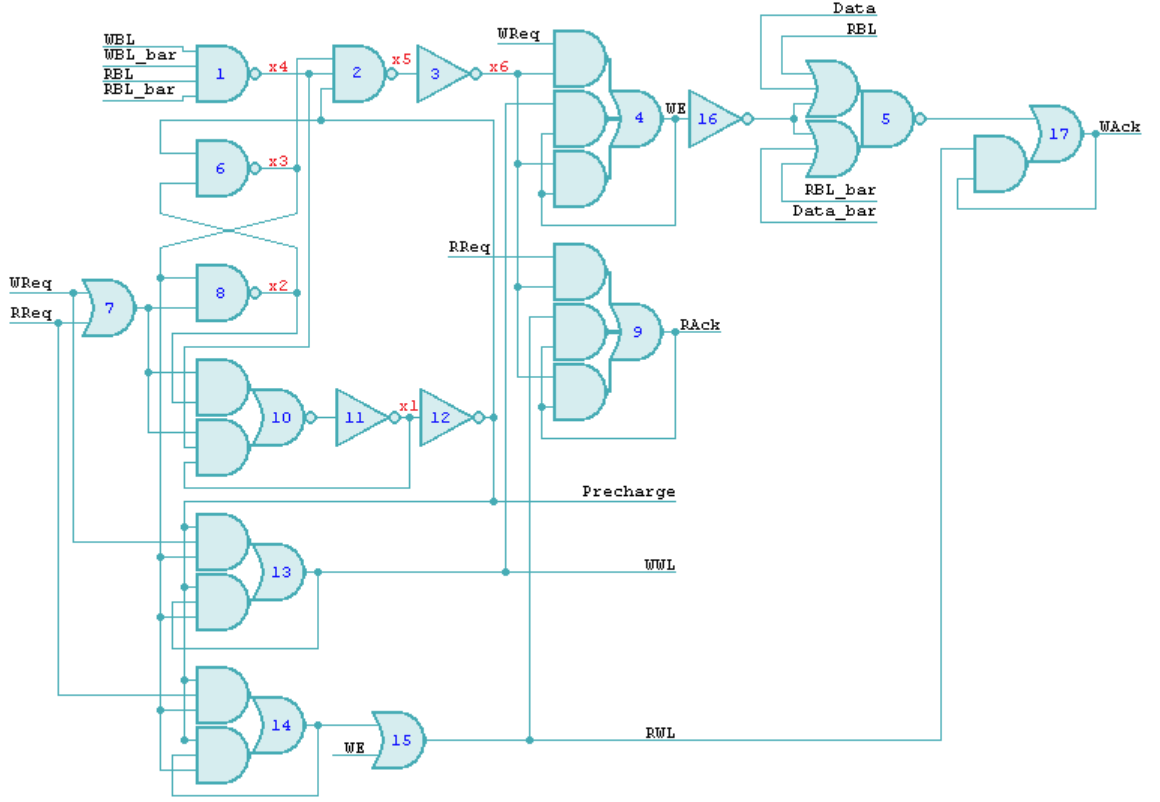


Figure 5.5 Proposed SI controller for the self-timed 10T SRAM.

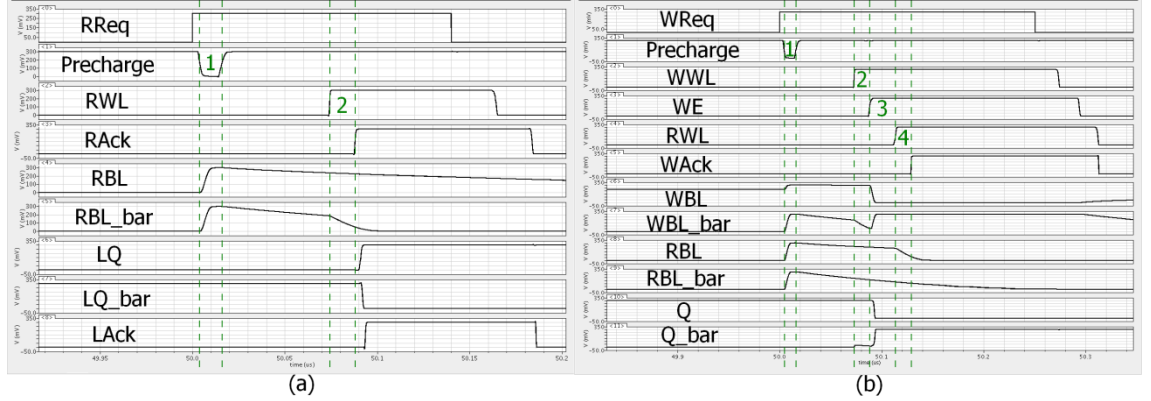


Figure 5.6 Waveforms of the proposed self-timed SRAM for (a) reading and (b) writing.

### 5.3.1 Investigations on the Proposed Bit-Cell Based Technique

This section investigates the robustness of the proposed design, which aims to operate down to near sub-threshold region while supporting large bit-lines. Accordingly, a column containing 256 such 10T SRAM, controlled by the proposed timing controller is tested across a wide range of PVT variations that covers all process corners (TT, FF, SS, SNFP and FNFP), voltage from nominal value down to 0.3V, and temperatures from -50°C up to 125°C.

Just to recap, the corner test is regarded as successful only if corresponding following conditions are satisfied.

1. After receiving the request signal, the timing controller has to generate the signals in the order depicted in Figure 5.4.
2. If the operation is writing, it has to end up with flipping the cell and the cell has to hold the new data until withdrawing the acknowledgment signal.
3. If the operation is reading, it has to end up with latching the data in the SI-latch and the cell has to stay settled until withdrawing the acknowledgment signal.
4. After taking down the request signal, the timing controller has to reset itself by withdrawing all signals in the order depicted in Figure 5.4.

More than 300 simulations were conducted, in which all runs of all process and temperature corners satisfy the above conditions for all VDDs ranging from nominal value down to 0.4V, which demonstrates the ability of the proposed self-timed SRAM to address the raised issue. Nonetheless, some failures appear at 0.3V, for which several experiments were carried out to investigate the failure mechanism and its causes via examining the timing diagram of the critical signals. The typical failure was found to reside in the ability of some operational conditions to dynamically discharge the writing-bit-lines and trigger gate-1 before timing controller triggers gate-13. To clarify this matter, the experiment is repeated again under the worst case corner captured in the last step and with huge delay inserted at the output of gate-13. This magnifies the issue as shown in Figure 5.7, in which gate-13 output is deliberately delayed and during the delay time, gate-1 is triggered by the dynamic effects of process variations. This results in generating the acknowledgment signal before the actual writing as shown in the timing diagram. This hazard violates the controller protocols and breaks the above first and second conditions since the WE is issued before WL and WAck is

generated before the actual writing. It is true that this situation happens only under a high level of process variations associated with a large delay in gate-13, a case rarely happening in real silicon. However, it is the aim of this research to provide a robust design in order to mitigate all cases of process variations.

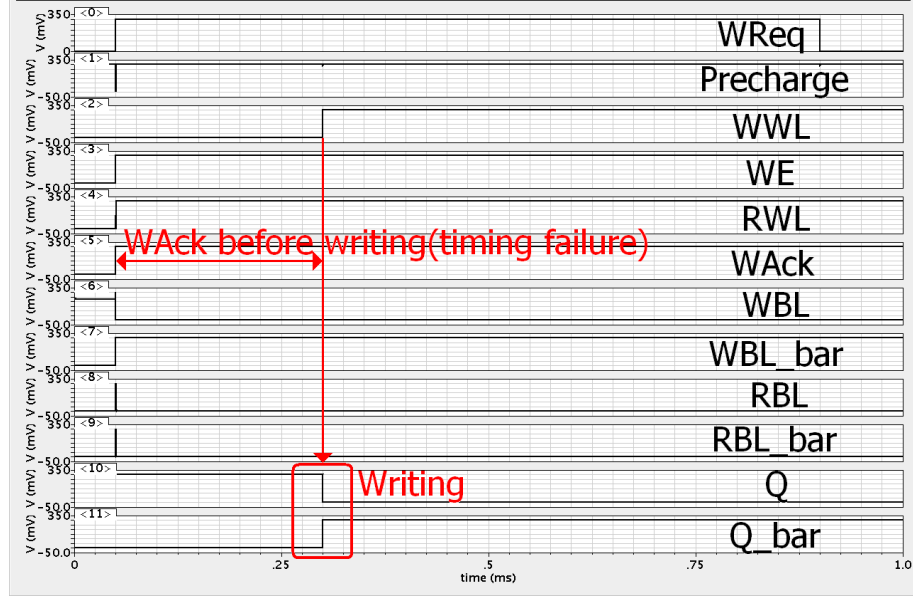


Figure 5.7 Waveforms of a timing failure case in the 10T self-timed SRAM.

In conclusion, the proposed 10T self-timed SRAM outperforms the 6T one in terms of supporting four times larger bit-line with the same level of robustness. However, in order to combine between this feature and near sub-threshold operation, a solution is required to either suppress or at least compensate the bit-line discharging currents caused by the corner conditions. Accordingly, the next couple of sections propose different design techniques to address this issue.

#### 5.4 Bit-line Keeper: a Peripheral Circuit Based Technique

In this section, the research proposed to compensate the bit-line currents wasted by the dynamic effects of process variations to suppress the timing failure captured above. Towards this goal, a bit-line keeper is added to each bit-line, in charge of the failure, to compensate its leakage current. Figure 5.8 shows the circuit diagram of the bit-line keeper [5]. The circuit operates in a clever way by continuously compensating the lost current so long

as it is not deliberately taken down by any other circuit, hence eliminating the aforementioned timing hazard.

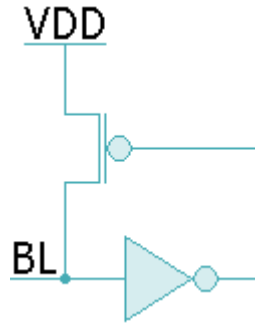


Figure 5.8 The circuit diagram of the bit-line keeper.

Adding the bit-line keeper to the last experiment, confirms that for whatever delay at gate-13, the overall system works robustly according to the design goals. Figure 5.9 shows that despite the overall circuitry experiencing high variations, and gate-13 has a delay of more than 200 $\mu$ s, which will never occur in real silicon, the overall system operate robustly.

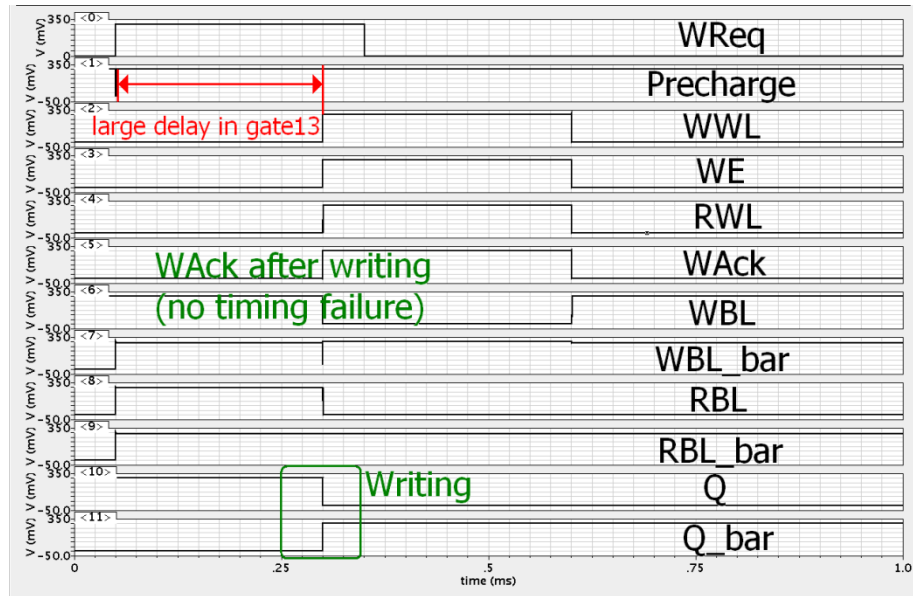


Figure 5.9 Waveforms of the 10T self-timed SRAM with no timing failure.

#### 5.4.1 Investigations on the Proposed Peripheral Circuit Based Technique

The previous experiment is repeated again after attaching the bit-line keepers to a bank containing 256 $\times$ 128 such 10T cells and controlled by the proposed timing controller. The experiment involves 310 simulations to cover all process corners (TT, FF, SS, SNFP and FNFP), VDD from nominal value

down to 0.3V and temperatures from -50°C up to 125°C. The obtained results confirmed the full functionality across the mentioned range. Figure 5.10 shows the writing time for such a bank at 0.3V for all process and temperature corners, which are coded in the horizontal axis as corner/temperature. The black part in each bar represents the time required for the actual writing, while the grey part indicates the time needed by the controller to issue the acknowledgment signal, named CD stands for Completion Detection.

It is worth highlighting that this level of robustness is acquired by adding the keeper circuit, which is smaller than half of the 6T SRAM cell, therefore, for a bit-line with 256 cells its area overhead is less than 0.4%.

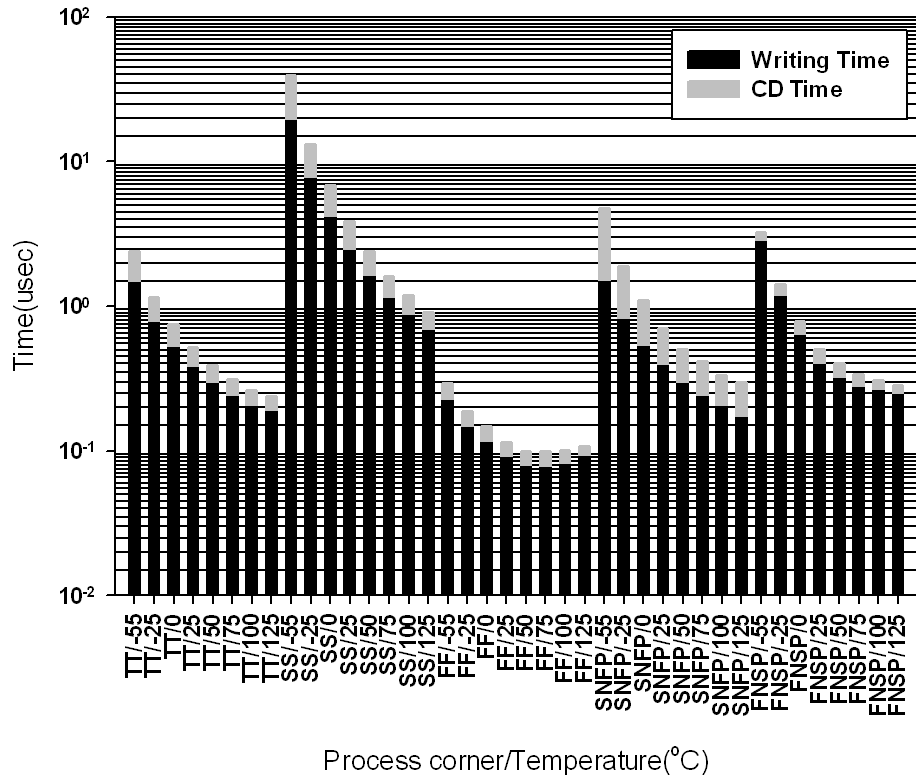


Figure 5.10 Writing time for 256x128 SRAM bank at 0.3V.

Investigating the results gained from the last experiment confirmed an important feature of the proposed design, which was achieved unintentionally. It is the ability of the proposed design to employ one of the data columns to bundle the timing of the whole bank without the need of adding a redundant column. In contrast, all previous bundling techniques appear in [6, 7] or even the one introduced here in the third chapter require a redundant col-



umn in order to bundle other data columns. Moreover, all these techniques deliberately worsen the timing of the dummy column so that it can cover the timing of the worst case cell in the bank. For instance, [6, 7] deteriorate the timing by internally connecting the bit-cell in such a way that reflect some worst case conditions while the one proposed earlier in this work does flip the cell data each time.

Here, the ability of the proposed design to bundle the whole bank with the timing of any arbitrary data column is proved from the results in Figure 5.11. The experiment selected the best case timing column among 128 columns and involved the following four writing operations, which covers all data combinations:

1. Write same data to the selected column, and flip other columns.
2. Write same data to the selected column, and other columns.
3. Flip the selected column, and write the same data to other columns.
4. Flip the selected column, and other columns.

The numbers above are corresponding to the numbers in the Figure 5.11 below each timing waveforms, where each shows the data in the selected and other columns as well as the request and acknowledgment signals. In all cases, the WAck signal is generated only after the data settle in all data columns, which is indicated by the green arrow in each subplot. The results in Figure 5.11 were double-checked across the 310 corners mentioned above with all of them passing the design goals.

Certainly, if the bundling column is selected to be the last column, the interconnect delay between the peripheral circuits and the last column will be added to the safety margin represented by the green arrow in the timing waveforms, nevertheless, that is not necessary, which grants the designer the freedom of choice.

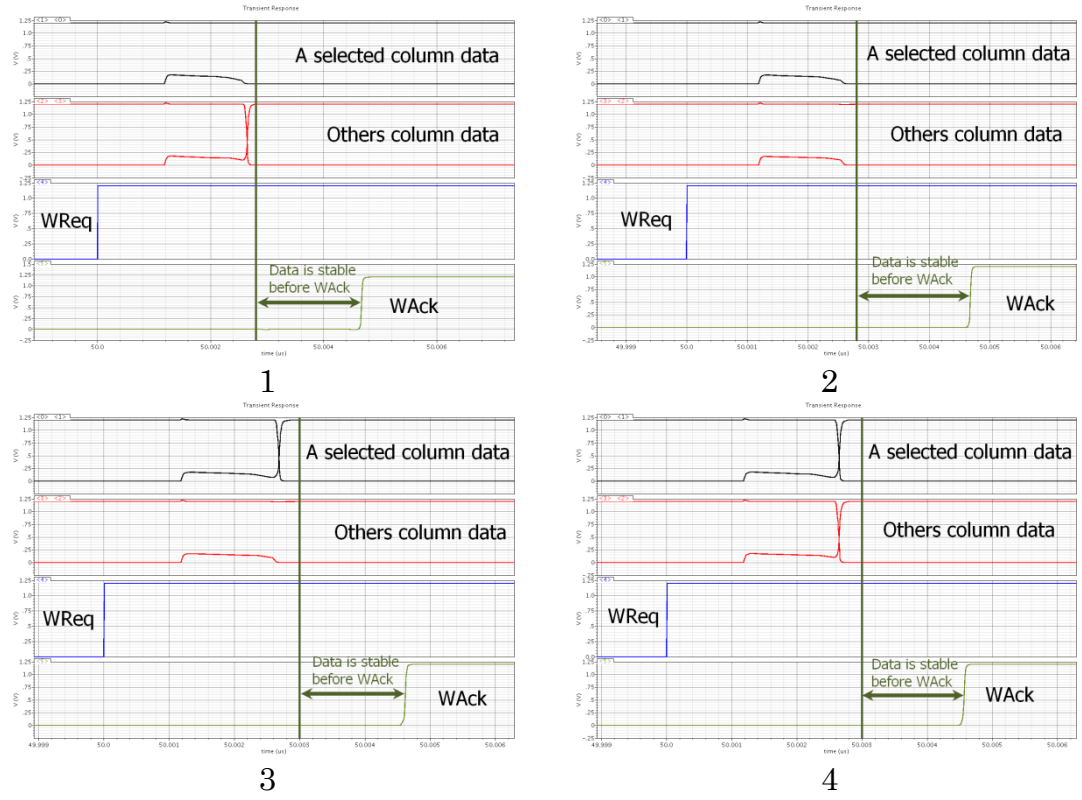


**Figure 5.11 Timing diagram of writing operation that shows the data in the bundling and bundled columns.**

In conclusion, adding the bit-line keepers to the proposed 10T self-timed SRAM gives it the opportunity to work robustly near the sub-threshold region while supporting large bit-lines. As an unprecedented achievement, which has not yet been reported either in synchronous or asynchronous SRAM, the proposed design is able to employ one of the data columns as a bundling column, which was proven across a wide range of PVT variations. This achievement improves the SRAM area density as well.

## 5.5 Virtual Ground: a Voltage Level Based Technique

By the end of section 5.3, this research acquired a new self-timed SRAM based on the 10T bit-cell, which is able to work robustly down to 0.4V across a wide range of PT variations. In that section, it is found that, there is a timing hazard happening below 0.4V at some corners, which is then addressed at section 5.4 by introducing the bit-line keeper. Moreover, keeper is categorized as a peripheral circuit based technique, which compensates the bit-line leakage currents.

This section aims to propose a new design that improves the energy efficiency of the 10T self-timed SRAM with keepers. This opportunity clearly appears after careful inspection of the last design, in which three events were found to waste useless amounts of energy as follows.

1. All bit-lines are precharged, however, only reading ones suffice for monitoring the bit-cell. Hence, it is suggested to precharge the reading bit-lines only to save the wasted energy from two aspects, preserving the charging currents and decreasing the precharging time.
2. Keepers compensate the wasted bit-line current by wasting more, where a better solution is to suppress the wastage rather than compensate for it. Accordingly, it is recommended to suppress the leakage current by means of a virtual ground, a well known design technique introduced before for synchronous SRAM [8, 9].
3. Writing-word-line is enabled before the write driver for no purpose. If, however, they are swapped, both the driving current of the access transistors and the time during which they are enabled will be decreased and that saves energy.

Unfortunately, the first and last recommendations require updating some gates in the timing controller to consider the new signal sequences while the second suggestion requires introducing a new signal to control the virtual ground of all cells in the same row. Firstly, the 10T bit-cell needs the update shown in Figure 5.12. VGND is the virtual ground control signal, when it is low, the reading bit-lines have no path to the ground and therefore it maintains its current, however, when it is high, the discharging path is recovered and the cell works as usual. According to the suggested signals sequence, including the added one for virtual ground, the new STG specifications are shown in Figure 5.13 for reading and writing.

In this STG, one more event is added to the reading operation, exactly after precharging the reading-bit-lines and before opening the reading-word-line, which is to assert the VGND signal to recover the discharging path of the

accessed row. Moreover, withdrawing the RReq signal means resetting VGND signal as well. This step is also included in the writing operation in addition to moving WWL+ signal after WE+. Everything else is the same as before, even the way of detecting the completion of the operation.

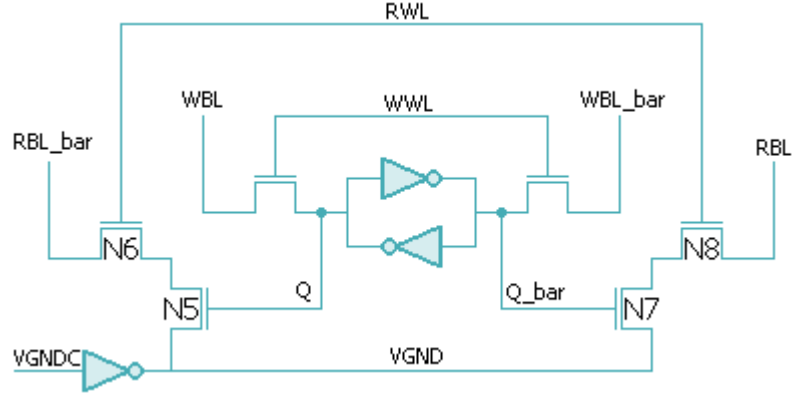
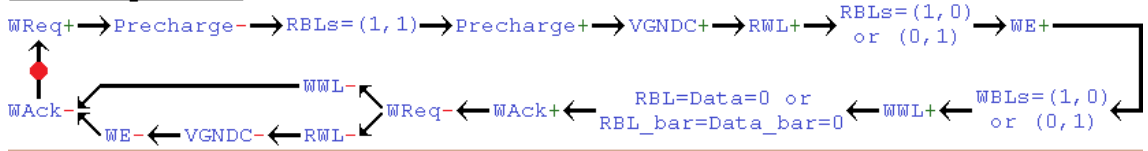


Figure 5.12 10T SRAM cell with the virtual ground terminal.

Writing STG:



Reading STG:

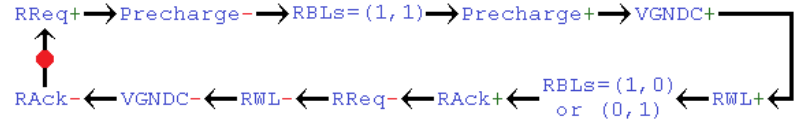


Figure 5.13 STGs specifications for writing and reading of the 10T SRAM with VGND.

As usual, the combined STGs are passed to Petrify [4] and the outputs are optimized manually to obtain the SI timing circuit in Figure 5.14.

This timing controller has been designed in a smart way that enables it to control the timing of several SRAM cells and structures. As a general condition, any differential SRAM cell that has the reading word-line detached from the writing word-line can be used with this timing controller, nevertheless, if the bit-lines are shared between reading and writing they must be separated. This condition contains but is not restricted to the following SRAM cells: 1) the 10T SRAM cell shown in Figure 5.12, 2) the 8T SRAM cell in [10], 3) the 9T SRAM cell in [11], and 4) the ST-2 SRAM cell in [12]. This timing controller can also control the bit-cell with either virtual or real

ground based on the terminal VGND in the controller. If VGND terminal in the controller is connected to GND, then any of the previously mentioned cells can be used with real ground. However if VGND terminal in the controller is connected to VDD, then any cell with virtual ground can be employed. Finally, bit-line keeper can be added if the required robustness level needs it.

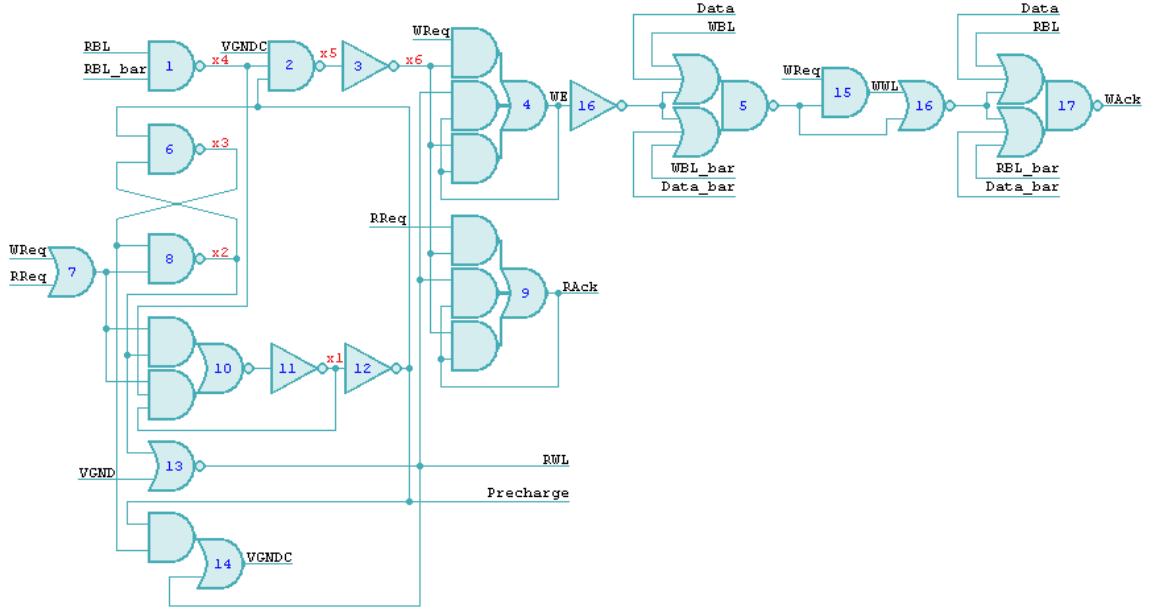


Figure 5.14 Possible realization of the timing circuit for the 10T SRAM with VGND.

In conclusion, this timing controller is smartly designed to be used with a wide variety of bit-cell structures either with virtual or real ground while employing the keeper if needed. Interestingly, this circuit has fewer gates than the previous one (Figure 5.5).

### 5.5.1 Investigations on the Proposed Voltage Level Based Technique

In order to prove the claimed energy efficiency of the suggested modifications, this section conducts a comparison study between the current and previous designs to find out how effective the changes are.

Firstly, in contrast to the previous design, it is found by simulation that the current design does not have the ability to bundle the whole bank with any arbitrary data column nor even with the last column. This is mainly caused by the timing discrepancy between writing the same data to the bundling

column and flipping the bundled columns, a similar situation to the 6T. That requires adding a redundant column to each bank and flipping the data in that column every writing operation.

Following this fact, a fair comparison is carried out between the two designs using the same benchmark as before. The results of the comparison are shown in the figure below, which shows the saving acquired by the current design in terms of energy with respect to the previous design.

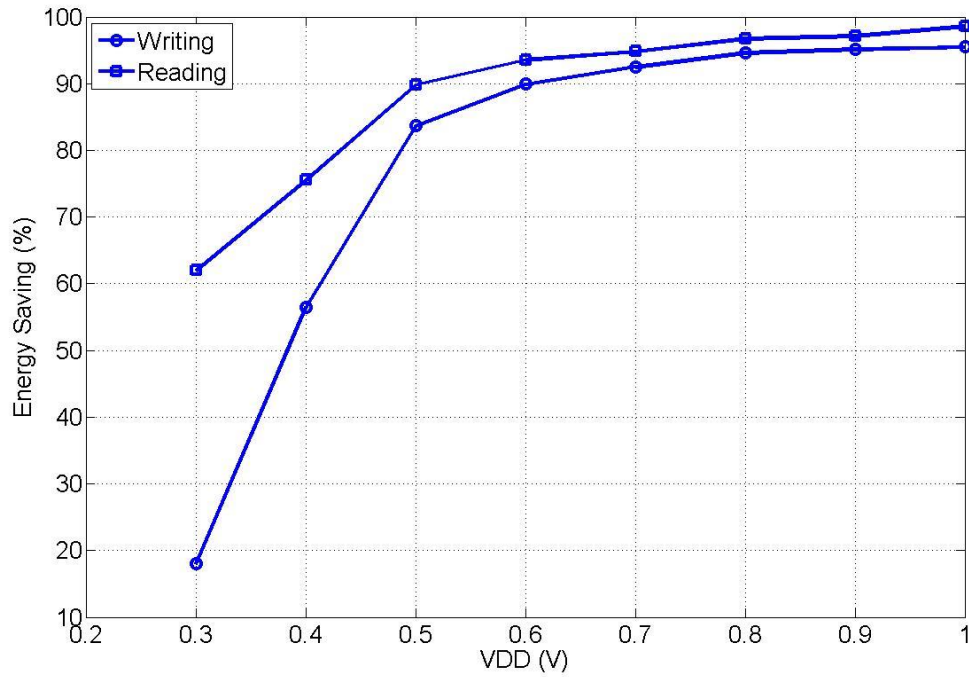


**Figure 5.15** Energy saving during writing and reading in the 10T SRAM with VGND.

The obtained information illustrate that the suggested modifications save a considerable amount of energy while achieving the same level of robustness. The saving is directly proportional to the supplied voltage.

## 5.6 Conclusions

The results obtained from the third chapter confirmed the ability of the SI timing circuit to robustly operate the SRAM across a wide range of VDD variations starting from the nominal value down to 0.4V. The fourth chapter supported this fact by data measured from real silicon. Nevertheless, low-voltage sub-threshold operation is one of the requirements in energy conscious environments (e.g. energy harvesting and portable systems). There-

fore, it is the aim of this research to operate the SRAM robustly down to the sub-threshold region, or at least near it, while supporting large bit-lines. Hence, this chapter is dedicated for that goal.

The work in this chapter was started by preliminary analysis to investigate the failure issue near the sub-threshold region and that was found to be the inability of the controller to generate the acknowledgment signal after successful writing due to two main reasons. The former is the dependency upon the nMOS access transistors to propagate logic one while the latter is the leakage from un-accessed cells. The latter increases as the bit-line length increases and hence it limits the area density of the SRAM. Following that investigation, the chapter explored some SRAM design techniques to address the mentioned issue.

According to the categorization of the SRAM design techniques described in the second chapter, the first solution is a bit-cell based technique, which involved proposing a new 10T bit-cell to address the aforementioned matter. The new cell features a new method of detecting the completion via charging the bit-line instead of discharging it and employing stacked transistors to decrease the leakage from un-accessed cells. Based upon the simulation data, the solution is able to support large bit-lines while operating robustly down to 0.4V. However, near sub-threshold operation failed due to timing hazard in the controller protocols caused by the dynamic effects of the process variations.

Then the study introduced the bit-line keeper, which is a peripheral circuit based technique, in order to compensate for the leakage currents, which cause the timing hazard. Adding that component to the design enabled it to reach the design goal by supporting large bit-lines and working robustly down to near sub-threshold region.

The careful inspections of the last design suggested several modifications to increase the energy efficiency of the whole design. The main recommendation is suppressing the leakage by the means of virtual ground technique instead of compensating it with the keeper. Accordingly, the bit-cell and its

timing controller are updated to accommodate the suggestions. The new timing circuitry is smartly designed to allow it to be used with a wide variety of bit-cell structures, four of them were listed above, with either virtual or real ground. The obtained results confirm saving considerable amount of energy for the same level of robustness.

## 5.7 References

1. H. Noguchi *et al.*, "Which is the Best Dual-Port SRAM in 45-nm Process Technology? - 8T, 10T Single End, and 10T Differential -" in *Integrated Circuit Design and Technology and Tutorial, 2008. ICICDT 2008. IEEE International Conference on*, 2008, pp. 55-58.
2. S. Jens and S. Furber, *Principles of Asynchronous Circuit Design: A Systems Perspective*: Springer, 2001.
3. J. M. Alain, "The Limitations to Delay-Insensitivity in Asynchronous Circuits," presented at the Proceedings of the sixth MIT conference on Advanced research in VLSI, Boston, Massachusetts, USA, 1990.
4. J. Cortadella *et al.*, "Petrify: A Tool for Manipulating Concurrent Specifications and Synthesis of Asynchronous Controllers," *IEICE TRANSACTIONS on Information and Systems*, vol. E80-D, pp. 315-325, 1997.
5. R. K. Krishnamurthy *et al.*, "A 130-nm 6-GHz 256 × 32 Bit Leakage-Tolerant Register File," *Solid-State Circuits, IEEE Journal of*, vol. 37, pp. 624-632, 2002.
6. C. Meng-Fan, Y. Sue-Meng, and C. Kung-Ting, "Wide  $V_{DD}$  Embedded Asynchronous SRAM with Dual-Mode Self-Timed Technique for Dynamic Voltage Systems," *Circuits and Systems I: Regular Papers, IEEE Transactions on*, vol. 56, pp. 1657-1667, 2009.
7. B. S. Amrutur and M. A. Horowitz, "A Replica Technique for Wordline and Sense Control in Low-Power SRAM's," *Solid-State Circuits, IEEE Journal of*, vol. 33, pp. 1208-1219, 1998.
8. N. Verma and A. P. Chandrakasan, "A 256 kb 65 nm 8T Subthreshold SRAM Employing Sense-Amplifier Redundancy," *Solid-State Circuits, IEEE Journal of*, vol. 43, pp. 141-149, 2008.
9. C. Ik Joon *et al.*, "A 32 kb 10T Sub-Threshold SRAM Array with Bit-Interleaving and Differential Read Scheme in 90 nm CMOS," *Solid-State Circuits, IEEE Journal of*, vol. 44, pp. 650-658, 2009.
10. J. P. Kulkarni *et al.*, "A Read-Disturb-Free, Differential Sensing 1R/1W Port, 8T Bitcell Array," *Very Large Scale Integration (VLSI) Systems, IEEE Transactions on*, vol. 19, pp. 1727-1730, 2011.
11. L. Zhiyu and V. Kursun, "Characterization of a Novel Nine-Transistor SRAM Cell," *Very Large Scale Integration (VLSI) Systems, IEEE Transactions on*, vol. 16, pp. 488-492, 2008.
12. J. P. Kulkarni *et al.*, "Process Variation Tolerant SRAM Array for Ultra Low Voltage Applications," in *Design Automation Conference, 2008. DAC 2008. 45th ACM/IEEE*, 2008, pp. 108-113.
13. S. G. Narendra and A. P. Chandrakasan, *Leakage in Nanometer CMOS Technologies*: Springer, 2006.



## Chapter 6. Conclusions and Future Work

### 6.1 Introduction

This chapter ends the thesis by concluding the whole project and proposing promising follow-on research studies. Therefore, the current chapter is divided into two main sections, the first is the conclusions, and the second is the future work.

### 6.2 View and Review

The story of the current technologies began after Jack Kilby introduced the IC in 1958 [1], and M. M. (John) Atalla and Dawon Kahng invented the Silicon MOSFET transistor in 1959 [2]. Certainly, this story has many other unsung heroes, however, the mentioned are the most important milestones of the technology journey [3].

Since then and the industry has been driven towards increasing the performance and functionality of the computational logic while decreasing its manufacturing cost and power consumption, which is achieved via downsizing the dimensions of the components embedded in the ICs. This clearly appears when comparing early ICs, which had a line width of  $25.4\text{ }\mu\text{m}$  with that one in 1972 with a gate length of  $6.0\text{ }\mu\text{m}$  [4, 5]. At that time, most of the research were directed towards the scaling process, as a promising field. For instance, in 1974, a scaling method was proposed in [6], which assumed that all the device parameters are either shrunk or increased by the same factor (e.g.  $K$ ). More precisely, the technique involves scaling all device dimensions, threshold voltage, supply voltage, and drain current by  $1/K$ . Consequently, the gate area and charge will be reduced by  $1/K^2$ , and circuit performance will be increased by  $K$ . Moreover, if the chip size is kept fixed, the

number of transistors per die will be increase by  $K^2$  every generation. If all these conditions are satisfied, the result will be increasing the functionality and performance of the IC every generation while keeping the power consumption constant, accordingly, this scaling is called ideal scaling [5, 7].

Nevertheless, the actual scaling has been more aggressive than the ideal one, due to the fact that the goals of the latter lag substantially behind the dream of the industry. That aggressive scaling scales key parameters of the device independently and the results are significant increase in the performance of the die and the number of transistors it has with marginal decrease in the supply voltage and threshold voltage. Accordingly, the die power consumption increased by several orders of magnitude, more specifically, it roughly doubled every two years [5, 8]. This considerable growth in power consumption makes it one of the main design concerns for both portable and non-portable systems. In the case of battery alone powered systems, the problem is even worse as the increase in power cannot be accommodated by the improvement in the battery capacity, which only doubles every ten years [8]. In addition to the limitations in battery capacity, in many cases, maintaining and replacing batteries are impossible, inconvenient, costly, or hazardous. This suggests developing a new generation of microelectronic systems that can be self-powered, the opportunity of which was made clear by the advances in both the field of micro-generators, and low power electronics. In the scope of that, this research study attempted to propose a proof of concept for enabling energy harvesting microelectronics via introducing several design methods for this area. The investigations conducted by this study concentrate on SRAM, as it occupies the majority of the chip area and affects most of its performance parameters, moreover, it is a vital component for all computational logic.

The first experiment in this research analysed the behaviour of the SRAM under variable VDD, a typical case in energy harvesting systems. The experiment confirmed the unsuitability of the simple chain of basic gates to bundle the SRAM timing in a highly variable supply voltage environment, otherwise, the wastage of resources might reach up to three times of the re-

quired amount. Accordingly, this research proposed to regulate the data flow inside the SRAM system based on the actual speed of the circuit via employing handshaking protocols and eliminate all timing assumptions. Nevertheless, the literature affirms that SRAM has not yet benefited from completion detection, especially for writing, due to an erroneous speculation that writing acknowledgment is difficult or even impossible to implement in SRAM. Thereafter, the study carried on by proposing a dynamic technique to detect the completion of both reading and writing in SRAM. Moreover, the obtained behavioural specifications were successfully synthesized in a fully SI circuit realisation for the aim of robust operation. The designed circuitry was employed in an SRAM system, where the whole design was proved, by simulation, to have the ability of working under highly variable VDD. Furthermore, the timing signals issued by the circuitry reports all activities inside the bit-cell, not only the completion of the whole operation but further the completion of each stage the main operation has. Interestingly, the task of monitoring the cell is achieved via a basic NAND gate. In contrast to conventional SRAM, the proposed one is able to function while the system changes the operational mode (DVS) with no need to stop working or waiting the supply voltage to settle down. In contrast to synchronous SRAM, the timing circuit proposed here has the ability to control both the performance and energy of the SRAM via only one knob, the VDD. Based on that design, another design was proposed which is faster but less safe as it depends upon bundling the whole SRAM with the handshaking signals from last column. Despite that, the bundling technique is still safer than those in the literature since it reflects real operation in real cells while other techniques reflect worst case timing in dummy cells.

Following this step, it was the time to prove the actual functionality in real silicon. Hence, the proposed design was combined with some other testing circuitry to test the whole design in an asynchronous and autonomous manner. The whole design showed full functionality down to above the sub-threshold region under high process variations, which encouraged taping out the chip. Nevertheless, the testing goals landed the chip in a situation requiring dual supply voltage along with a proper signal communication

technique between them and dual cell design methods. All these challenges were addressed via the right techniques by mastering several EDA tools. After receiving the chip, the testing environment was designed, which involves designing and fabricating a PCB fully powered and controlled by one of the latest  $\mu\text{C}$ , namely, PIC32MX795F512L. The portable demonstration system was completed and upon that, the testing was conducted, where the results confirm the ability of the SI SRAM to tolerate VDD variations up to 64% of the nominal value in 90nm technology. A small design mistake was found which limits the minimum operational voltage of the chip, nevertheless, this mistake made a clear opportunity for the researcher to design a reference free voltage sensor.

Finally, the research concentrates on expanding the proposed design technique to support large bit-lines and operate the SRAM down to near the sub-threshold region. Towards this aim, several SRAM design techniques were employed after analysing the main limitations in the previous design. Starting from bit-cell based techniques, a new 10T cell was proposed along with its SI timing controller, both of which were later combined with bit-line keepers, a voltage level based technique, to achieve the mentioned goal. Thereafter, a new design was proposed to improve the energy efficiency of it by employing a virtual ground, a peripheral circuit based technique, to suppress the leakage rather than compensate for it. The table below provides a brief comparison between the main advantages and disadvantages of different designs proposed in this thesis.

**Table 6.1 Comparison between the designs proposed in the thesis**

Design	Advantages	Disadvantages
6T Full SI SRAM	-Robust down to 0.4V	-Max 64 cells/bit line -Slow
6T Bundled SRAM	-Robust down to 0.4V -Fast	-Requires a redundant bit line -Max 64 cells/bit line
10T with keeper	-Robust down to 0.3V -Up to 256 cells/bit line	-67% area overhead/cell -High energy consumption
10T with VGND	-Robust down to 0.3V -Up to 256 cells/bit line -Low energy consumption	-67% area overhead/cell

### 6.3 Prospective Future Research

The investigations, analysis, and experiments conducted during this research along with the obtained results from real silicon suggested several promising proposals for the future research.

According to the ITRS reports, clock-less designs will be increased in future SoC [9, 10], in which the majority of the area is occupied by the memory. This highly probable prediction encourages designers to investigate self-timed memory system in more details and optimize its operation to satisfy most of the applications requirements.

Firstly and most importantly, reliability is a crucial metric for all memory systems, especially in low power and energy harvesting systems, as lowering the VDD badly deteriorates reliability. Process variations have different impacts on different components of a memory subsystem. For instance, the high leakage currents in submicron technologies are generally considered as a main concern in terms of power consumption and more recently in terms of fault modelling [11]. Mostly, variations affect the threshold voltage and eventually the leakage and latency. Nonetheless, the proposed SI SRAM covers the latency related faults as previously demonstrated.

In a highly reliable system, fault detection is vital. The earlier a fault is detected, the better a system is. Conventionally, the faults are detected by a series of writing and reading and/or some dedicated hardware. However, as the proposed self-timed SRAM uses closed loop control, all operations are controllable. For instance, previous chapters showed a writing fault, which causes a deadlock eventually. The same problem can happen in reading. As an example, during reading, after precharging, if the leakage current is high, it will discharge the bit lines and eventually reading acknowledgment is generated wrongly. These leakage faults can be detected either from deadlocks or from wrong relationships in control signals.

Asynchronous handshaking protocols can be verified via different techniques, for instance, in [12] a low cost method was proposed to check the handshaking protocols during the run time of asynchronous circuits. Accord-

ing to the obtained results, the design is able to detect both deadlocks and wrong relationships in the protocols.

Moreover, Data Retention Voltage (DRV) is an important parameter of a highly reliable system for low power operations. For idle memory banks, lowering the supply to the DRV level enables dramatic reduction of the wastage energy. Nevertheless, the DRV depends on the extremes of local mismatch variations, where design time decisions may need to be so conservative as to render this technique useless or at least less efficient.

Several and different DRV tracking techniques have been already proposed and the most important of them were discussed previously. While each method advances the state of the art in some aspects, it suffers from many limitations. In conclusion, to the best of the researcher's knowledge and until the date of writing this chapter, there is no fully on-chip design that can detect the actual DRV of the SRAM bank during the runtime and control the voltage level accordingly without sacrificing the stored data.

On the other hand, with the self-timed memory, when the supply voltage is reduced to a certain point, the controller stops working properly because of the sensing mechanism embedded in the controller as discussed previously. From the experiments in the previous chapters, it is clear that in that situation the data is still correct, but the sensing mechanism stops working. The voltage that the memory stops working at is still higher than the DRV, however, it is very close to the minimum energy point.

Consequently, such self-timed SRAM can be regarded somehow as self-sensing for usable DRV and an asynchronous deadlock or conflict detector can then be employed to generate a warning signal to raise system voltage.

In summary, the future research might concentrate on designing a new memory controller that is able to bind the DRV with some signals and gives the user the opportunity to calibrate the safe margin between the actual DRV and the generated DRV in order to cope with the error rate of the ap-

plication. Nevertheless, the controller must have the ability to determine the actual DRV on-chip.

Other research projects might focus upon improving the area density of self-timed memory via enhancing the strength of the completion signal, which can be achieved by partitioning the bit-lines and adding some logic after each partition in order to save the safe operation of the complete timing path.

The future research should not overlook the clear opportunity of designing reference free voltage sensors. The feasibility of this idea has already been supported by data from real silicon and now it just requires more analysis and investigation. According to the design and obtained results, such a sensor is very cheap in terms of area and energy while it provides high accuracy and similarity between the design time output and the silicon data.

Finally, it is certainly a good idea for upcoming research to benefit from the robustness of self-timed memory system in the context of high performance processors.

## 6.4 References

1. Texas Instruments, *An Interview with Jack Kilby* [online]. Available: [www.ti.com/corp/docs/kilbyctr/interview.shtml](http://www.ti.com/corp/docs/kilbyctr/interview.shtml).
2. D. Kahng, "A Historical Perspective on the Development of MOS Transistors and Related Devices," *Electron Devices, IEEE Transactions on*, vol. 23, no. 7, pp. 655-657, 1976.
3. C.-T. Sah, "Evolution of the MOS Transistor-from Conception to VLSI," *Proceedings of the IEEE*, vol. 76, pp. 1280-1326, 1988.
4. G. E. Moore, "Progress in Digital Integrated Electronics," in *Electron Devices Meeting, 1975 International*, 1975, pp. 11-13.
5. H. Iwai, "CMOS Technology-Year 2010 and Beyond," *Solid-State Circuits, IEEE Journal of*, vol. 34, pp. 357-366, 1999.
6. R. H. Dennard *et al.*, "Design of Ion-Implanted MOSFET's with Very Small Physical Dimensions," *Solid-State Circuits, IEEE Journal of*, vol. 9, pp. 256-268, 1974.
7. H. Iwai, "Roadmap for 22 nm and Beyond (Invited Paper)," *Microelectronic Engineering*, vol. 86, pp. 1520-1528, 7// 2009.
8. J. M. Rabaey, *Low Power Design Essentials*: Springer London, Limited, 2009.
9. B. M. Al-Hashimi, *System-on-Chip: Next Generation Electronics*: The Institution of Engineering and Technology, 2006.
10. The International Technology Roadmap for Semiconductors, *ITRS Home* [online]. Available: <http://www.itrs.net/>.
11. S. G. Narendra and A. P. Chandrakasan, *Leakage in Nanometer CMOS Technologies*: Springer, 2006.
12. D. Shang *et al.*, "Low-Cost Online Testing of Asynchronous Handshakes," in *Test Symposium, 2006. ETS '06. Eleventh IEEE European*, 2006, pp. 225-232.

## Appendix A. Hardware Supplements

### A.1 Tool Path

The only format that the foundry requires in order to tape-out any chip is the GDS file, which contains all needed information about the silicon and metal layers inside the chip. For successful conversion of the schematic to a GDS or Stream file, the designer is required to employ and master several EDA tools provided by different companies, mostly developed by Cadence Design Systems, Inc. ([www.cadence.com](http://www.cadence.com)), Synopsys, Inc. ([www.synopsys.com](http://www.synopsys.com)) and Mentor Graphics ([www.mentor.com](http://www.mentor.com)). Firstly, the researcher started by defining what is called a “tool path”, which is the combination of different tools that he is planning to use so as to convert the schematic to the Stream. After that, he is required to configure each tool in such a way that allows it to accept the output from the previous tool, manipulate it, and pass it to the next one in a sequential way starting from schematic and ending by GDSII file.

The design story, of HoliSRAM, started by employing Virtuoso (from Cadence) to convert the complete schematic, obtained previously, to a net-list, which describes, in writing, all components involved in the design together with the connections between them. The description covers all hierarchies’ level down to the transistor level.

After generating the net-list of the whole chip, the job is handed over to the Encounter (from Cadence), in which the designer first prepares the chip floor by defining a separate region for each power domain. This is a primary step required before placing each cell instance in its corresponding domain, and routing both the power and signal connections to it. Following floor-



planning, the designer imported the net-list, obtained by Virtuoso, into Encounter. Accordingly, Encounter places the abstract view of all instances of every cell involved in the chip in its right position and routes all connections internally between all instances and externally to the I/O pins. The abstract view contains certain physical information about the cell, which includes the bounding box, signal connections and wiring blockages to tell the P&R tool what the needed area for that instance is, and where the ports of the instance and the obstructions inside it are. Encounter requires this brief information in order to optimally place each instance and route its corresponding connections. Certainly, before placing the abstract views of the cells, the designer is required to generate the abstract views for those full-custom cells, which were designed in-house. Figure A.1 shows the final view in Encounter after placing all instances and routing all connections. At that stage, it is required to export the whole design to a special file called Design Exchange Format (DEF) in order to be passed to the following tool in the tool path.

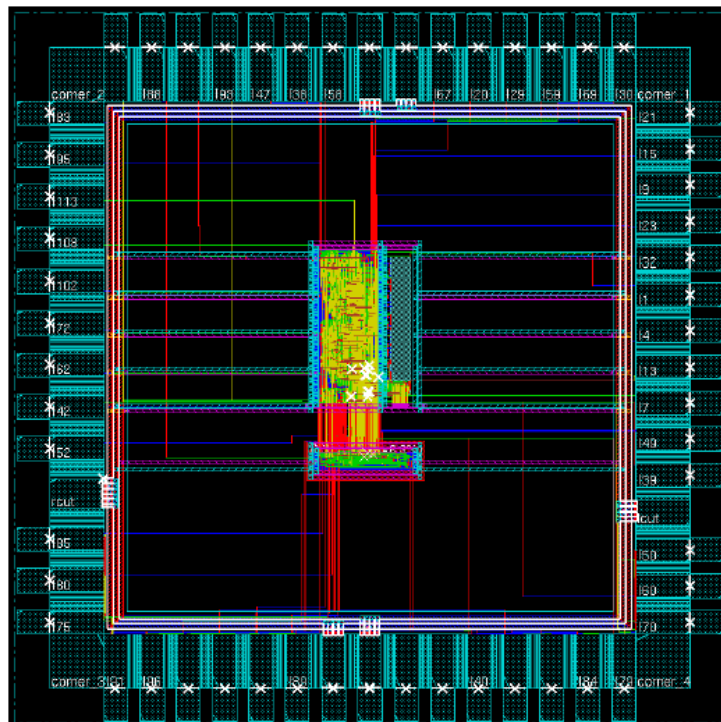


**Figure A.1 The final view of the SRAM chip after P&R.**

After generating the DEF file, Virtuoso takes another round of design by importing the DEF file and substituting the abstract view of each instance

with its actual layout to end up with what is shown in Figure A.2. This figure shows the layout of the entire chip with all involved cells compiled and connected internally together and externally to the I/O pins. The next step is the verifications, which require a GDSII file, therefore, the current design file is Streamed out.

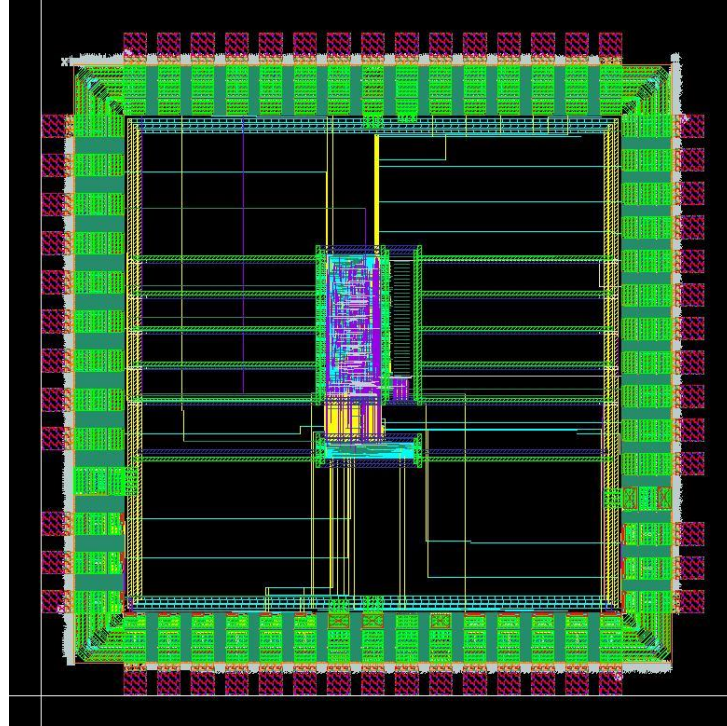


**Figure A.2 SRAM chip after replacing abstract views with corresponding real layouts.**

The obtained GDSII file is handed over this time to a tool called Calibre (from Mentor Graphics), which is the tool recommended by the foundry for verifications. By employing Calibre, the designer checked whether the layers inside the entire chip is manufacturable, a test better known as Design Rule Check (DRC), and whether the silicon and metal layers in the layout file are exactly the same as the transistors and connections in the schematic view, a test better known as Layout Versus Schematic (LVS). Certainly, it is the designer's responsibility to make sure that all in-house designed cells are DRC and LVS clean before replacing them in Virtuoso in the previous step.

Following the verifications, the design is now ready for the last step, which can be entitled chip assembly. By the end of this step, the entire chip is assembled and its bond-pads are connected to the pins of the package as Fig-

ure A.3 shows, where the package selected for HoliSRAM is PGA84. Finally, the exported GDSII file is sent to IMEC for fabrications and packaging.

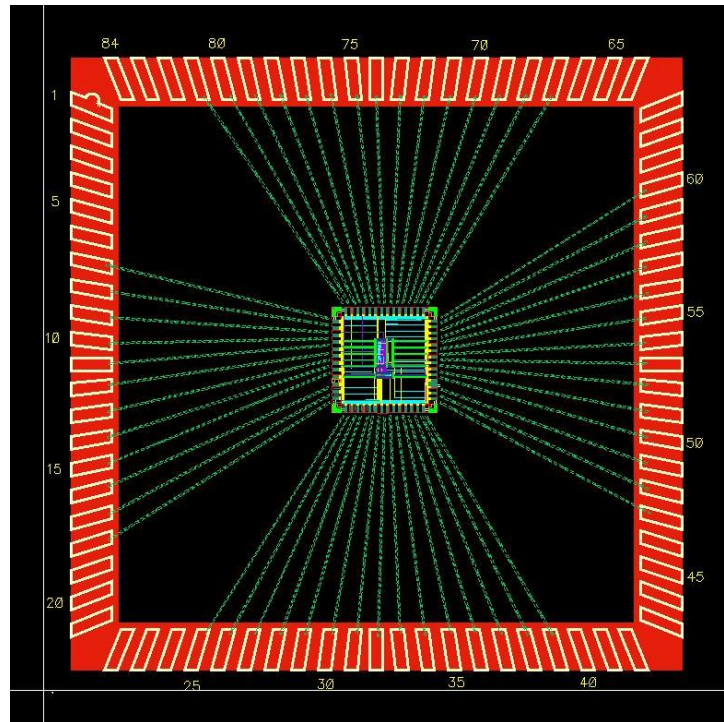


Figure A.3 HoliSRAM chip completely designed and packaged in PGA84.

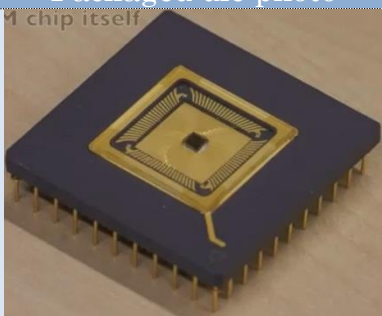

## A.2 Introduction

This appendix contains more details about the works related to the chips fabrication and testing involved in this project.

## A.3 Chip Gallery

The table below lists all the silicon chips that the researcher designs and fabricates during his study. Explicitly, he contributes by designing and laying out the full-custom and analogue part of two pieces of silicon, which are the HoliSRAM chip and the reference free voltage sensors. The former and latter are fabricated using UMC 90nm and 180nm respectively. Importantly, both silicon dies have correct functionality according to the design goals. In addition, he completely designed all parts of another SRAM chip using TSMC 130nm technology.

**Table A.1 Chip Gallery**

Technology	Packaged die photo	Main design goal
UMC 90nm		Demonstrate the ability of truly self-timed SRAM to tolerate high variations in supply voltage
UMC 180nm		Demonstrate the capability of the asynchronous logic to accurately sense the on-chip voltage without reference voltage

## A.4 Demonstration PCB

Figure A.4 to Figure A.6 below show the complete schematic of the portable demonstration board.

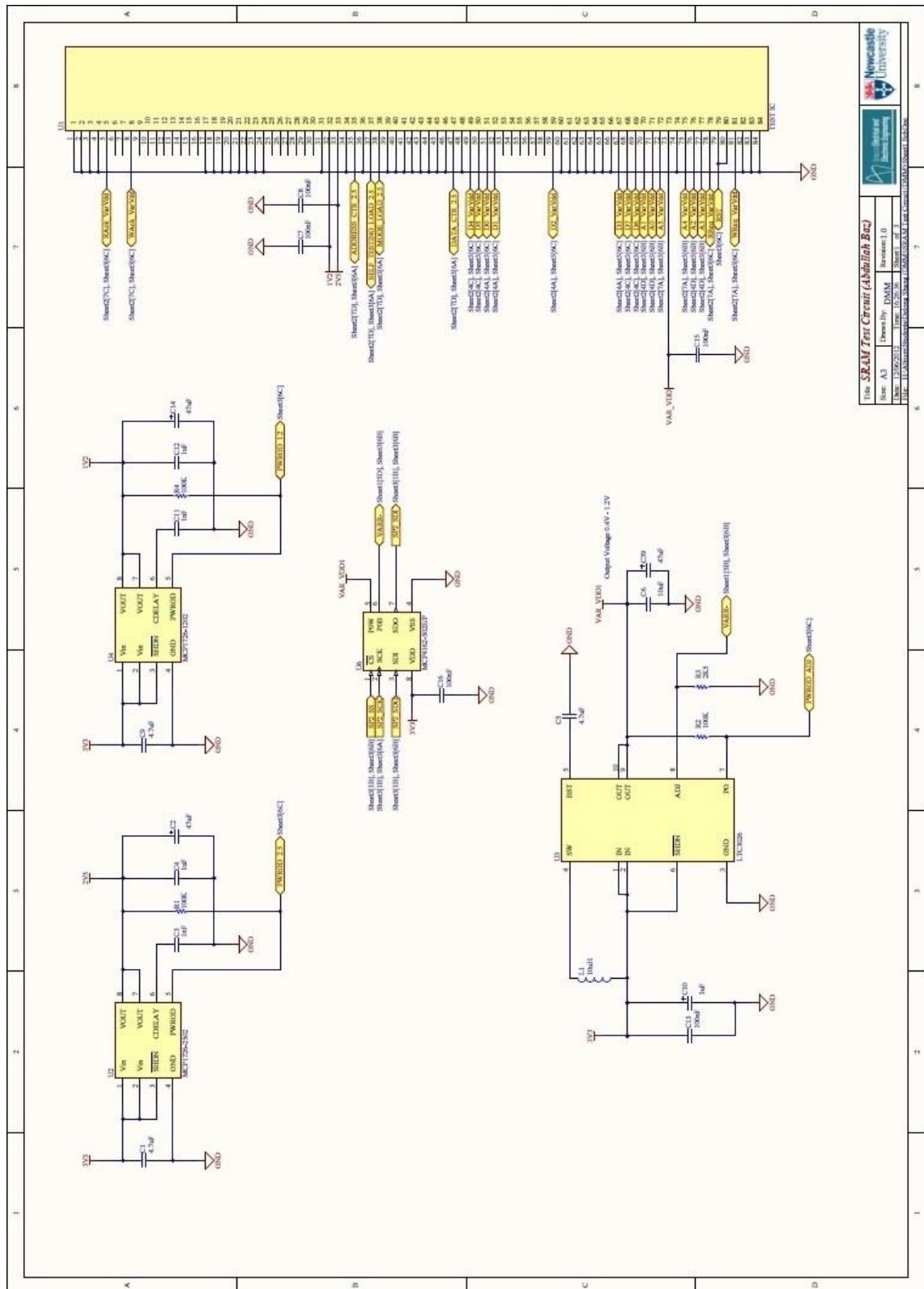


Figure A.4 Schematic of the demonstration PCB page 1/3.







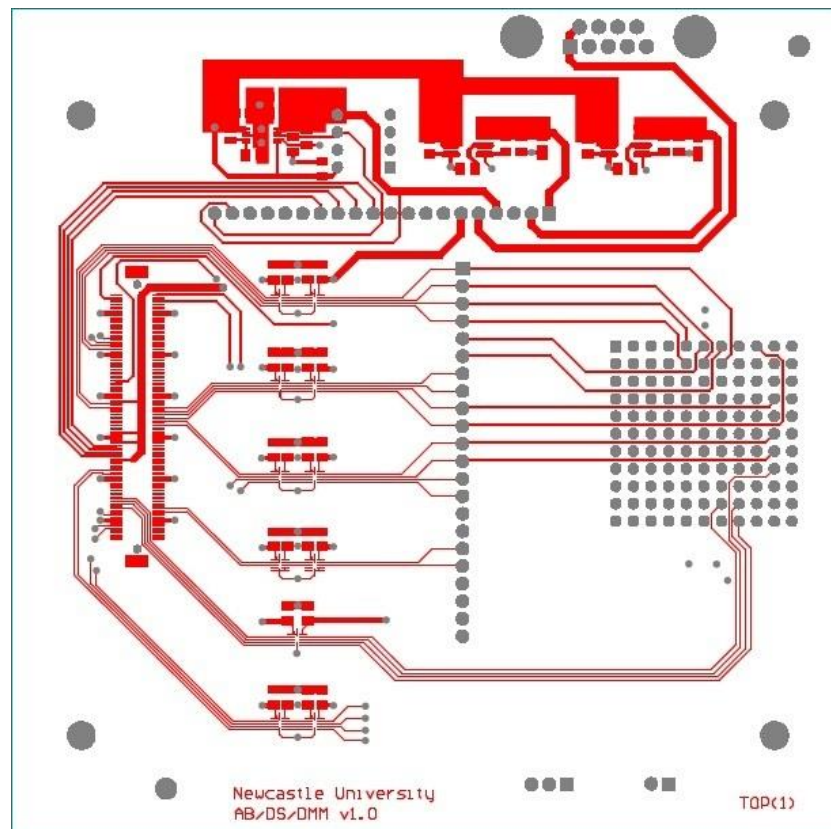


Figure A.7 Layer-1 of the demonstration PCB.

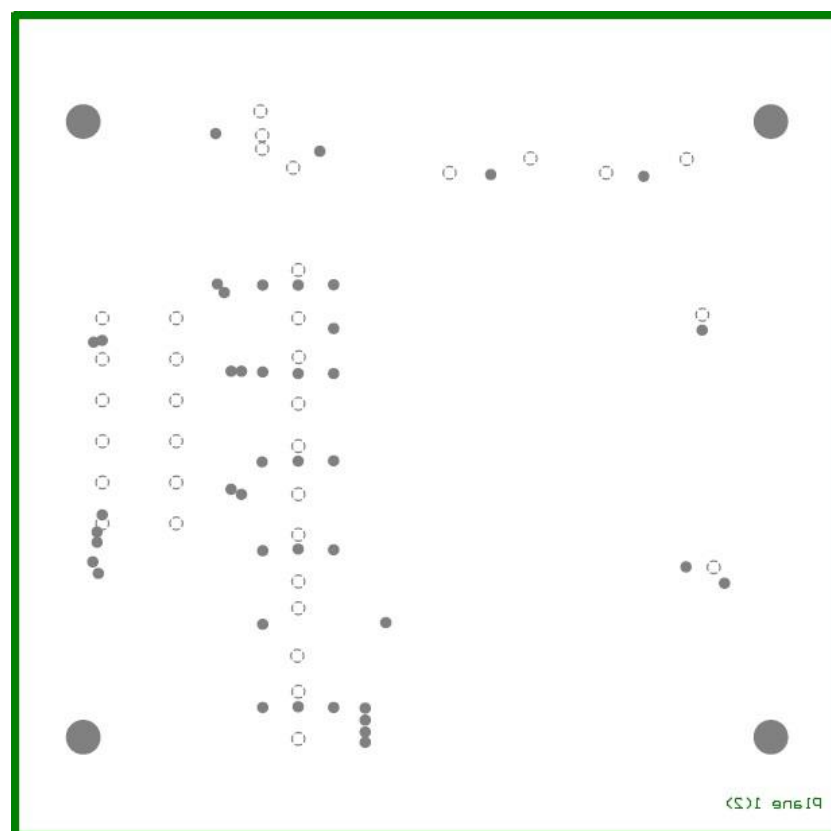


Figure A.8 Layer-2 of the demonstration PCB.



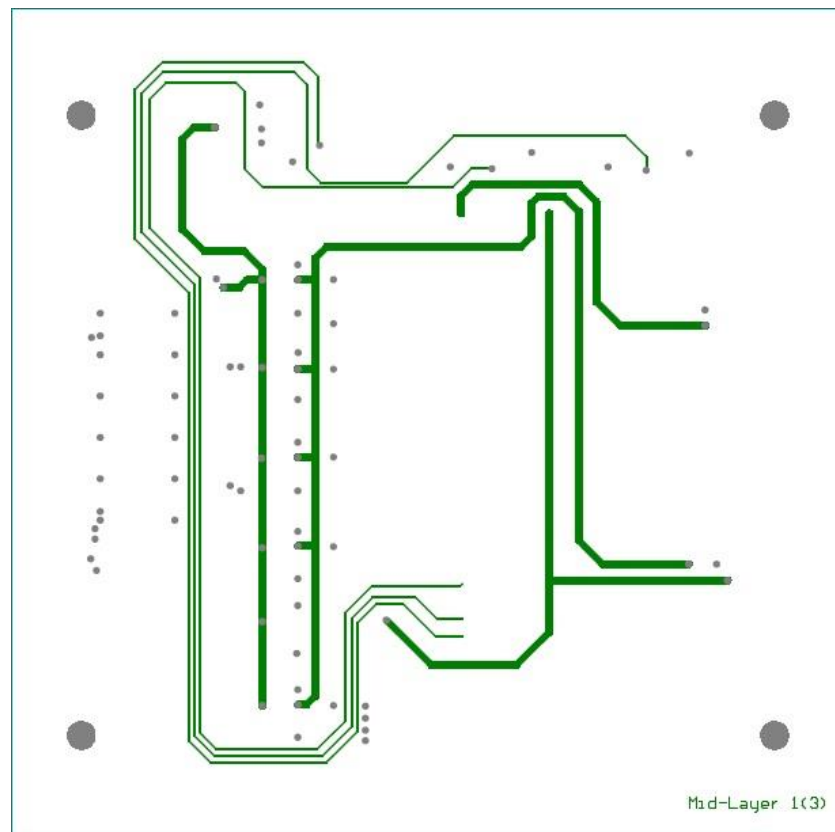


Figure A.9 Layer-3 of the demonstration PCB.

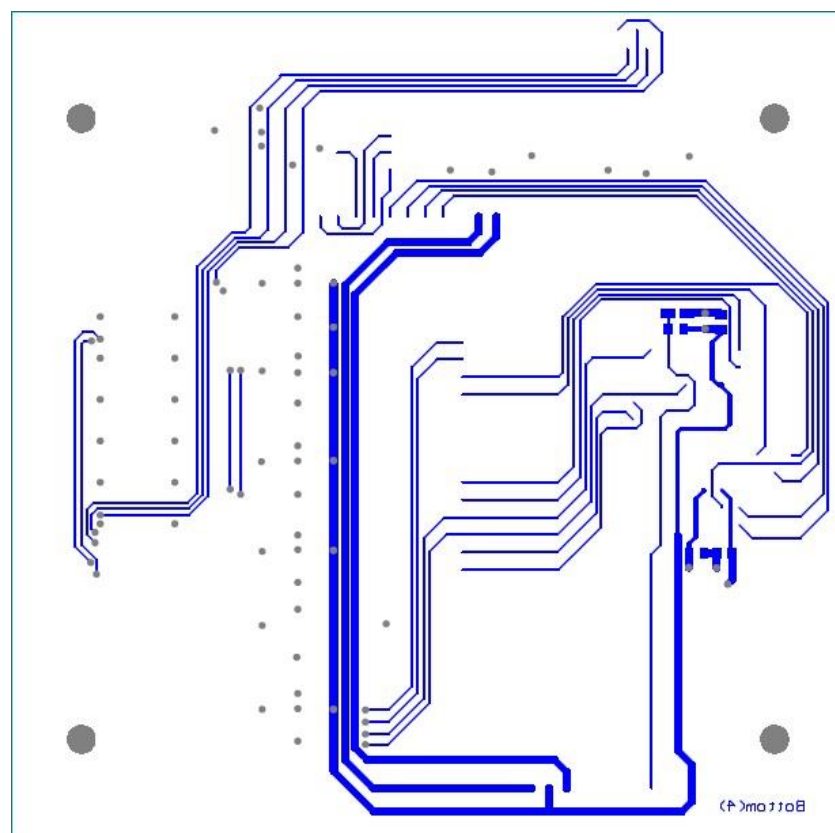


Figure A.10 Layer-4 of the demonstration PCB.



```

#pragma config POSCMOD = XT           // Primary Oscillator
#pragma config IESO = OFF            // Internal/External Switch-over
#pragma config FSOSCEN = OFF         // Secondary Oscillator Enable
#pragma config CP = OFF              // Code Protect
#pragma config BWP = OFF             // Boot Flash Write Protect
#pragma config PWP = OFF             // Program Flash Write Protect
#pragma config ICESEL = ICS_PGx2    // ICE/ICD Comm Channel Select
#pragma config DEBUG = OFF           // Debugger Disabled for Starter Kit

#define SYS_FREQ (80000000)

unsigned char SCCValue=224, portEOut=0, data[64];
void DelayMs(float msec);
void SetVDD(unsigned char VDDValue, unsigned char powerMode, unsigned char portEOut);
void WriteToAddress();
void ReadFromAddress();
void WriteToSRAM();
void ReadFromSRAM();

int main(void)
{
    SYSTEMConfig(SYS_FREQ, SYS_CFG_WAIT_STATES | SYS_CFG_PCACHE);
    DBINIT();

    unsigned char typeOfOperation=0;
    unsigned int config = 0b00010000000000001000011000100000, i;
    SpiChnOpen(2, config, 8);
    SPI2BUF = 0x00F2;
    while(!SPI2STATbits.SPIRBF);

    AD1PCFG = 0x7FFF;
    // PORTB = Digital;RB15 = analog
    AD1CON1 = 0x0000;
    // SAMP bit = 0 ends sampling and starts converting
    AD1CHS = 0x000F0000;
    // Connect RB15/AN15 as CH0 input in this example RB15/AN15 is the input
    AD1CSSL = 0;
    AD1CON3 = 0x0002;
    // Manual Sample, TAD = internal 6 TPB
    AD1CON2 = 0;
    AD1CON1SET = 0x8000;
    // turn on the ADC

    mPORTESetPinsDigitalOut(0b11111111);
    mPORTBSetPinsDigitalOut(0x3FFF);
    mPORTCSetPinsDigitalOut(0x0006);

    mPORTEWrite(SCCValue);
    DelayMs(0.001); // 1 usec
    mPORTEWrite(SCCValue+256);

    mPORTBWrite(0);
    mPORTCWrite(0);
    mPORTEWrite(SCCValue+256);
    mPORTBWrite(4094);
    mPORTCWrite(0);
    mPORTEWrite(8+SCCValue+256);
    DelayMs(0.01);
    mPORTBWrite(4094);
    mPORTCWrite(0);
    mPORTEWrite(SCCValue+256);
    mPORTBWrite(0);
    mPORTBWrite(10752);
    mPORTBWrite(0);
    mPORTBWrite(51);
    mPORTBWrite(0);
    mPORTBWrite(16127);
    mPORTCWrite(0);
    mPORTEWrite(4+SCCValue+256);
    DelayMs(0.01);
    mPORTBWrite(16127);
    mPORTCWrite(0);
    mPORTEWrite(SCCValue+256);
    mPORTBWrite(0);
    mPORTBWrite(10803);

    portEOut=0;
    DBPRINTF("\n");
    DBPRINTF("\n");

```

```

        DBPRINTF("\n");
        DBPRINTF("Hi, \n");
        DBPRINTF("I'm the first Self-Timed SRAM in the world, called HoliSRAM. \n");
        DBPRINTF("Welcome to this demonstration, which is developed by Abdullah Baz.
\n");
        DBPRINTF("In Newcastle University, school of EEE. \n");
        DBPRINTF("The current date and time are (" __DATE__ " , " __TIME__ ") \n");

        for(i=0; i<64; i++)
            data[i] = 48;

        while(1)
        {
            typeOfOperation=0;
            while(typeOfOperation!=49 && typeOfOperation!=50 && typeOfOperation!=51
&& typeOfOperation!=52)
            {
                DBPRINTF("Please select the type of the operation: (1 to write to
a specific address, 2 to read from a specific address, 3 to write to the whole SRAM, 4
to read from the whole SRAM). \n");
                DBGETC(&typeOfOperation);
            }
            if(typeOfOperation==49)
                WriteToAddress();
            else if(typeOfOperation==50)
                ReadFromAddress();
            else if(typeOfOperation==51)
                WriteToSRAM();
            else if(typeOfOperation==52)
                ReadFromSRAM();
        }

        DBPRINTF("Program terminated. Click HALT and then RESET to stop the microcontrol-
ler. \n");
        return 0;
    }

void DelayMs(float msec)
{
    unsigned int tWait, tStart;
    tWait=(SYS_FREQ/2000)*msec;
    tStart=ReadCoreTimer();
    while((ReadCoreTimer()-tStart)<tWait); // wait for the time to pass
}

void SetVDD(unsigned char VDDValue, unsigned char powerMode, unsigned char portEOut)
{
    if(powerMode==49)
    {
        if(VDDValue==49) //1.2 V
            SPI2BUF = 0x00F2;
        else if(VDDValue==50) //1.1 V
            SPI2BUF = 0x0092;
        else if(VDDValue==51) //1.0 V
            SPI2BUF = 0x0082;
        else if(VDDValue==52) //0.9 V
            SPI2BUF = 0x0072;
        else if(VDDValue==53) //0.8 V
            SPI2BUF = 0x0072;
        else if(VDDValue==54) //0.7 V
            SPI2BUF = 0x0040;
        else if(VDDValue==55) //0.6 V
            SPI2BUF = 0x0032;
        else if(VDDValue==56) //0.5 V
            SPI2BUF = 0x0012;
        else if(VDDValue==57) //0.4 V
            SPI2BUF = 0x0000;

        while(!SPI2STATbits.SPIRBF); // wait for TX complete
    }
    else if(powerMode==50)
    {
        if(VDDValue==49) // 1.2 V
        {
            mPORTEWrite(portEOut+96);
            DelayMs(0.001); // 1 usec
            mPORTEWrite(portEOut+96+256);
        }
        else if(VDDValue==50) // 1.1 V

```

```

        {
            mPORTEWrite(portEOut+32);
            DelayMs(0.001); // 1 usec
            mPORTEWrite(portEOut+32+256);
        }
        else if(VDDValue==51 || VDDValue==52) // 0.9 V
        {
            mPORTEWrite(portEOut+160);
            DelayMs(0.001); // 1 usec
            mPORTEWrite(portEOut+160+256);
        }
        else if(VDDValue==53) // 0.8 V
        {
            mPORTEWrite(portEOut+64);
            DelayMs(0.001); // 1 usec
            mPORTEWrite(portEOut+64+256);
        }
        else if(VDDValue==54 || VDDValue==55 || VDDValue==56 || VDDValue==57) //
0.6 V
        {
            mPORTEWrite(portEOut+192);
            DelayMs(0.001); // 1 usec
            mPORTEWrite(portEOut+192+256);
        }
    }
}

void WriteToAddress()
{
    unsigned int getWack=0x0000, i=0, risingTimer, fallingTimer, j=0, risingEdgeNo=0,
fallingEdgeNo=0, ADCValue, realAddress=0;
    unsigned char address[2], isWrongAddress=1, powerMode=0, VDDMode=0, VDDValue=0,
VDDUpperLimit=0, VDDLLowerLimit=0;
    unsigned short portBOut=0;
    float VDD;

    mPORTBSetPinsDigitalOut(0x3FFF); //Data & Address
    mPORTCSetPinsDigitalOut(0x0002); //WReq
    mPORTFSetPinsDigitalIn(0x0001); //Wack

    while(isWrongAddress)
    {
        address[0]=0;
        address[1]=0;
        DBPRINTF("Please enter the address you want to write to (between 0 and
63):\n");
        DBGETS(address, sizeof(address));
        if( address[1]==0 && address[0]>=48 && address[0]<=57 )
            isWrongAddress=0;
        else if( address[1]>=48 && address[1]<=57 && address[0]>=49 && ad-
dress[0]<=53 )
            isWrongAddress=0;
        else if( address[0]==54 && address[1]>=48 && address[1]<=51 )
            isWrongAddress=0;
    }

    if(address[1]==0)
        realAddress=address[0]-48;
    else
        realAddress=(address[0]-48)*10+(address[1]-48);

    DBPRINTF("Please enter the data you want to write (only one character):\n");
    DBGETC(&data[realAddress]);

    portBOut=data[realAddress]+realAddress*256;

    portEOut=0;
    mPORTEWrite(portEOut+SCCValue+256);
    mPORTBWrite(portBOut);

    while(powerMode!=49 && powerMode!=50)
    {
        DBPRINTF("Please select the type of the power supply: (1 for regulator
and 2 for SCC). \n");
        DBGETC(&powerMode);
    }

    while(VDDMode!=49 && VDDMode!=50)
    {

```

```

        DBPRINTF("Please select the supply voltage mode: (1 for stable and 2 for
variable). \n");
        DBGETC(&VDDMode);
    }

    if(VDDMode==49) //stable supply voltage
    {
        while(!(VDDValue>=49 && VDDValue<=57))
        {
            DBPRINTF("Please enter the supply voltage value: (1 for 1.2 V, 2
for 1.1 V, 3 for 1.0 V, 4 for 0.9 V, 5 for 0.8 V, 6 for 0.7 V, 7 for 0.6 V, 8 for 0.5 V,
9 for 0.4 V). \n");
            DBGETC(&VDDValue);
        }

        SetVDD(VDDValue, powerMode, portEOut);
        DelayMs(1000);

        AD1CON1SET = 0x0002;
        // start sampling ...
        DelayMs(1);
        // for 100 ms
        AD1CON1CLR = 0x0002;
        // start Converting
        while (!(AD1CON1 & 0x0001));
        // conversion done?
        ADCValue = ADC1BUF0;
        // yes then get ADC value
        VDD=0.00322265625*ADCValue;

        risingEdgeNo=1;
        fallingEdgeNo=1;

        for(i=0;i<20;i++)
        {
            mPORTCWrite(0x0002);
            getWack=0x0000;
            risingTimer=0;
            while(!(getWack&0x0001 || risingTimer>1000))
            {
                risingTimer++;
                getWack=mPORTFReadBits(BIT_0);
            }
            if(risingTimer==1)
            {
                DBPRINTF("Wack rising edge number %01u at %1.3f V \n",
risingEdgeNo, VDD);
                risingEdgeNo++;
            }
            else if (risingTimer>1000)
            {
                DBPRINTF("Wack cannot be generated at %1.3f V \n", VDD);
                break;
            }
            mPORTCWrite(0x0000);
            getWack=0xFFFF;
            fallingTimer=0;
            while(!( (~getWack)&0x0001 || fallingTimer>1000))
            {
                fallingTimer++;
                getWack=mPORTFReadBits(BIT_0);
            }
            if(fallingTimer==1)
            {
                DBPRINTF("Wack falling edge number %01u at %1.3f V \n",
fallingEdgeNo, VDD);
                fallingEdgeNo++;
            }
            else if (fallingTimer>1000)
            {
                DBPRINTF("Wack cannot be withdrawn at %1.3f V \n", VDD);
                break;
            }
        }
    }
    else if(VDDMode==50) //variable supply voltage
    {
        while(!(VDDUpperLimit>=49 && VDDUpperLimit<=57))
        {

```

```

        DBPRINTF("Please enter the upper limit of the supply voltage: (1
for 1.2 V, 2 for 1.1 V, 3 for 1.0 V, 4 for 0.9 V, 5 for 0.8 V, 6 for 0.7 V, 7 for 0.6 V,
8 for 0.5 V, 9 for 0.4 V). \n");
        DBGETC(&VDDUpperLimit);
    }
    while(!(VDDLLowerLimit>=49 && VDDLLowerLimit<=57))
    {
        DBPRINTF("Please enter the lower limit of the supply voltage: (1
for 1.2 V, 2 for 1.1 V, 3 for 1.0 V, 4 for 0.9 V, 5 for 0.8 V, 6 for 0.7 V, 7 for 0.6 V,
8 for 0.5 V, 9 for 0.4 V). \n");
        DBGETC(&VDDLLowerLimit);
    }

    j=VDDUpperLimit;
    SetVDD(j, powerMode, portEOut);
    DelayMs(1000);

    AD1CON1SET = 0x0002;
    // start sampling ...
    DelayMs(1);
    // for 100 ms
    AD1CON1CLR = 0x0002;
    // start Converting
    while (!(AD1CON1 & 0x0001));
    // conversion done?
    ADCValue = ADC1BUF0;
    // yes then get ADC value
    VDD=0.00322265625*ADCValue;

    risingEdgeNo=1;
    fallingEdgeNo=1;

    for(i=0;i<20;i++)
    {
        mPORTCWrite(0x0002);
        getWack=0x0000;
        risingTimer=0;
        while(!(getWack&0x0001 || risingTimer>1000))
        {
            risingTimer++;
            getWack=mPORTFReadBits(BIT_0);
        }
        if(risingTimer==1)
        {
            DBPRINTF("Wack rising edge number %01u at %1.3f V \n",
risingEdgeNo, VDD);
            risingEdgeNo++;
        }
        else if (risingTimer>1000)
            DBPRINTF("Wack cannot be generated at %1.3f V \n", VDD);
        mPORTCWrite(0x0000);
        if(risingTimer==1)
        {
            getWack=0xFFFF;
            fallingTimer=0;
            while(!( (~getWack)&0x0001 || fallingTimer>1000))
            {
                fallingTimer++;
                getWack=mPORTFReadBits(BIT_0);
            }
            if(fallingTimer==1)
            {
                DBPRINTF("Wack falling edge number %01u at %1.3f V
\n", fallingEdgeNo, VDD);
                fallingEdgeNo++;
            }
            else if (fallingTimer>1000)
                DBPRINTF("Wack cannot be withdrawn at %1.3f V \n",
VDD);
        }
        else
            DelayMs(4800);
        j++;
        if(j>VDDLLowerLimit)
            j=VDDUpperLimit;
        SetVDD(j, powerMode, portEOut);
        DelayMs(1000);

        AD1CON1SET = 0x0002;

```

```

        // start sampling ...
        DelayMs(1);
        // for 100 ms
        AD1CON1CLR = 0x0002;
        // start Converting
        while (!(AD1CON1 & 0x0001));
        // conversion done?
        ADCValue = ADC1BUF0;
        // yes then get ADC value
        VDD=0.00322265625*ADCValue;
    }
}

void ReadFromAddress()
{
    unsigned int getRAck=0x0000, getData=0x0000, i=0, risingTimer, fallingTimer, j=0,
    risingEdgeNo=0, fallingEdgeNo=0, ADCValue, realAddress=0;
    unsigned char address[2], isWrongAddress=1, powerMode=0, VDDMode=0, VDDValue=0,
    VDDUpperLimit=0, VDDLowerLimit=0;
    unsigned short portBOut=0;
    float VDD;

    mPORTBSetPinsDigitalIn(0x00FF); //Data
    mPORTBSetPinsDigitalOut(0x3F00); //Address
    mPORTCSetPinsDigitalOut(0x0004); //RReq
    mPORTFSetPinsDigitalIn(BIT_1); //RAck

    while(isWrongAddress)
    {
        address[0]=0;
        address[1]=0;
        DBPRINTF("Please enter the address you want to read from (between 0 and
63):\n");
        DBGETS(address, sizeof(address));
        if( address[1]==0 && address[0]>=48 && address[0]<=57 )
            isWrongAddress=0;
        else if( address[1]>=48 && address[1]<=57 && address[0]>=49 && ad-
dress[0]<=53 )
            isWrongAddress=0;
        else if( address[0]==54 && address[1]>=48 && address[1]<=51 )
            isWrongAddress=0;
    }

    if(address[1]==0)
        realAddress=address[0]-48;
    else
        realAddress=(address[0]-48)*10+(address[1]-48);

    portBOut=realAddress*256;

    portEOut=2;
    mPORTEWrite(portEOut+SCCValue+256);
    mPORTBWrite(portBOut);

    while(powerMode!=49 && powerMode!=50)
    {
        DBPRINTF("Please select the type of the power supply: (1 for regulator
and 2 for SCC). \n");
        DBGETC(&powerMode);
    }

    while(VDDMode!=49 && VDDMode!=50)
    {
        DBPRINTF("Please select the supply voltage mode: (1 for stable and 2 for
variable). \n");
        DBGETC(&VDDMode);
    }

    if(VDDMode==49) //stable supply voltage
    {
        while(!(VDDValue>=49 && VDDValue<=57))
        {
            DBPRINTF("Please enter the supply voltage value: (1 for 1.2 V, 2
for 1.1 V, 3 for 1.0 V, 4 for 0.9 V, 5 for 0.8 V, 6 for 0.7 V, 7 for 0.6 V, 8 for 0.5 V,
9 for 0.4 V). \n");
            DBGETC(&VDDValue);
        }
    }
}

```



```

        SetVDD(VDDValue, powerMode, portEOut);
        DelayMs(1000);

        AD1CON1SET = 0x0002;
        // start sampling ...
        DelayMs(1);
        // for 100 ms
        AD1CON1CLR = 0x0002;
        // start Converting
        while (!(AD1CON1 & 0x0001));
    // conversion done?
    ADCValue = ADC1BUF0;
    // yes then get ADC value
    VDD=0.00322265625*ADCValue;

    risingEdgeNo=1;
    fallingEdgeNo=1;

    for(i=0;i<20;i++)
    {
        mPORTCWrite(0x0004);
        getRAck=0x0000;
        risingTimer=0;
        while(!(getRAck&0x0002 || risingTimer>1000))
        {
            risingTimer++;
            getRAck=mPORTFReadBits(BIT_1);
        }
        if(risingTimer==1)
        {
            DBPRINTF("Rack rising edge number %01u at %1.3f V \n",
risingEdgeNo, VDD);
            risingEdgeNo++;
            DBPRINTF("Output data of address %01u is: %c \n", realAd-
dress, data[realAddress]);
        }
        else if (risingTimer>1000)
        {
            DBPRINTF("Rack cannot be generated at %1.3f V \n", VDD);
            break;
        }
        mPORTCWrite(0x0000);
        getRAck=0xFFFF;
        fallingTimer=0;
        while(!(~getRAck)&0x0002 || fallingTimer>1000))
        {
            fallingTimer++;
            getRAck=mPORTFReadBits(BIT_1);
        }
        if(fallingTimer==1)
        {
            DBPRINTF("Rack falling edge number %01u at %1.3f V \n",
fallingEdgeNo, VDD);
            fallingEdgeNo++;
        }
        else if (fallingTimer>1000)
        {
            DBPRINTF("Rack cannot be withdrawn at %1.3f V \n", VDD);
            break;
        }
    }
}
else if(VDDMode==50) //variable supply voltage
{
    while(!(VDDUpperLimit>=49 && VDDUpperLimit<=57))
    {
        DBPRINTF("Please enter the upper limit of the supply voltage: (1
for 1.2 V, 2 for 1.1 V, 3 for 1.0 V, 4 for 0.9 V, 5 for 0.8 V, 6 for 0.7 V, 7 for 0.6 V,
8 for 0.5 V, 9 for 0.4 V). \n");
        DBGETC(&VDDUpperLimit);
    }
    while(!(VDDLLowerLimit>=49 && VDDLLowerLimit<=57))
    {
        DBPRINTF("Please enter the lower limit of the supply voltage: (1
for 1.2 V, 2 for 1.1 V, 3 for 1.0 V, 4 for 0.9 V, 5 for 0.8 V, 6 for 0.7 V, 7 for 0.6 V,
8 for 0.5 V, 9 for 0.4 V). \n");
        DBGETC(&VDDLLowerLimit);
    }
}

```

```

        j=VDDUpperLimit;
        SetVDD(j, powerMode, portEOut);
        DelayMs(1000);

        AD1CON1SET = 0x0002;
        // start sampling ...
        DelayMs(1);
        // for 100 ms
        AD1CON1CLR = 0x0002;
        // start Converting
        while (!(AD1CON1 & 0x0001));
    // conversion done?
    ADCValue = ADC1BUF0;
    // yes then get ADC value
    VDD=0.00322265625*ADCValue;

    risingEdgeNo=1;
    fallingEdgeNo=1;

    for(i=0;i<20;i++)
    {
        mPORTCWrite(0x0004);
        getRAck=0x0000;
        risingTimer=0;
        while(!(getRAck&0x0002 || risingTimer>1000))
        {
            risingTimer++;
            getRAck=mPORTFReadBits(BIT_1);
        }
        if(risingTimer==1)
        {
            DBPRINTF("Rack rising edge number %01u at %1.3f V \n",
risingEdgeNo, VDD);
            risingEdgeNo++;
            DBPRINTF("Output data of address %01u is: %c \n", realAd-
dress, data[realAddress]);
        }
        else if(risingTimer>1000)
            DBPRINTF("Rack cannot be generated at %1.3f V \n", VDD);
        mPORTCWrite(0x0000);
        if(risingTimer==1)
        {
            getRAck=0xFFFF;
            fallingTimer=0;
            while(!(~getRAck)&0x0002 || fallingTimer>1000))
            {
                fallingTimer++;
                getRAck=mPORTFReadBits(BIT_1);
            }
            if(fallingTimer==1)
            {
                DBPRINTF("Rack falling edge number %01u at %1.3f V
\n", fallingEdgeNo, VDD);
                fallingEdgeNo++;
            }
            else if (fallingTimer>1000)
                DBPRINTF("Rack cannot be withdrawn at %1.3f V \n",
VDD);
        }
        else
            DelayMs(4800);
        j++;
        if(j>VDDLowerLimit)
            j=VDDUpperLimit;
        SetVDD(j, powerMode, portEOut);
        DelayMs(1000);

        AD1CON1SET = 0x0002;
        // start sampling ...
        DelayMs(1);
        // for 100 ms
        AD1CON1CLR = 0x0002;
        // start Converting
        while (!(AD1CON1 & 0x0001));
    // conversion done?
    ADCValue = ADC1BUF0;
    // yes then get ADC value
    VDD=0.00322265625*ADCValue;
    }

```

```

    }
}

void WriteToSRAM()
{
    unsigned int getWack=0x0000, i=0, risingTimer, fallingTimer, j=0, ADCValue;
    unsigned char powerMode=0, VDDMode=0, VDDValue=0, VDDUpperLimit=0, VDDLowerLim-
it=0;
    unsigned short portBOut=0;
    float VDD;

    portEOut=0;

    // Fill string buffer with null chars
    for(i=0; i<64; i++)
        data[i] = '\0';
    DBPRINTF("Please type up to 64 characters long string. \n");
    // Store it in our buffer
    DBGETS(data, sizeof(data));
    // In case more than 64 characters entered, set last byte in buffer = null
    data[64] = 0;

    mPORTBSetPinsDigitalOut(0x3FFF); //Data & Address
    mPORTCSetPinsDigitalOut(0x0002); //WReq
    mPORTFSetPinsDigitalIn(0x0001); //Wack

    while(powerMode!=49 && powerMode!=50)
    {
        DBPRINTF("Please select the type of the power supply: (1 for regulator
and 2 for SCC). \n");
        DBGETC(&powerMode);
    }

    while(VDDMode!=49 && VDDMode!=50)
    {
        DBPRINTF("Please select the supply voltage mode: (1 for stable and 2 for
variable). \n");
        DBGETC(&VDDMode);
    }

    if(VDDMode==49) //stable supply voltage
    {
        while(!(VDDValue>=49 && VDDValue<=57))
        {
            DBPRINTF("Please enter the supply voltage value: (1 for 1.2 V, 2
for 1.1 V, 3 for 1.0 V, 4 for 0.9 V, 5 for 0.8 V, 6 for 0.7 V, 7 for 0.6 V, 8 for 0.5 V,
9 for 0.4 V). \n");
            DBGETC(&VDDValue);
        }

        SetVDD(VDDValue, powerMode, portEOut);
        DelayMs(1000);

        AD1CON1SET = 0x0002;
        // start sampling ...
        DelayMs(1);
        // for 100 ms
        AD1CON1CLR = 0x0002;
        // start Converting
        while (!(AD1CON1 & 0x0001));
        // conversion done?
        ADCValue = ADC1BUF0;
        // yes then get ADC value
        VDD=0.00322265625*ADCValue;

        for(i=0; i<64; i++)
        {
            portBOut=data[i]+i*256;
            mPORTBWrite(portBOut);

            mPORTCWrite(0x0002);
            getWack=0x0000;
            risingTimer=0;
            while(!(getWack&0x0001 || risingTimer>1000))
            {
                risingTimer++;
                getWack=mPORTFReadBits(BIT_0);
            }
            if(risingTimer==1)

```

```

        DBPRINTF("Wack rising edge of address %0lu at %1.3f V \n",
i, VDD);
        else if (risingTimer>1000)
        {
            DBPRINTF("Wack of address %0lu cannot be generated at
%1.3f V \n", i, VDD);
            break;
        }
        mPORTCWrite(0x0000);
        getWack=0xFFFF;
        fallingTimer=0;
        while(!((~getWack)&0x0001 || fallingTimer>1000))
        {
            fallingTimer++;
            getWack=mPORTFReadBits(BIT_0);
        }
        if(fallingTimer==1)
            DBPRINTF("Wack falling edge of address %0lu at %1.3f V
\n", i, VDD);
        else if (fallingTimer>1000)
        {
            DBPRINTF("Wack of address %0lu cannot be withdrawn at
%1.3f V \n", i, VDD);
            break;
        }
    }
}
else if(VDDMode==50) //variable supply voltage
{
    while(!(VDDUpperLimit>=49 && VDDUpperLimit<=57))
    {
        DBPRINTF("Please enter the upper limit of the supply voltage: (1
for 1.2 V, 2 for 1.1 V, 3 for 1.0 V, 4 for 0.9 V, 5 for 0.8 V, 6 for 0.7 V, 7 for 0.6 V,
8 for 0.5 V, 9 for 0.4 V). \n");
        DBGETC(&VDDUpperLimit);
    }
    while(!(VDDLLowerLimit>=49 && VDDLLowerLimit<=57))
    {
        DBPRINTF("Please enter the lower limit of the supply voltage: (1
for 1.2 V, 2 for 1.1 V, 3 for 1.0 V, 4 for 0.9 V, 5 for 0.8 V, 6 for 0.7 V, 7 for 0.6 V,
8 for 0.5 V, 9 for 0.4 V). \n");
        DBGETC(&VDDLLowerLimit);
    }

    j=VDDUpperLimit;
    SetVDD(j, powerMode, portEOut);
    DelayMs(1000);

    AD1CON1SET = 0x0002;
    // start sampling ...
    DelayMs(1);
    // for 100 ms
    AD1CON1CLR = 0x0002;
    // start Converting
    while (!(AD1CON1 & 0x0001));
    // conversion done?
    ADCValue = ADC1BUF0;
    // yes then get ADC value
    VDD=0.00322265625*ADCValue;

    for(i=0; i<64; i++)
    {
        portBOut=data[i]+i*256;
        mPORTBWrite(portBOut);

        mPORTCWrite(0x0002);
        getWack=0x0000;
        risingTimer=0;
        while(!(getWack&0x0001))
        {
            DelayMs(1000);
            getWack=mPORTFReadBits(BIT_0);
            DelayMs(1000);
            if(getWack==0x0001)
                DBPRINTF("Wack rising edge of address %0lu at %1.3f
V \n", i, VDD);
            else if(getWack!=0x0001)
            {
                DBPRINTF("Wack of address %0lu cannot be generated

```

```

at %1.3f V \n", i, VDD);

        j++;
        if(j>VDDLLowerLimit)
            j=VDDUpperLimit;
        SetVDD(j, powerMode, portEOut);
        DelayMs(1000);

        AD1CON1SET = 0x0002;
        // start sampling ...
        DelayMs(1);

        // for 100 ms
        AD1CON1CLR = 0x0002;
        // start Converting
        while (!(AD1CON1 & 0x0001));
        // conversion done?
        ADCValue = ADC1BUF0;
        // yes then get ADC value
        VDD=0.00322265625*ADCValue;
    }
}
mPORTCWrite(0x0000);
getWack=0xFFFF;
while(!((~getWack)&0x0001))
{
    DelayMs(1000);
    getWack=mPORTFReadBits(BIT_0);
    DelayMs(1000);
    if(getWack==0x0000)
        DBPRINTF("Wack falling edge of address %0lu at
%1.3f V \n", i, VDD);
    else if(getWack==0x0001)
    {
        DBPRINTF("Wack of address %0lu cannot be withdrawn
at %1.3f V \n", i, VDD);

        j++;
        if(j>VDDLLowerLimit)
            j=VDDUpperLimit;
        SetVDD(j, powerMode, portEOut);
        DelayMs(1000);

        AD1CON1SET = 0x0002;
        // start sampling ...
        DelayMs(1);

        // for 100 ms
        AD1CON1CLR = 0x0002;
        // start Converting
        while (!(AD1CON1 & 0x0001));
        // conversion done?
        ADCValue = ADC1BUF0;
        // yes then get ADC value
        VDD=0.00322265625*ADCValue;
    }
}

j++;
if(j>VDDLLowerLimit)
    j=VDDUpperLimit;
SetVDD(j, powerMode, portEOut);
DelayMs(1000);

AD1CON1SET = 0x0002;
// start sampling ...
DelayMs(1);

// for 100 ms
AD1CON1CLR = 0x0002;
// start Converting
while (!(AD1CON1 & 0x0001));
// conversion done?
ADCValue = ADC1BUF0;
// yes then get ADC value
VDD=0.00322265625*ADCValue;
}

}

void ReadFromSRAM()
{

```

```

        unsigned int getRAck=0x0000, getData=0x0000, i=0, risingTimer, fallingTimer, j=0,
        ADCValue;
        unsigned char powerMode=0, VDDMode=0, VDDValue=0, VDDUpperLimit=0, VDDLowerLim-
        it=0;

        unsigned short portBOut=0;
        float VDD;

        portEOut=2;

        mPORTBSetPinsDigitalIn(0x00FF); //Data
        mPORTBSetPinsDigitalOut(0x3F00); //Address
        mPORTCSetPinsDigitalOut(0x0004); //RReq
        mPORTFSetPinsDigitalIn(BIT_1); //RAck

        while(powerMode!=49 && powerMode!=50)
        {
            DBPRINTF("Please select the type of the power supply: (1 for regulator
            and 2 for SCC). \n");
            DBGETC(&powerMode);
        }

        while(VDDMode!=49 && VDDMode!=50)
        {
            DBPRINTF("Please select the supply voltage mode: (1 for stable and 2 for
            variable). \n");
            DBGETC(&VDDMode);
        }

        if(VDDMode==49) //stable supply voltage
        {
            while(!(VDDValue>=49 && VDDValue<=57))
            {
                DBPRINTF("Please enter the supply voltage value: (1 for 1.2 V, 2
                for 1.1 V, 3 for 1.0 V, 4 for 0.9 V, 5 for 0.8 V, 6 for 0.7 V, 7 for 0.6 V, 8 for 0.5 V,
                9 for 0.4 V). \n");
                DBGETC(&VDDValue);
            }

            SetVDD(VDDValue, powerMode, portEOut);
            DelayMs(1000);

            AD1CON1SET = 0x0002;
            // start sampling ...
            DelayMs(1);
            // for 100 ms
            AD1CON1CLR = 0x0002;
            // start Converting
            while (!(AD1CON1 & 0x0001));
            // conversion done?
            ADCValue = ADC1BUF0;
            // yes then get ADC value
            VDD=0.00322265625*ADCValue;

            for(i=0;i<64;i++)
            {
                portBOut=i*256;
                mPORTBWrite(portBOut);

                mPORTCWrite(0x0004);
                getRAck=0x0000;
                risingTimer=0;
                while(!(getRAck&0x0002 || risingTimer>1000))
                {
                    risingTimer++;
                    getRAck=mPORTFReadBits(BIT_1);
                }
                if(risingTimer==1)
                {
                    DBPRINTF("Rack rising edge of address %01u at %1.3f V \n",
                    i, VDD);
                    DBPRINTF("Output data of address %01u is: %c \n", i, da-
                    ta[i]);
                }
                else if (risingTimer>1000)
                {
                    DBPRINTF("Rack of address %01u cannot be generated at
                    %1.3f V \n", i, VDD);
                    break;
                }
            }
        }
    }

```

```

        mPORTCWrite(0x0000);
        getRAck=0xFFFF;
        fallingTimer=0;
        while(!((~getRAck)&0x0002 || fallingTimer>1000))
        {
            fallingTimer++;
            getRAck=mPORTFReadBits(BIT_1);
        }
        if(fallingTimer==1)
            DBPRINTF("Rack falling edge of address %0lu at %1.3f V
\n", i, VDD);
        else if (fallingTimer>1000)
        {
            DBPRINTF("Rack of address %0lu cannot be withdrawn at
%1.3f V \n", i, VDD);
            break;
        }
    }
}
else if(VDDMode==50) //variable supply voltage
{
    while(!(VDDUpperLimit>=49 && VDDUpperLimit<=57))
    {
        DBPRINTF("Please enter the upper limit of the supply voltage: (1
for 1.2 V, 2 for 1.1 V, 3 for 1.0 V, 4 for 0.9 V, 5 for 0.8 V, 6 for 0.7 V, 7 for 0.6 V,
8 for 0.5 V, 9 for 0.4 V). \n");
        DBGETC(&VDDUpperLimit);
    }
    while(!(VDDLLowerLimit>=49 && VDDLLowerLimit<=57))
    {
        DBPRINTF("Please enter the lower limit of the supply voltage: (1
for 1.2 V, 2 for 1.1 V, 3 for 1.0 V, 4 for 0.9 V, 5 for 0.8 V, 6 for 0.7 V, 7 for 0.6 V,
8 for 0.5 V, 9 for 0.4 V). \n");
        DBGETC(&VDDLLowerLimit);
    }

    j=VDDUpperLimit;
    SetVDD(j, powerMode, portEOut);
    DelayMs(1000);

    AD1CON1SET = 0x0002;
    // start sampling ...
    DelayMs(1);
    // for 100 ms
    AD1CON1CLR = 0x0002;
    // start Converting
    while (!(AD1CON1 & 0x0001));
    // conversion done?
    ADCValue = ADC1BUF0;
    // yes then get ADC value
    VDD=0.00322265625*ADCValue;

    for(i=0;i<64;i++)
    {
        portBOut=i*256;
        mPORTBWrite(portBOut);

        mPORTCWrite(0x0004);
        getRAck=0x0000;
        risingTimer=0;
        while(!(getRAck&0x0002))
        {
            DelayMs(1000);
            getRAck=mPORTFReadBits(BIT_1);
            DelayMs(1000);
            if(getRAck==0x0002)
            {
                DBPRINTF("Rack rising edge of address %0lu at %1.3f
V \n", i, VDD);
                DBPRINTF("Output data of address %0lu is: %c \n",
i, data[i]);
            }
            else if(getRAck!=0x0002)
            {
                DBPRINTF("Rack of address %0lu cannot be generated
at %1.3f V \n", i, VDD);
                j++;
                if(j>VDDLLowerLimit)
                    j=VDDUpperLimit;
            }
        }
    }
}

```

```

        SetVDD(j, powerMode, portEOut);
        DelayMs(1000);

        AD1CON1SET = 0x0002;
        // start sampling ...
        DelayMs(1);
        // for 100 ms
        AD1CON1CLR = 0x0002;
        // start Converting
        while (!(AD1CON1 & 0x0001));
        // conversion done?
        ADCValue = ADC1BUF0;
        // yes then get ADC value
        VDD=0.00322265625*ADCValue;
    }
}
mPORTCWrite(0x0000);
getRAck=0xFFFF;
while(!((~getRAck)&0x0002))
{
    DelayMs(1000);
    getRAck=mPORTFReadBits(BIT_1);
    DelayMs(1000);
    if(getRAck==0x0000)
        DBPRINTF("Rack falling edge of address %01u at
%1.3f V \n", i, VDD);
    else if(getRAck==0x0002)
    {
        DBPRINTF("Rack of address %01u cannot be withdrawn
at %1.3f V \n", i, VDD);

        j++;
        if(j>VDDLLowerLimit)
            j=VDDUpperLimit;
        SetVDD(j, powerMode, portEOut);
        DelayMs(1000);

        AD1CON1SET = 0x0002;
        // start sampling ...
        DelayMs(1);
        // for 100 ms
        AD1CON1CLR = 0x0002;
        // start Converting
        while (!(AD1CON1 & 0x0001));
        // conversion done?
        ADCValue = ADC1BUF0;
        // yes then get ADC value
        VDD=0.00322265625*ADCValue;
    }
}

j++;
if(j>VDDLLowerLimit)
    j=VDDUpperLimit;
SetVDD(j, powerMode, portEOut);
DelayMs(1000);

AD1CON1SET = 0x0002;
// start sampling ...
DelayMs(1);
// for 100 ms
AD1CON1CLR = 0x0002;
// start Converting
while (!(AD1CON1 & 0x0001));
// conversion done?
ADCValue = ADC1BUF0;
// yes then get ADC value
VDD=0.00322265625*ADCValue;
}
}
}

```